Keratins act as global coordinators of tissue spreading through mechanosensitive feedback

by

Suyash Naik

October, 2025

A thesis submitted to the
Graduate School
of the
Institute of Science and Technology Austria
in partial fulfillment of the requirements
for the degree of
Doctor of Philosophy

Committee in charge:

Michael Sixt, Chair Carl-Philipp Heisenberg Edouard Hannezo Jiri Friml Xavier Trepat



The thesis of Suyash Naik, titled <i>Keratins act as global coordinators of tissue spreading through mechanosensitive feedback</i> , is approved by:				
Supervisor : Car	I-Philipp Heisenberg, ISTA, Klosterneuburg, Austria			
	Signature:			
Co-supervisor:	Edouard Hannezo, ISTA, Klosterneuburg, Austria			
	Signature:			
Committee Me	mber: Jiri Friml, ISTA, Klosterneuburg, Austria			
	Signature:			
Committee Me	mber: Xavier Trepat, Institute for Bioengineering of Catal	onia, Spain		
	Signature:			
Defense Chair:	Michael Sixt, ISTA, Klosterneuburg, Austria			
	Signature:			

© by Suyash Naik, October, 2025

CC BY-SA 4.0 The copyright of this thesis rests with the author. The whole thesis is licensenced under the CC BY-SA 4.0 except chapter 3 section 1, which is covered under the CC-BY-ND 4.0 copyright. The contents of this thesis except for Chapter 3 section 1 are licensed under a Creative Commons Attribution-ShareAlike 4.0 International. Under this license, you may copy and redistribute the material in any medium or format for both commercial and non-commercial purposes. You may also create and distribute modified versions of the work. This on the condition that: you credit the author and share any derivative works under the same license. Copyrighted by CC BY-ND 4.0 for chapter 3.1 allows to copy and redistribute the material in any medium or format for both commercial and non-commercial purposes. This on the condition that: you credit the author and do not distribute modified versions of the work.

ISTA Thesis, ISSN: 2663-337X

ISBN: 978-3-99078-069-5

I hereby declare that this thesis is my own work and that it does not contain other people's work without this being so stated; this thesis does not contain my previous work without this being stated, and the bibliography contains all the literature that I used in writing the dissertation.

I accept full responsibility for the content and factual accuracy of this work, including the data and their analysis and presentation, and the text and citation of other work.

I declare that this is a true copy of my thesis, including any final revisions, as approved by my thesis committee, and that this thesis has not been submitted for a higher degree to any other university or institution.

I certify that any republication of materials presented in this thesis has been approved by the relevant publishers and co-authors.

Signature:		
J		
	Suyash Naik	
	October, 2025	

Abstract

Epithelial spreading plays a pivotal role in the development of organisms especially those such as zebrafish which require the epithelial enveloping layer (EVL) to spread to cover the substantial yolk surface during gastrulation. Epiboly requires the transition of the epithelium with cuboidal cells to form a thin, flat squamous epithelial sheet. During this transition, the cells show tissue-scale mechanosensation with mechanisms such as direct mechanical control over the axis of cell division.

Cytoskeletal intermediate filaments play a crucial role in vertebrate cells, not only facilitating mechanical stability but also helping facilitate the mechanosensitive response of the cell. Mechanosenstivity displayed by intermediate filaments is due not just to their interesting physical properties but also to their interactions with other cytoskeletal elements such as actin and microtubules. Keratin is the predominant intermediate filament expressed in the EVL. It expresses concomitantly with the gastrulation movements of the developing embryo. Our work focuses on understanding the role and dynamics of the keratin cytoskeletal network in modulating the physical aspects of EVL spreading. We demonstrated with the combination of physical characterisation and manipulations of the EVL, utilising a variety of biophysical tools and microscopy, the mechanistic role of keratin in tissue spreading.

Generating novel genetic morphants and mutants, we probe the effect that the loss of the keratin network has on the physiology of the epithelium and the developing embryo. We show that the changing organisation of the keratin network is important for changing EVL physical properties as the stress imposed on the EVL increases during epiboly. By modelling the epithelium, we study how the mechanical heterogeneity in an epithelium can feed back into a mechanical loop to the maturation of the keratin network and hence affect the mechanics of the epithelium. However, unlike what would be predicted by the effect of intermediate filaments in acting as a security belt and increasing the resistance of the epithelium, we observe that loss of keratin leads to a delay in the EVL movement. Using both local aspirations of the YSL and EVL ablations, we demonstrate the mechanistic facilitation of actin mechanosensation in a keratin-dependent manner.

Furthermore, using chemical inhibitors of microtubule polymerisation, we provide insight into the mechanisms underlying the organisation and distribution of keratin. Interestingly, the phenotype observed upon this loss of microtubules shows that keratins interact with the nucleus through microtubular interactions. Together with these diverse observations, we describe the mechanosensory feedback between resilience and that is critical for uniform and robust spreading of the epithelium.

Acknowledgements

To Carl-Philipp Heisenberg and Edouard Hannezo, this work could have only been done under your critical guidance, 'Thank you!'. It was my aim as I started my PhD to perform interdisciplinary work that combines the different scales of biomechanics to understand developmentally critical processes. Your support while letting me explore and discover different directions of the project was an incredibly fulfilling experience. I also appreciate the critical feedback that helped me formulate my untempered raw conceptual intuitions into falsifiable hypotheses and empirically grounded scientific conclusions. I cannot give enough credit to the preceptive discussions we have had *over coffee* over the years, and I look forward to carrying the insights I have gained about breaking down complex interconnected mechanisms into their most parsimonious, explanatory core. I would also like to thank Xavier Trepat and Jiri Friml for being a part of my thesis committee and providing me with invaluable feedback and support through our meetings. These discussions and feedback were critical in shaping and furthering my PhD project.

A special and deeply heartfelt thanks goes to Roland and Preeti, whose mentorship and guidance during the earliest stages of my doctoral journey gave me both the direction and the confidence to explore uncharted territories. Their patience, encouragement, and belief in me shaped the foundation of my research and my growth as a scientist.

I am profoundly grateful to all of my lab members, who have been a constant source of support, inspiration, and friendship throughout my PhD. Shayan, Silvia, Karla, Conny, Daniel, and Feyza—thank you for teaching me not only about the intricacies of science, but also about resilience, collaboration, and life itself. I carry forward many of your lessons both inside and outside the lab. To Diana, Ste, Nikhil, Carolina, Tushna, Viraj, David and other postdocs in the lab, your generosity with your time, your insightful discussions, and your willingness to challenge my thinking made me a sharper, more critical researcher.

This journey would not have been the same without Laura, Xin, Prajwal, and Roksi, with whom I've had the privilege of sharing my own mirrored experiences. Being able to guide and learn from you at the same time has been one of the most rewarding aspects of my PhD, and I am grateful for the camaraderie, laughter, and solidarity we shared along the way. Finally, a very special thanks to Koni and Irene, whose kindness, patience, and constant willingness to lend a hand were indispensable. Whether it was helping me navigate the practicalities of lab life or stepping in when my molecular biology experiments refused to cooperate. My labs have been my training grounds—not just for science, but for finding my voice, learning to express my ideas, and standing before an audience that constantly pushed me to think deeper and clearer. For those I may have missed in these lines—please know that your presence and support have been invaluable. The fact that these words come at the very end of my thesis reflects less on the depth of my gratitude and more on how difficult it is to capture the breadth of my appreciation.

To my dearest friends—Sarath, Patricia, Laura, Divyansh, and Djordje—you carried me through some of the most challenging times, from lockdowns and cyberattacks to moments of personal struggle and health issues. Your unwavering love, encouragement, and laughter gave me strength when I needed it most.

I am deeply grateful to Verena and everyone at the fish facility for their unwavering dedication and care over the years. Their hard work in maintaining the health of the fish and the smooth operation of the facility has been essential to the success of my research. I especially want to thank Gabby, Terza, Mo, Cris, Yann, Nasser, and the other members of the IOF facility for their constant support, technical expertise, and readiness to step in whenever help was needed. Their efforts have provided me with a stable and reliable environment in which to carry out my experiments. I also greatly appreciate their work in maintaining the microscopes, which has ensured that they were always in excellent condition and available when I needed them. Without their skill, attention to detail, and genuine commitment to supporting researchers, much of my work would not have been possible. I look forward to learning more from you in the future.

I would also like to thank my parents and my sister Jivika, who have always been supportive of my dreams and aspirations. Himani who has been a pillar of support and understanding throughout this journey. Her encouragement during the most challenging times, her ability to celebrate the small victories with me, and her steady belief in my abilities have meant more than words can capture. She has been my anchor, reminding me to keep perspective, and my inspiration.

I would also like to thank the LSF and Cryo facility at ISTA, which have been helpful in my experiments. I would also like to acknowledge FWF and JKU Nanocell for providing funding for my PhD research. EMBO and FWF for providing funding for travel grants to attend conferences.

About the Author

Suyash Naik completed an Integrated BS-MS degree at the Indian Institute of Science Education and Research, Pune with completing the requirements for his MS thesis at Laboratory of Molecular Physio-Medicine (Lp2M), CNRS Côte d'Azur University. He joined IST Austria to pursue a Ph.D. co-supervised by Carl-Phillip Heisenberg and Edouard Hannzeo in September 2018. His main research interests focus on understanding developmentally critical processes through the study of biomechanics across different scales. While at ISTA, he has worked on uncovering the mechanics of intermediate filaments during early developmental process such as zebrafish epithelial spreading. His work during his undergraduate studies revolved around the biomechanics of a marine invertebrate organism, Hydra, and has been published in the Journal of Experimental Biology. During his PhD he has contributed to one publication in Developmental Cell and presented his work as a lead author in several international conferences including invited talks at European Intermediate Filaments and Gordon Conference. Alongside his PHD, he is actively involved in outreach and mentorship, being an organiser for the online seminar series Connecting intermediate filaments and has led PhD Balance, a volunteer-run organisation that helps academia provide spaces to grow together and talk about mental health.

List of Collaborators and Publications

Suyash Naik, Yann-Edwin Keta, Kornelija Pranjic-Ferscha, Édouard Hannezo, Silke Henkes, and Carl-Philipp Heisenberg. Keratins coordinate tissue spreading by balancing spreading forces with tissue material properties. *bioRxiv*, 2025

This publication has been incorporated in this thesis as Chapter 3, Section 1.

Table of Contents

Αŀ	tract	vii
Ac	nowledgements	viii
Αŀ	out the Author	x
Lis	of Collaborators and Publications	хi
Ta	le of Contents	xiii
Lis	of Figures	xiv
1	Introduction 1.1 Morphogenesis in multicellularity	1 2 6 13
2	Material and Methods 2.1 Experimental model and Subject Details 2.2 Analysis of keratin expression 2.3 Generation of keratin Crispr Cas9 mutants 2.4 Cloning of expression constructs 2.5 mRNA and morpholino injections 2.6 Sample preparation and fluorescence imaging 2.7 UV ablation/cutting 2.8 Pipette aspiration 2.9 Analysis of actomyosin flows 2.10 EVL cell tracking automation 2.11 Keratin network segmentation 2.12 EVL primary cell culture	17 17 18 19 20 21 21 22 23 23 23 24
3	Results 3.1 Mechanosensitive regulation of keratin organization co-ordinate tissue spreading 3.2 Keratin promotes persistence of AJs and TJs	25 25 63 65
4	Discussion	71

List of Figures

1.1	Cytoskeletal architecture of a cell showing general localization and strucutre of cytoskeletal and junctional elements	4
1.2	Schematic of epithelial cell shapes observed in different epithelial packing	8
1.3	Schematic of EVL spreading during epiboly	11
1.4	Basic organization of intermediate filament structures	14
1.5	Rim and spoke organization of keratin filaments	15
3.1	Keratin network maturation in the EVL.	36
3.2	Pulling forces promote keratin expression within the EVL.	38
3.3	Loss of keratin expression diminishes EVL epiboly movements.	40
3.4	Mechanical force percolation within the EVL is dependent on keratin	.0
J. 1	expression.	41
3.5	Vertex model of EVL spreading in the presence and absence of keratin	
	expression.	43
3.6	Actin flow alignment within the YSL is dependent on keratin expression.	46
3.7	Keratin expression and localization during epiboly	48
3.8	Tension-dependent regulation of keratin expression within the EVL	50
3.9	Effect of dominant negative keratin 18 expression on keratin network	
	formation and EVL epiboly	52
3.10	Effect of dominant negative keratin 18 expression on keratin network	
	formation and EVL epiboly	54
3.11	Micropipette aspiration experimental data and Maxwell model	55
3.12	Time and velocity scales for the EVL micropipette aspiration experiment	
	and parameters of the Maxwell model	57
3.13	Actin-keratin flows within the YSL	59
3.14	Ecadherin expression in the EVL upon keratin knockdown	63
3.15	Occludin-GFP expression in the EVL upon keratin knockdown	65
3.16	Keratin structure upon dissolution of microtubules before epiboly initiation	66
3.17	Keratin structure upon dissolution of microtubules after shield stage	67
3.18	Keratin structure upon dissolution of microtubules after shield stage	68
3.19	Keratin structure upon dissolution of microtubules after shield stage	68
3.20	Keratin structure reorganization leading to clearing around the nucleus upon	
	microtubule dissolution	69

CHAPTER 1

Introduction

1.1 Morphogenesis in multicellularity

The transition from unicellular to multicellular life marks one of the most significant evolutionary milestones, allowing organisms to overcome the constraints of single-cell systems through specialization and division of labour. Evolution into multicellular life allowed for the development of complex mechanisms that led to the diversity of morphology in the Tree of Life. Guided by both mechanical and chemical signaling pathways, multicellular organization gives rise to cellular patterns whose formation and arrangement can be mathematically described, notably demonstrated by Turing's seminal work on morphogenesis [2]. A simple interaction between molecules that could diffuse and lead to a reaction with cells could generate complex patterns. Remarkably, these patterns explain diverse complex patterns that metazoans produce in initially uniform tissues. Although metazoan embryos start off as a roughly uniform embryonic state, generally a spherical, symmetric embryo, during development, they undergo massive transformations to acquire diverse shapes. Understanding the process of morphogenesis relies on understanding not just the signals that transform the developing embryo but also the physical changes that accompany the shape changes. Initiating as a single-cell embryo, successive rounds of cell division generate numerous cells that progressively specialize and acquire distinct functions and spatial identities. These cells collectively self-organize into specific, patterned tissue layers—namely, the ectoderm, mesoderm, and endoderm—which subsequently give rise to diverse organs and structures within metazoans.

Early evidence points to epithelial specialization as a pivotal innovation in the transition from single cellular, multifunctional cells to complex multicellular organisms with a defined division of functional environments [3]. Epithelial tissues play a central role by providing flexible yet stable structural frameworks, which appear prominently and consistently in developmental tissue atlases across a broad spectrum of organismal body plans. Consequently, epithelia serve as key model systems for investigating the fundamental mechanisms that define and control morphological outcomes in metazoans. Epithelial frameworks effectively mediate morphogenesis by coordinating changes through processes such as cell arrangement and tissue shape. The physical forces exerted by cellular mechanics—including differential adhesion, cortical tension, and cytoskeletal contraction—are critical in influencing morphogenesis, thereby shaping the diverse morphological structures observed in multicellular life [4, 5, 6].

1.2 Cellular Mechanics driving morphogenesis

Cellular processes that can exert forces in metazoans driving morphogenesis involve diverse mechanisms that can affect cell number, affinity, contractility, size, shape, and position. A variety of mechanisms exist that allow cells to control and regulate each of these aspects to allow for precise control of morphogenesis.

1.2.1 Growth and Death

Tissue growth during development is primarily controlled through the control of cell growth, cell divisions, and cell death (apoptosis). Biochemical and mechanical signals spatiotemporally control cell divisions in developing embryos. Maternal RNAs and proteins establish initial patterns, which are further refined by the embryo's own signaling networks [7]. These patterns determine the axes and gradients that guide cell behavior. During most developmental paradigms, the single cellular fertilized embryo undergoes several rounds of division before morphogenetic processes take place. Spatio-temporal control of division can lead to diverse shapes in various organisms, such as the bending of bird beaks, the sizes of fly wings, and the scales of crocodiles [8, 9, 10]. While cell divisions are a major driver of tissue growth cell growth also plays an equally important role in tissue growth. Cell growth is usually limited early in development until zygotic expression is initiated, but often precedes cell division later in embryonic development [11]. The molecular basis of the cell size checkpoint is not entirely understood, but some evidence implicates the nuclear-to-cytoplasmic ratio as a critical determinant in this regulation. As the cell grows larger beyond a checkpoint dependent on the cytoplasmic to DNA volume, the cell cycle kinases that regulate cell division can act and initiate mitosis of cells [12]. The growth of cells and an increase in cell volume are primarily controlled through extracellular growth factors. Growth factors, such as epidermal growth factor signalling patterns, are set up by the deposition of factors by the mother or through signal patterns during the organism's development. Cell size is tightly regulated in some tissues, such as the Drosophila wing, and can influence tissue architecture. Growth factor signaling, metabolic nutrients and pathways that metabolize them, control the balance between cell growth and division. Growth factors can stimulate intracellular pathways to stimulate protein and nuclear biosynthesis. The mTOR pathway, as an paradigmatic example, integrates environmental cues to regulate cell growth and division, ensuring that tissues achieve the correct size and shape [10].

In zebrafish, the development of dorso-ventral patterning is dependent on the animal-vegetal patterning set up in the oocyte. The breaking of the germinal vesicle and the balbiani body movement lead to the formation of the animal-vegetal polarity [7]. Polarity and axis specification perform a crucial role in setting up gradients and determining cell divisions in the embryo. Cell divisions are a regulated function of tissues in development that are dependent on numerous signals. In certain tissues, such as the Drosophila imaginal discs, the tissue size is regulated regardless of the cell size by regulation of the number of divisions[13]. Mechanisms that regulate divisions depend on various mechanisms that include but are not limited to a determination of the nuclear vs the cytosplasmic volume of the cell and cell cycle regulating kinases such as cdk. As cell division grows the tissue during development, cell death leads to the opposite effect, reducing the size of the tissue. Various signals can affect the decision between cell division and cell death in a growing tissue, some of which are directly dependent on the state of the tissue. Apoptotic forces can generate forces at the local as well as tissue level due to localized recruitment of the contractile apparatus of the cell, the actomyosin

cytoskeleton [14, 15].

1.2.2 Cytoskeletal mediated regulation of physical properties

The mechanics of a cell controlled largely through a set of proteins constituting the cytoskeleton and adhesive machinery, are crucial in allowing single cells to join together and form a tissue (Fig 1.1). The adhesive complexes of vertebrates are diverse, with different sets of junctions providing distinct functional elements to cells. The junctional diversity of cellular affinity can be through junctional components: Adherens Junctions (AJs), Tight junctions (TJs), and Desmosomes (Fig 1.1). This diversity enables the different junction components to perform specific functions and interact with specific cytoskeletal elements. Tight junctions are a critical barrier protein that maintains a fence which prevents the mixing of membrane proteins between the apical and basolateral membranes, and a gate function which controls the paracellular passage of ions and solutes between cells. Adherens junctions are adhesive protein complexes located at cell-cell contact sites, primarily in epithelial and endothelial tissues. They are essential for maintaining tissue structure, mechanical strength, and cellular organization [16]. The core of the complex is made up of the cadherin complex proteins, such as Ecadherin, and catenin proteins such as β -catenin and α -catenin. Both TJs and AJs associate with the actin cortex and regulate the dynamics of actin. Desmosomes, however, form with specific desmosomal cadherins, forming a dense plaque that interacts specifically with intermediate filaments [17]. They are calcium-sensitive cadherin proteins that are especially prominent in stratified squamous and simple epithelia, where they play a key role in resisting mechanical stress and maintaining tissue cohesion. The tissue-specific expression of desmosomes in tissues under extreme stress, such as cardiac muscles allows cells to regulate their adhesive fucntion depending on their role and function[18]. Differetial adhesion affects how cells interact with each other and can allow for different cells to attach to each other[19, 20]. The adhesion complexes mediate signalling, regulating cell shape, polarity, and mechanical stability in the cells. Armadillo family proteins such as palkoglobin and β -catenin can shuttle between the adhesive junction and the nucleus, acting as transcriptional regulators. Through this regulation, adhesive junctions can dynamically regulate the cellular cytoskeleton such as the actin cortex and the intermediate filament network[21, 22, 23].

The cytoskeleton provides structural support, enables intracellular transport, facilitates cell shape changes and motility, and coordinates force generation and signaling essential for the morphogenesis of tissues. The cellular cytoskeleton consists of a diverse array of filamentous protein networks—primarily actin filaments, microtubules, and intermediate filaments—that collectively support cytoskeletal functions. Each of these cytoskeletal systems has diverse, sometimes interdependent functions: from generating force by the activity of myosin in actomyosin networks, transporting materials across the cell, and helping organize organelles by the microtubules, and maintaining mechanical integrity (or so thought of so far) by intermediate filaments.

Actin forms the quintessential framework of the cell that drives major structural and shape changes in the cell (Fig 1.1). Actin and proteins that bind it form complex networks in the cells, from forming a thin cortex under the plasma membrane to rings that can divide the cells during cytokinesis[24]. The structures that actin networks are organized into are broadly classified as filamentous networks: linear, aligned filaments most often organized by formin and branched networks: Tree-like, branched filaments often organized by proteins such as Arps[25]. Actin filaments additionally exist in two forms in the cells: globular g-actin and filamentous f-actin, which exhibit polarity with a fast-growing "plus" (barbed) end and a

1. Introduction

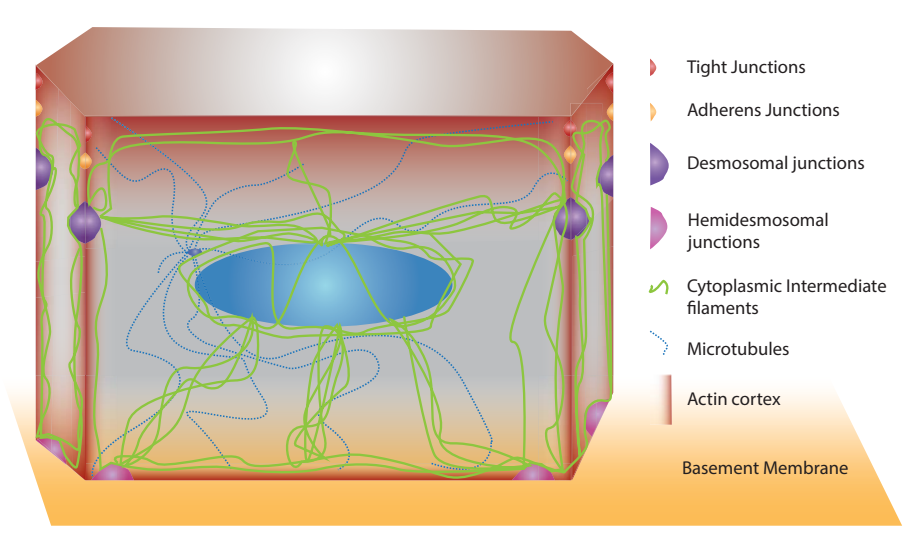


Figure 1.1: Cytoskeletal architecture of a cell showing general localization and strucutre of cytoskeletal and junctional elements

slower-growing "minus" (pointed) end. Actin networks generate forces by both the association of and action of myosin in the network and the addition of monomers at either end of the actin filament [26, 27]. This allows the actin cytoskeleton to alter the mechanics of the cell surface, including surface tension, which affects how cells interact with their environment. Differential adhesion and surface tension can allow for cell neighbour exchanges, leading to large-scale cell rearrangements that are necessary for spreading, and compartmentalization of cell populations during morphogenesis [28]. An essential component of this function is myosin, a motor protein that interacts with actin filaments, using the energy from ATP hydrolysis to generate force and movement. In addition to this active motor activity, myosin binding to actin can also act as a cross-linker that changes the stability of the actin cortex [29, 30]. Microtubules form a network of filaments that are crucial to the transport of intracellular cargo inside the cell and the mechanical stability of the cell (Fig 1.1). Similar to actin, they are polarized filaments with a plus end that grows, which has exposed β -tubulin, and a minus end that is capped by α -tubulin, the two monomers of microtubules. Microtubules are highly dynamic, undergoing cycles of assembly (polymerization) and disassembly (depolymerization), which are regulated by microtubule-associated proteins and cellular signals crucial for cell cycle mechanics [31]. They are a critical part of the motile machinery of single cells such as cilia and flagella and the spindle apparatus. In addition to large-scale modifications, post-translational modifications such as acetylation are also important responses to stress and cellular metabolic changes in the cell [32].

Intermediate filaments(IF) are the most diverse family of cytoskeletal proteins, made up of a wide variety of proteins such as keratins, vimentin, and lamins. Intermediate filaments are made up of fibrous proteins that form apolar homo or heterofilaments. The form networks both inside the cytoplasm and inside the nucleus. No known motors bind to intermediate filaments but there exists a class of proteins that mediate interactions between intermediate filaments and other cytoskeleton elements known as plakin proteins. Similar to microtubules various post translational modifications have been identified for regulating IF assembly, dynamics, and function within the cell. A variety of PTMs such as phosphorylation, glycosylation, sumoylation, acetylation, prenylation, and ubiquitination exist that can influence the mechanical properties, stability, and interactions of IFs [33]. Understanding the functions of intermediate filaments in the cytoskeleton Intermediate filaments and their dynamic roles in development have been

discussed in detail in section 1.4 of this chapter. Together, these cytoskeletal elements can affect the properties of the cell such that the shape and the surface tension, which can affect large-scale tissue mechanics, hence affecting the morphogenetic movements of a tissue. These mechanisms have been extensively described in the developmental mechanics of epithelial tissue, which not only serve as an excellent model to study biomechanics but also as a crucial malleable tissue for morphogenesis.

1.2.3 Cytoskelton facilitated mechanical properties of cells

Cytoskeletal proteins affect mechanical properties of cells that can lead to changes in tissue shape size and position of cells. The forces produced by the cytoskeleton and changing properties of the cellular cortex the cytoskeleton can affect the shape, spindle orientations, ionic balances in cells.

The cytoskeletal architecture controls the cell morphology critically by forming a variety of structures such as rings and the cortex (for actin), asters (for microtubules) and a rim and spoke network (for intermediate filaments). Dynamic changes in their support and organization affect the membrane and its functions associated with proteins such as ion channels and transporters [34, 35]. Under osmotonic shocks that cause changes to cell volumes actin cytoskeleton undergoes dynamic reorganization and polymerization that are usually independent of change in total actin in the cell [36]. Osmotic shock driven polymerization and depolymerization of the actin cytoskeleton is regulated by signalling pathways that activate actin-binding proteins, kinases, phosphatases, and small GTPases [37]. Additionally actin cytoskeleton is also crucial in responding to mechanical cues from the environment via focal adhesions, integrating extracellular forces into intracellular responses. Actin cortex organization is central to shape regulation. The filaments and their interacting proteins, such as Arps and formins, can change the organization between branched and filamentous polymerization. At the cell cortex, these can generate protrusive structures like lamellipodia, filopodia, and microvilli. Actin can also form stress fibers that, with antiparallel actin filaments and myosin II motors, generate contractile tension.

Microtubules, as well, are essential for maintaining and dynamically regulating cell shape. They indirectly influence cell volume by organizing the cell's interior, supporting membrane trafficking, and integrating mechanical signals. Modulating the mechanical properties of the cell cortex and cytoplasm is a critical driver of shape change, enabling cells to adapt to mechanical cues, migrate, divide, and differentiate. Microtubules are critical in determining the polarity of the cells. They can also interact with the actin organisation by delivering of signaling proteins and mechanical feedback. These mechanisms act in concert to allow cells to exert forces on their environments. Active force production as well as the regulation of mechanical properties is critical for the movement of cells. Adhesion protein regulation is generally precisely spatiotemporally regulated as cells move, under direct mechanical feedback from the cytoskeleton.

When cells join together to form tissues, these mechanical components and the interactions are critical in mediating diverse mechanical functions required for morphogenesis.

1.3 Epithelial morphogenesis in metazoans

As membranes separate the exterior to the interior of the single cells, epithelia perform a similar function in metazoans. Epithelial tissues possess specialized features that make them uniquely suited for compartmentalization. These attributes emerge as early as the diploblastic metazoans in evolutionary history [38]. However, ongoing debate within the field concerns to whether the mono-layered tissues in Cnidarians and Porifera, such as jellyfish and hydra, exhibit all the hallmarks of true epithelia[39, 3]. This debate about classifying tissues into different classes of organisms helps clarify the simple principles that underlie the essential function and physical organization of epithelial tissues.

Adhesion proteins mediate cellular connections, facilitate signaling, serve as organizational hubs for cytoskeletal elements, and contribute to barrier functions critical for maintaining tissue integrity. The role of barrier functions of epithelia in metazoans can not be understated in its importance to morphogenesis. This intricate interplay between the cytoskeleton and adhesion proteins not only ensures the structural and functional stability of tissues but also enables the dynamic remodelling required for morphogenesis, paving the way for the development of complex multicellular organisms.

1.3.1 Features of epithelia

A crucial feature that most succinctly defines epithelia is their ability to define and differentiate compartments that make multicellular organisms. This ability allows multicellular organisms to differentiate internal environments from the exterior or between different compartments of the organism. In this section, we explore the features and components of the epithelial architecture that are essential for this function in metazoans.

In epithelial tissues, features that mediate critical functions are modulated through mechanisms, such as apicobasal cell polarity, adhesive junctions between their apical and lateral domains, and a basement membrane [40]. Precise cytoskeletal spatiotemporal organization allows for the specification and maintenance of these features defining epithelia [41, 42]. This precise spatiotemporal organization is mediated through conserved principles throughout the tree of life, primarily those that involve the polarization of apical and basal surfaces[43].

Apicobasal polarity is a fundamental feature of epithelial cells, enabling them to organize into cohesive sheets that perform specialized functions. This polarity is characterized by the distinct segregation of cellular components into apical and basolateral domains. The specification of apicobasal polarity is necessary for positioning and maintenance of the adhesive contacts between epithelial cells. Additionally, the organization of distinct basal and apical domains allows for polarized exocytosis required for various functions that require the segregation of molecules such as ion channels, signaling factors, and extracellular membrane components[44]. The apical domain is most often present at the contactless exterior surface (in the case of non-luminal epithelia) or on the hollow lumen (in the case of tubular epithelia). This surface is characterized by the presence of apical protein complexes and lipids such as PI(4,5)P2. The basal surface, on the other hand, is specifically identified by the presence of so-called basal markers such as SCRB complex proteins, the kinase PAR1, and the lipid PI(3,4,5)P3 [45, 46]. The lateral contact between cells is, interestingly, the surface that demarcates the boundary and interaction between these mutually antagonistic surfaces. The lateral surfaces of epithelial cells host the junction component, SJs in invertebrates and TJs & AJs in vertebrate systems that are critical in isolating the specific components that define these domains.

This segregation is mediated by so-called polarity proteins such as par proteins, crumbs complex (Crb) and aPKC/ Lethal giant larvae (LGL) complexes [46]. These complexes interact and organize the cytoskeleton depending on the domains [47]. The structural organization of the apical domain and the cytoskeleton surrounding it is crucial in the function of epithelial cells. Apical polarization is responsible for the organization of the lateral and apical cell-cell junctions[47, 48].

Although the way apicobasal polarity is mediated in vertebrates vs invertebrates is similar, the organization of adhesion complexes is quite different. In invertebrates such as the model organism Drosophila, the apical cell-cell junction is mediated by adherens junctions. In vertebrates, the apical contact is mediated by Tight junctions (TJs), while the zona adherens, right below these, mediate the adhesive contact. Tight junctions are crucial in maintaining the barrier between cells, and, together with adherence, junctions play an organizer role in mediating connections between the actin and microtubular cytoskeleton. In addition, in vertebrates, macula adherens can be found below the zona adherens, forming the desmosomal contacts between cells. Unlike TJs, these adhesions are known to be major interaction sites for intermediate filaments, important for their subcellular organization [49]. These adhesion proteins are also crucial in mediating binding to basement membranes, which are extracellular composites of several large glycoproteins that provide structural support and functional inputs to cellular functions [50].

Basement membranes are secreted in a diverse tissue-specific fashion, dynamically regulated based on the physiological state of the tissue. Basement membranes are critical for functional tissues, providing a dynamic structural support to most tissues. In mammals such as mice, laminin-111 is among the first ECM proteins expressed, with its three chains (α 1, β 1, and γ 1) detectable as early as the two-cell stage [51]. However, these membranes are usually absent or play a less prominent role in early morphogenesis; hence, epithelial barriers and their mechanics are critical in organizing the mechanics.

1.3.2 Mechanical organization of epithelia

Epithelial tissues exhibit a remarkable diversity in cellular morphology, a characteristic that underpins their varied physiological roles across organ systems. The mechanical properties are critical in regulating the shapes of epithelial tissues [52, 53, 54]. Based on the shape of constituent cells and the number of layers they form, epithelia are broadly categorized into several structural types: squamous, cuboidal, columnar, pseudostratified, and stratified epithelia (Fig 1.2). These structural differences are not merely morphological but are tightly correlated with specific functional mechanical adaptations, ranging from passive exchange of substances to active secretion, absorption, and protection.

Simple Squamous Epithelium

This type consists of a single layer of flattened, thin cells. Due to their minimal thickness, squamous epithelia are highly permeable and are thus ideally suited for facilitating passive processes such as diffusion and filtration. They line surfaces where rapid exchange is essential, such as the alveoli of the lungs, glomeruli of the kidneys, internal linings of organs and the inner walls of blood and lymphatic vessels (endothelium). Their structural simplicity is critical for the trade-off between mechanical barrier and efficient trans-barrier transport.

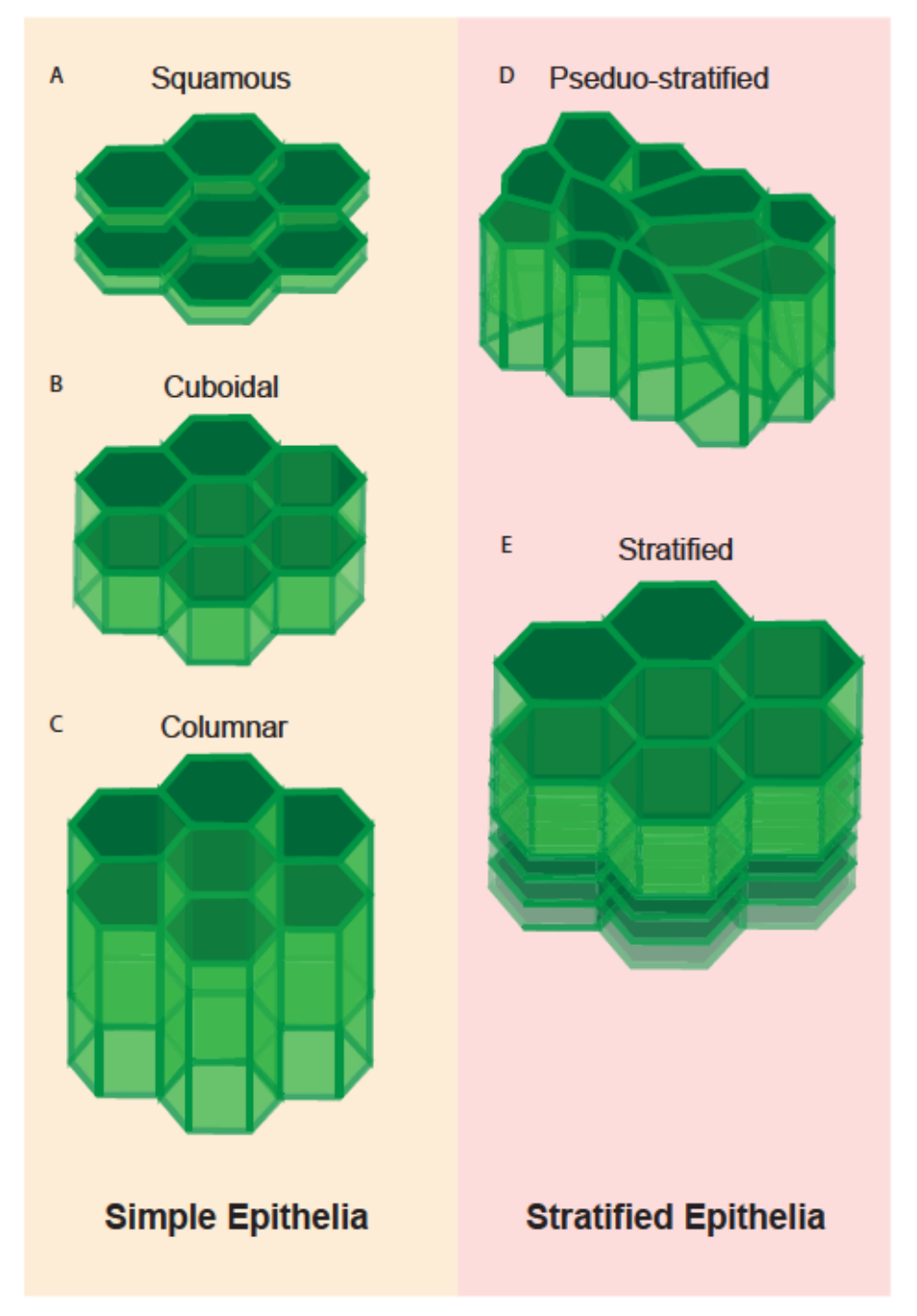


Figure 1.2: Schematic of epithelial cell shapes observed in different epithelial packing A Schematic representing squamous epithelia (left top) which are formed by a barrier of thin flat cells B Schematic representing cuboidal epithelial tissue (left middle), which consists of cube-like cells that are equidimensional. C Schematic representing columnar epithelial tissues (left bottom), which are made up of columnar cells that are longer than their horizontal surfaces. D Schematic representing pseudo-stratified epithelial tissues that are made up of epithelial cells that like simple epithelia all share a basal layer but unequal occupation in the two layers giving the impression of being divided in multiple layers E Schematic representing stratified epithelial tissues that are made up of multiple layers of epithelial cells, often with each layer made up of different types of epithelial packing.

Simple Cuboidal Epithelium

Comprised of cube-shaped cells with roughly equal dimensions in all planes, this epithelium typically performs absorptive and secretory functions. The relatively larger cytoplasmic volume compared to squamous cells allows for the accommodation of organelles involved in active transport and metabolic processes. This epithelial type commonly lines glandular ducts, the surface of ovaries, and renal tubules, where it contributes to the controlled exchange and modification of substances.

Simple Columnar Epithelium

Columnar epithelia are composed of tall, rectangular cells arranged in a single layer. These cells frequently exhibit apical specializations such as microvilli (forming a brush border to enhance surface area for absorption) or motile cilia (which aid in the propulsion of mucus and other substances). This type is predominant in the lining of the gastrointestinal tract, from the stomach to the rectum, where it mediates the absorption of nutrients and the secretion of digestive enzymes and mucus. The vertical elongation of the cells provides spatial separation of functional domains—apical, lateral, and basal—enabling finely tuned vectorial transport.

Pseudostratified Epithelium

Despite appearing multilayered due to the varying positions of nuclei within the cells, all cells in pseudostratified epithelium contact the basement membrane. This illusion of stratification often accompanies functional complexity. Most notably found in the respiratory tract (pseudostratified columnar ciliated epithelium with goblet cells), it combines mucus production and ciliary movement to protect against inhaled pathogens and particulates. The integrated functions of secretion and clearance are tightly coordinated through this structural arrangement.

Stratified Epithelium

Unlike simple epithelia, stratified epithelia consist of multiple cell layers, offering robust mechanical protection. The most common subtype, stratified squamous epithelium, is adapted to resist physical and chemical stress. In areas exposed to abrasion—such as the skin, oral cavity, esophagus, and vagina—it may be keratinized to form a tough, waterproof barrier. Non-keratinized variants, retaining surface nuclei, are found in moist internal linings. Other forms, such as stratified cuboidal or stratified columnar epithelia, are less common and typically found in glandular ducts, contributing to both protection and limited secretion.

In summary, the classification of epithelial tissues by cellular shape and layering reflects a precise tuning of form to function. The structural specialization of each epithelial packing permits a wide range of physiological tasks, from passive exchange to protective insulation and complex secretory dynamics. This morphological and functional diversity is a hallmark of epithelial adaptability across metazoan life.

1.3.3 Morphogenetic movements of epithelia

Epithelial tissues play a crucial role in mediating morphogenetic movements by shaping the organism through co-ordinate cellular behaviors and mechanical forces. Epithelial tissues are essential mechanical elements in developing organisms, serving as crucial barrier structures defending against external environmental challenges while orchestrating intricate cellular interactions essential for embryonic growth and organogenesis [55]. Developmental morphogenesis

1. Introduction

of an organism involves a magnitude of challenges as the embryo takes shape[56, 57, 58]. This change of form and function is influenced by physical and chemical factors, including the environment and the organism's interactions. Embryonic epithelia are important during this morphogenesis due to their function as a barrier and regulatory tissue to maintain control over these factors[55, 47].

Epithelial cohesion balances cell adhesion and contractile tension, allowing cells to defrom and retain their integrity depending on contextual demands. A critical feature underlying the plasticity and diversity of epithelial function is the tissue fluidity arising from local active forces acting at cell junctions. Epithelial tissue responds in a viscoelastic manner to forces applied, behaving like elastic solids under short-term stress but viscously flowing under longer-term deformations [59]. Under sustained stress, epithelial tissues can undergo permanent topological changes through cell rearrangements and junctional remodeling. Collectively these behaviours organize multiscale mechanical frameworks in which tissue-scale outcomes are attained by local cellular activities guided by mechanical and biochemical signals.

During morphogenesis, epithelial tissues perform complex rearrangements and shape changes of cells within sheets, including movements such as invagination, ingression, involution, intercalation, and Collective migration. These morphogenetic movements lead to changes in the shapes of epithelial tissues that can organize into varied shapes required for morphogenesis. Invagination is mediated by coordinated movement of the cells such that the apical surfaces move to form tubular inpockets. Apical constriction of the cells, Basal relaxation and wedging, vertical telescoping are some of the mechanisms with which the epithelial cells bend to invaginate. Regulation of cell mechanics and the movement of cells are critical for these mechanisms that lead to invagination [60, 61]. Similar to invagination of the entire epithelial sheet, individual cells also can ingress into the sheet a process that is critical for straified epithelia formation as well as occurs during epithelial to mesenchymal transition. Apical cell constriction is important for this as well, but unlike in the case of involution, ingression also requires the cells to lose contact with their neighbours and move inwards [62]. Intercalation of cells is a critical mechanism by which cells can exchange neighbours while maintaining the apico-basal architecture and barrier integrity. Dynamic regulation of actomyosin density at the junctions is critical in mediating this process [63, 64, 65].

Collective migration in epithelial tissues is crucial for allowing morphogenetic changes while maintaining tissue integrity [66, 67]. Upon injury or a migratory signal, cells coordinate their movements over multiple cell scales by mechanosensitive signalling by the cells at the edge, called leader cells. Polarization and intracellular pulling forces from the leading cells lead to mechanosensitive changes in the follower cells [66]. This effect is observable through multiple cell distances over the epithelia. Actomyosin contractility plays a critical role in such coordinated movement. During development, actomyosin networks across cells can organize in tandem to generate forces across length scales. For example, in the Drosophila embryo, planar-polarized actomyosin ribbons function as "denoising" mechanisms, ensuring precise formation of tissue folds and boundaries [68].

Epithelial morphogenesis in zebrafish

Teleost embryos serve as an exceptional model system for elucidating morphogenesis during early vertebrate development [69, 70, 58]. Unlike mammalian embryos, fish embryos must address the distinctive challenge posed by engulfing and utilizing a substantial anuclear yolk mass[71]. While notable developmental variations exist between the two prominent teleost model organisms, Danio rerio (zebrafish) and Oryzias latipes (medaka), fundamental cellular

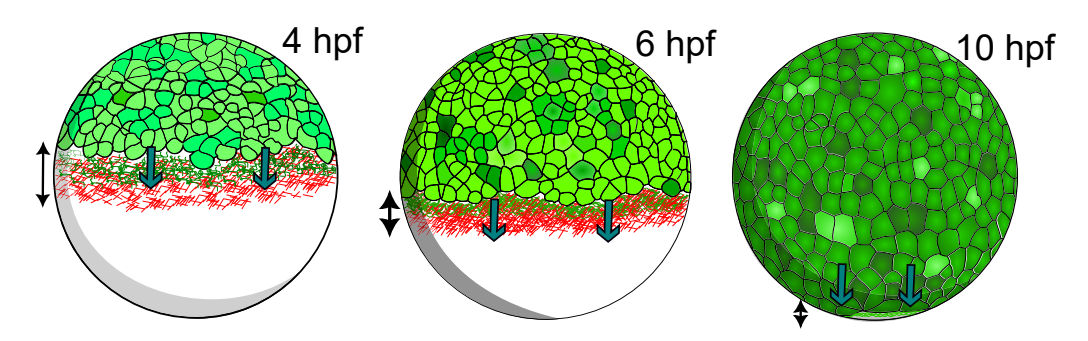


Figure 1.3: Schematic of EVL spreading during epiboly Schematic represents the spreading of the EVL and YSL starting at 4 hpf (left), to shield stage at 6hpf (center) and to the end of blastopore closure 10 hpf (right).

movements and developmental challenges remain remarkably conserved [72]. Embryogenesis in teleosts initiates with a polarized distribution of cytoplasm concentrated at the animal pole, covering approximately one-third of the embryonic surface.

As development proceeds, the embryo undergoes meroblastic cleavages where the cells divide on top of the yolk. The polarity that drives the segregation of the cytoplasm to the animal pole begins within the oocyte maturation cycle when the germinal vesicle (GV) breaks down. The breakdown of GV is a complex process that ends up breaking symmetry in the oocyte [73]. This process also leads to an increase in the egg volume and maturation of the egg. The establishment of animal polarity and maturation of the balbiani body that follows GV breakdown is directly associated with the micropyle precursor cell (MPC) formation by mutual competition. This cell is interesting as it forms the micropyle in the mature egg, which is essential for fertilization. Interestingly, this is perhaps the first process in which keratins are expressed and play a mechanical function during zebrafish development.

Krt18 serves as an early marker for MPC differentiation, indicating that intermediate filaments are involved in the cellular differentiation process[74]. This differentiation leads to rapid growth and distinctive shape of the MPC compared to the surrounding granulosa cells. Buc mutants interestingly show multiple MPC formations that form functional micropyles, suggesting a role of animal polarity in restricting this function specification[75]. Upon fertilization of the embryo, cytoplasm actively streams towards the animal pole, coinciding with karyokinesis [76, 77]. This leads to increase in the cellular volume, which undergoes meroblastic cleavages that divide the cell from the animal pole to the yolk.

Unlike in mammalian or other embryos that cleave holoblastically the cytokinetic furrow doesn't extend to the vegetal pole but rather divides the cells over the yolk surface. Species such as monotremes, avians, reptiles, and fish that contain telolecithal eggs show meroblastic cleavages. This creates an interesting challenge for the organism in terms of further development as the yolk serves as a major source of nutrition and signalling[78]. While embryos where yolk is completely or partially removed retain certain genetically encoded patterns, the loss of certain cell type determinants clearly exemplifies the necessity of the signalling components that are provided by the yolk [79].

The cell cycles as the embryo develops are initially synchronized but as the divisions develop the durations of the S-phases of cell cycles extend [80]. This is most obviously seen at division rounds 10 and further, where the cell cycles are almost asynchronous, but starting from round 4, the variance in the timing between cells continuously increases. This variance is driven through the geometry of the embryo that is surrounded by the yolk membrane and the animal

1. Introduction

plasma membrane.

As the cells continue to divide, the cells on the surface divide preferentially according to the shape, such that the cells reduce their height-to-radius ratio [81]. This leads to the formation of a thin layer of squamous epithelial cells, which later form the enveloping layer (EVL). Adhesion and proximity to the neighbouring cells is critical for EVL specification [82]. At the same time, zygotic gene activation occurs where genes specific to epithelial specification express [83]. The marginal cells surrounding the yolk undergo fusion to form a syncytium as the cells continue to divide to form a syncytial layer of tissue on the margin of the embryo called the yolk syncytial layer (YSL). Genes encoding various ion channels and epithelial-specific proteins are expressed in the EVL and YSL, which further drive their specification. FoxH1, Irf1 and Oct4 are critical in the specific expression of the EVL fate and regulate the mechanics of the EVL cells [84, 85, 86].

As gastrulation begins, the YSL serves as a driving motor driven by the retrograde flow of actin [71]. This flow of actin creats a pull towards the yolk through friction in a direction opposing the direction of the flow (Fig 1.3). Intermediate filaments, especially epithelial keratins, are expressed in these tissues as epiboly progresses, but their roles and interactions during development are so far unknown.

1.4 Intermediate filaments in epithelial development

The cytoskeleton of a cell plays a crucial role in its mechanical functions, through intracellular networks made up of actin, microtubules, and intermediate filaments. These networks are crucially mediated through interactions of specific domains in the monomeric architecture of the filaments. Direct covalent and hydrophobic interactions, weak interactions such as phase separation of the filaments, drive the formation of these networks and provide mechanisms for regulating the function of these networks. As discussed above in section 1.2.2, these cytoskeletal systems perform a myriad of functions to enable cellular movements that drive the morphogenesis of organisms. Among their functions in development, much is known about the role of actin, microtubules, and their interaction proteins; however, the regulation and functions of intermediate filaments are yet understudied.

Intermediate filaments form a complex class of cytoskeletal networks that perform crucial roles in various developmentally critical functions in tissues. The differences between intermediate filaments and other cytoskeletal networks are evident at the structural level. The expression of intermediate filaments is highly variable and cell-type specific, unlike actin and microtubules, which are expressed ubiquitously in cells. Actin microfilaments and microtubules are polar filaments with motor proteins that attach to them and provide mechanical forces through these interactions. The polarity of these cytoskeletal filaments is crucial to directional movement of the motor proteins, such as myosin, which moves toward the +end of actin filaments, and kinesin, the +end motor on microtubules, while dynein moves toward the -ve end of microtubules. Intermediate filaments, on the other hand, are the only cytoskeletal networks that are apolar and show no direct motor protein associations. The critical reason intermediate filaments are apolar is due to the structural organization of these filaments, which aligns them without a precise polar orientation within the filament. However, various interacting proteins have been identified that can mediate cross-talk and interactions with other cytoskeletal networks.

Intermediate filaments are of two major types: nuclear intermediate filaments and cytoplasmic intermediate filaments. Both share a similar structure, which is critical for their functions in organisms' developmental programs as mechanical supports of the cells. This classification is dependent on their physical location in the cell, with nuclear intermediate filaments being organized into the nuclear lamina at the nuclear envelope, and cytoplasmic IFs organized from the external nuclear lamina to the cell periphery. However, given their functional and structural diversity, various structural modifications exist in IFs that change distinct domains of the protein. Understanding their structural differences helps understand the organizational differences of these proteins.

1.4.1 Structural organization of intermediate filaments

Intermediate filaments are broadly classified into six types based on their structural and functional distinctions: Type I and Type II form the epithelial cytoskeletal filaments, keratins; Type III is reserved for homo-polymerizing filaments such as desmin, Vimentin and GFAP; Type IV are neurofilaments; Type V are the nuclear localizing lamins and Type VI are the special lens IFs phakinin and Filensin (Fig 1.4). At the molecular level, all intermediate filament proteins are composed of three distinct domains: a flexible N-terminal head, a central α -helical rod domain responsible for coiled-coil dimerization, and a variably sized C-terminal tail[87]. These domains represent the minimal structural modules required for filament assembly and are conserved across all IF types, despite substantial sequence variation and functional specialization[88].

1. Introduction

While the rod domain has been characterized structurally in detail, the head and tail domains, although structurally elusive, play critical roles in filament dynamics, cellular localization, and regulation through post-translational modifications and phase separation. In this section, we dive into the structural organization of intermediate filaments from their protein structure to the organization in cells.

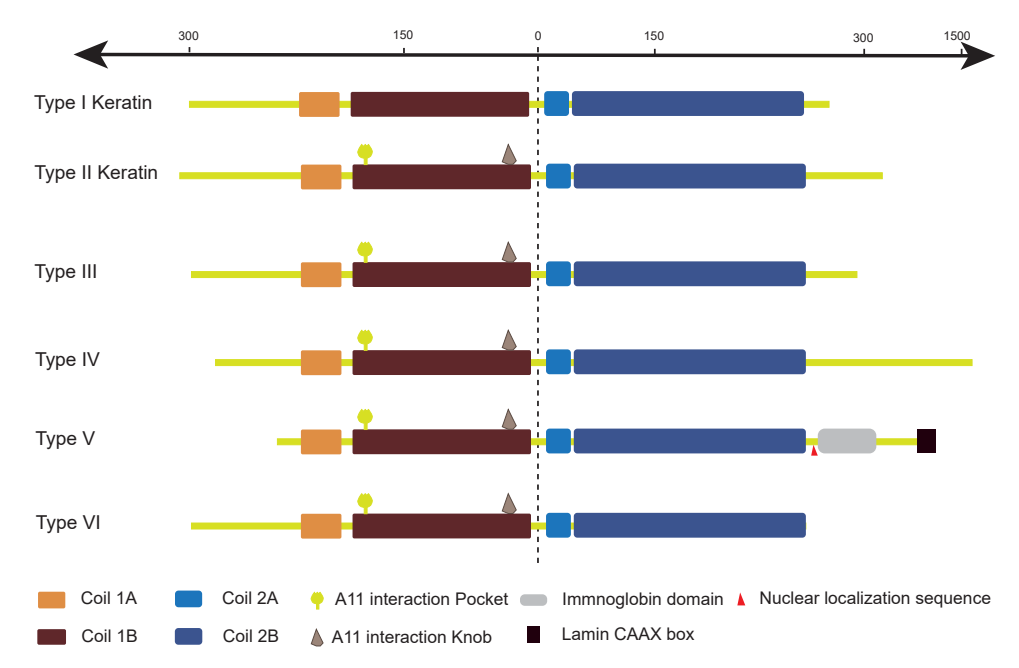


Figure 1.4: Basic organization of intermediate filament structures

Schematic representing the structural organization of intermediate filament proteins according to their family type. The major coil domains are represented as rectangular boxes; linkers, head and tail domains are shown as green lines connecting these boxes. The relative scale of the average of the amino acid sequences of these proteins is maintained to mark differences between structural organization of different filament types. The schematic is based off structures of IF detailed in [89].

The rod domain is critical in the dimerization of intermediate filaments, the first step of ULF organization. The rod domain is divided into four helical domains: 1A, 1B, 2A, 2B, which are separated by linker domains: L1, L12, L2. The structural assembly of all intermediate filaments is similar, except that keratin form via obligate heteropolymers of Type I and Type II filaments, whereas other types of IFs form homopolymers of the same filament. These linkers, once thought to be flexible hinges, have now been shown to adopt helical structures with significant bendability, contributing to the filament's mechanical resilience and adaptability[89]. A type I and Type II filament / homofilament pair to form a parallel heterodimer aligning head to head with each other. 2 heterodimers align antiparallel to each other to form a tetramer. The basic filament is formed by eight tetramers that associate laterally to form a unit length filament (ULF). A conserved symmetric anchoring knob -hydrophobic pocket mechanism at the 1B domain of the rod domain allows the interaction of the heteromeric filament. But the coils 1B and 2B are also involved in higher order IF assemblies above the dimeric forms. Depending on the orientations and exact domain binding different modes of alignment for different intermediate filaments have been observed. 1B and 2B are important in these alignments with alignment of 1B domains giving A11 alignment of the filaments and 2B domain alignment leading to A22 alignment [89]. When 1B domains are aligned with 2B A12 alignment is achieved. A12, A11 and A22 alignments are In different IF types

the pathways and mechanisms of elongation can be unique such as the compaction seen in vimentin filaments due to their hydrophobic residues. Lamins show head-to-tail polymerization of dimers before lateral association is seen. However it is clear that the interactions of the rod domains is essential for dimer formation. The head and tail unstructured domains, however, are critical for further network formation as headless filaments do not progress further than dimers [90]. The most evident structural difference between the nuclear and cytoplasmic intermediate filaments is the longer 1B rod and the presence of a nuclear localization signal (NLS) near an immunoglobulin motif at the C-terminal of the nuclear protein.

The vast structural diversity of intermediate filaments allows for functional and tissue-specific distribution, reflective of their specialized roles in cellular architecture and function [91]. Keratins, both type I and type II are epithelial-specific and are often used as clear markers for the epithelial fate. Heterodimeric acidic/basic keratin pairs assemble into filamentous networks bound to desmosomes and hemidesmosomes, thereby reinforcing epithelial resilience under mechanical stress and transmitting forces inside the cells. Type III IF proteins include desmin, GFAP, vimentin, and peripherin. Desmin localizes to Z-disks, intercalated discs, and sarcolemmal membranes in striated and smooth muscle, integrating myofibrils and organelles. GFAP is confined to astrocytes and ependymal cells in the central nervous system, with additional expression in specific non-neural cells such as renal glomeruli and Leydig cells. Vimentin, on the other hand, is a hallmark of mesenchymal cell fates, forming dynamic cytoskeletal scaffolds in fibroblasts, endothelial cells, leukocytes, and during epithelial-mesenchymal transition, anchoring organelles and contributing to cellular elasticity. Neurofilaments form a diverse class of type IV filaments characteristic of neurons, enriched in axons to support long-range transport. Nuclear lamins type V filaments are present in all somatic cells, forming the nuclear lamina beneath the inner nuclear membrane and contributing to nuclear structure and genome organization. They are supposed to be the most ancestral intermediate filament from which most intermediate filaments have evolved [92, 93]. Given their critical importance in epithelial tissues, including early developmental epithelia, and similarities with other cytoskeletal intermediate filaments, we discuss the currently proposed model of cytoplasmic intermediate filaments organisation called the rim and spoke model due to their structural organization in the cell (Fig 1.5) [88, 94].

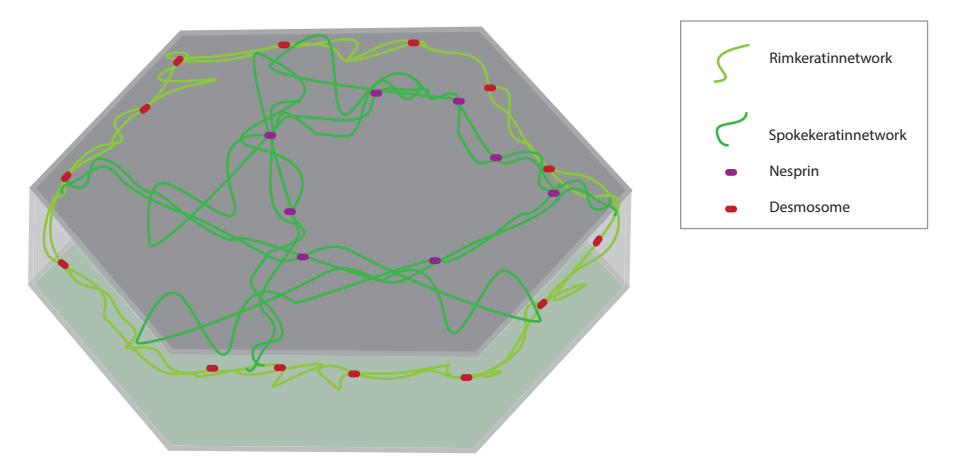


Figure 1.5: Rim and spoke organization of keratin filaments
Schematic representing the rim and spoke architecture of keratin intermediate filaments in a epithelial cell

1.4.2 The Rim

The Rim intermediate filament network is observed as a ring of intermediate filaments around the junction. Intermediate filaments on the junctional rim are associated with the junctions at desmosomes[94, 95]. The desmosomal cadherins, desmogleins and desmocollins, associate with intermediate filaments via the plakin family protein desmoplakin. The desmosome can be divided into three zones: the extracellular core (desmoglea), where the cadherin extracellular domains interact, the outer-dense plaque, where the desmosomal cadherins interact with plakoglobin and the N-terminal domain of desmoplakins, and the inner dense plaque, where the desmoplakins interact with intermediate filaments[96, 17]. Early attachment of intermediate filaments to the junction occurs at distinct points colocalized with desmosomal cadherins. At these focal points, keratin filaments can nucleate and grow further to elongate into a longer filament, hence establishing a ring-like network. The keratin-mediated connection is also proposed to function in positioning and tensioning the desmosomal proteins[47].

The connection between the desmosomes and keratin is mediated by desmoplakin. Loss of desmoplakin in different epithelial tissues has different effects on the accumulation of keratin and desmosomes depending on the epithelial tissue [97, 98, 99]. In the intestine, knockout of desmoplakin leads to a mislocalization of adhesion proteins but not of the keratin intermediate filaments [97]. However, in stratified epithelia from conditional mouse knockouts, desmoplakin knockouts affected keratin organization, especially in the suprabasal layers of the epithelia[99]. Interestingly, in the desmoplakin knockout epithelia, actin filaments showed an increased intracellular organization and decreased cell periphery accumulation, showing a close interaction of the two different cytoskeletal networks. This is in part mediated by the mechanosensitive regulation of these networks through an intricate connection of the rim with the cytoplasmic network of intermediate filaments.

1.4.3 The Spoke

The spoke network is formed as a combination of the nuclear and cytoplasmic network of intermediate filaments. The spoke-like filaments extend from the periphery of the cell to the nucleus, which in some cells look similar to spokes[100]. Additionally, their interactions with the nuclear lamina proteins, such as nesprins, lead to a network of keratins that cover the nucleus, called as the nuclear cage [101]. Loss of keratin or the interaction leads to a reorganization of nuclear shape, hence proving critical to nuclear mechanics as well as cellular mechanics. Interestingly, it has also been observed that the network can reorganize in certain cells under stress, such that the cytoplasmic network can transition from a disorganized cytoplasmic network into clear spokes that extend to the nucleus [102, 103]. These dynamic changes are usually observed under extreme stress, where strains of over 150% are experienced in the cells [104].

These interactions are facilitated by the interaction of the filaments with plakin proteins and other cytoskeletal proteins. Plakins are a diverse set of proteins that include plectin, BPAG1, desmoplakin, envoplakin, periplakin, and epiplakin. They are large modular cytolinker proteins that physically connect keratin IFs with other cytoskeletal networks (actin, microtubules), adhesion sites, and the nuclear surface [105]. Mechanosensitive interactions of plakins that mediate force mitigation through the keratin intermediate filament network are understudied in developing systems. However, numerous examples point to precise spatiotemporal regulation of the spoke intermediate filament network.

Material and Methods

2.1 Experimental model and Subject Details

For the experiments mentioned in this thesis, zebrafish (Danio Rerio) were maintained in the aquatics facility at ISTA with the help of the aquatics facility. Fish were maintained according to local animal ethical regulations regarding space and animal ethics (Breeding 2023-0.288.351). All experiments were done on embryos collected from parents that were set up together the evening before the specified developmental stages. All stages studied in this thesis were within the first 36 hours of development. The embryos were collected in the morning, sieved through a thin mesh and kept in an incubator at $28^{\circ}C$. Staging was done both according to time from fertilization as well as known developmental stages according to the developmental atlas [58, 106].

Transgenic lines used in this thesis:

- wild-type TL
- wild-type AB
- Tg(krt18:Krt18GFP)
- Tg(actb2:Utrophin-mcherry)
- Tg(actb2:Myl-mcherry)
- Tg(plakoglobin-GFP)
- Tg(actb2:Lifeact- GFP)
- Tg(acbt2:Utrophin-mcherry, krt18:Krt18GFP)

2.2 Analysis of keratin expression

Pre-existing single-cell(sc) RNA datasets were analysed using URD dataset portal in the Broad Single-Cell Portal. The expression level and localization were confirmed using qPCR and Fluorescence in situ hybridization (FISH). For qPCR, total RNA was extracted from 20 embryos at 1k (3.3 hpf), sphere (4 hpf), shield (6 hpf) and bud stage (9.5 hpf) using 750 μ l Trizol by

dechorionating the embryos followed by homogenizing by vortexing for 60-90 secs. The lyzed trizol samples were stored at -70 overnight so that all stages could be processed together. The RNA was isolated by adding 250 μ l of methanol and mixing thoroughly. The suspension was incubated at RT for 5 mins before centrifugation at 15000 g for 30 mins at 4°C such that phase separation into 3 phases was seen. The aqueous phase was isolated by tilting the tube while carefully avoiding the interphase and organic phase and transferring it to another tube. The RNA was precipitated using 500 µl isopropanol and incubation at RT for 10 mins. The suspension was centrifuged at $15,000 \times g$ for 10 minutes at 4°C to pellet the RNA. The supernatant was discarded and the pellet was washed twice with 70 % ethanol. The pellet was resuspended in 20 μ l Rnase free water. Any contaminations of genomic DNA were cleared using DNA-free™ DNA Removal Kit (Thermo Fisher Scientific) according to the manufacturers protocol. cDNA libraries were then made from 3 μg of RNA from each sample using Luna RT Supermix kit. cDNA amplification was tested using serial dilution from 1:1-1:10000 to generate standard curves and amplification efficiency was tested by generating a standard curves. Based on 90%-110% efficiency 1:100 dilution was used for amplification by gPCR. For normalisation, the elongation factor 1 α (EF1 α), as a housekeeping gene, was amplified but the expression efficiency for EF1 α was not stable during different stages of development.

The following primers for keratin(krt)4, 5, 8 and 18 were used:

krt4 forward: GCAGTCTATGAGGCTGAACTCC
krt4 reverse: CTCAGCCTTTGTTGAGCGGA
krt5 forward: ACTTCCTTCAAAACCTTCACC
krt5 reverse: CCAGATCCTGCTCCAAAAC
krt8 forward: CCACCTACAGCAAGAAAACC
krt8 reverse: AGAGATGAAGCCACTACCAC
krt18 forward: GTAACATCCAGCATCAGACG
krt18 reverse: CACAACCTTTCCATCCACC

The qPCR runs were performed on the Bio-Rad C1000 Thermal Cycler in triplicates using the Luna qPCR master mix.

2.3 Generation of keratin Crispr Cas9 mutants

To generate F0 crispant zebrafish embryos with targeted knockouts of keratin4 (krt4) and keratin8 (krt8), we employed a CRISPR-Cas9 approach utilizing the Alt-R CRISPR-Cas9 system from Integrated DNA Technologies (IDT). For each gene, three distinct guide RNAs (gRNAs) were designed to target separate exons, ensuring comprehensive disruption of the gene's coding sequence. The specific gRNA sequences used were as follows:

- 1. Keratin 4 (krt4)
 - 5'-[sequence]-3'
 - 5'-[sequence]-3'
 - 5'-[sequence]-3'
- 2. Keratin 8 (krt8)
 - 5'-[sequence]-3'
 - 5'-[sequence]-3'
 - 5'-[sequence]-3'

Each gRNA was prepared by annealing 1 μ L of crRNA (200 μ M) with 1 μ L of tracrRNA (200 μ M) in 1.5 μ L of IDT's Duplex Buffer. The mixture was heated to $95^{\circ}C$ for 5 minutes and

then cooled on ice to facilitate annealing. Subsequently, ribonucleoprotein (RNP) complexes were formed by combining the annealed gRNAs with Cas9 protein in equimolar ratios (1:1) and incubating at $37^{\circ}C$ for 15 minutes. For each gene, the injection mixture contained a total of 28.5 fmol (1000 pg) of the gRNA trio (approximately 9.5 fmol per gRNA) and 28.5 fmol (4700 pg) of Cas9 protein.

One-cell stage zebrafish embryos were microinjected with approximately 1–2 nL of the respective RNP complexes targeting krt4 or krt8. Post-injection, embryos were maintained at $28.5^{\circ}C$, and daily assessments were conducted to monitor survival rates and document phenotypic manifestations indicative of successful gene disruption. This methodological approach was adapted from established protocols for CRISPR-Cas9-mediated gene editing in zebrafish.

2.4 Cloning of expression constructs

Gateway and Gibson assembly were used to create pCS2 expression vectors from cDNA of zebrafish keratin genes. Total RNA was extracted from 20 WT embryos at 4 and 8 hpf after dechorionation using 750 μ l Trizol (Invitrogen). The cDNA library was generated with the Superscript III reverse transcription kit following the manufacturer's instructions. The coding region of zebrafish krt 18 was isolated using the following primers:

forward: 5'GGGGACAAGTTTGTACAAAAAAGCAGGCTTAATGAGTCTGAGAACAAGCTA CAGCG3'

reverse: 5'GGGGACCACTTTGTACAAAGAAAGCTGGGTTTTAAAGTTTCCTCTTTGGTTTCTGTGC3'

The dominant negative (DN) version of krt18 was generated by mutating the Arginine to Cysteine at position 93 using the following primers:

forward: 5'CATGCAGAACTTGAACGACTGTCTGGCCTCCTATCTGGAG3'

reverse: 5'CTCCAGATAGGAGGCCAGACAGTCGTTCAAGTTCTGCATG3' The template DNA was then digested using dpn1 and the cDNA fragments were cloned into a pDEST plasmid using Gateway cloning. After transformation in NEB 5-alpha Ecoli strain in a pCS2 plasmid, the clones with the correct sequences were selected using sequencing. For krt 8 and 4, the genomic fragments were isolated from cDNA libraries obtained from RNA of 8 hpf embryos as described above. The following primers were used to isolate specific DNA fragments:

krt8 forward: 5'GCATGGACGAGCTGTACAAGAAGACAGAAAACACACAAGGCAGGATGAG TACG3'

krt8 reverse: 5'GCTGGTTTTCTTACTATACGTACTCATCCTGCCTTGTGTGTTTTTCTGTCTTCTTG3'

krt4 forward: 5'GGCATGGACGAGCTGTACAAGCTCAAAGACACGGGGATCATGTCGACGC GCTCTATCTCT3'

krt4 reverse: 5'GTAATACGACTCACTATAGTTCTAGAGGCTTAATAGCGTTTACTGCTGA CGGTGG3'

The PCR products were then integrated to generate entry vectors via recombining with pDONR(P1-P2) (Lawson#208) and the entry clone was further recombined with pCS-N-term-mEmerald (Lawson #223) or pCS-N-term-mCherry (Lawson #362) destination vector (krt4-mcherry, krt8-mcherry, krt4-mEmerald, krt8-mEmerald) or p3E mNeonGreen, pCS2-Dest (Lawson #444) for C-terminal tagging (DNkrt18).mRNA for expression was trasnscribed using the SP6 mMachine kit (Ambion).

2.5 mRNA and morpholino injections

Morpholinos were obtained from Gene Tools, LLC. Morpholino sequences were obtained from previously published research as described in [84].

krt4 MO: 5'AGACCTGGTTGACATGATGCCTGTG3'

krt8 MO: 5'GGTTTTCTTGCTGTAGGTGGACATC3'

krt18 MO: 5'TGTAGCTTCTTCTCAGACTCATGGT3'

FoxH1 MO: 5'TACTTAACCCTACCTCTGATAAAGT3'

human beta globin MO: 5'CCTCTTACCTCAGTTACAATTTATA3'

The morpholinos targeting keratins were translation blocking MOs and prevented formation of protein from the spliced sequence. For FoxH1 MO, a splice-disrupting MO was selected. Based on sequence similarity using BLAST, each of these MOs showed specificity to their respective transcripts and the morphology of the keratin network was assessed as an additional factor to control the effect. A gradient of concentrations from 0.5 ng to 3.0 ng of each MO was tested to observe the phenotype and any off-target effects. For experiments involving keratin 4 and keratin 8 MO knockdowns 1ng of each was injected into the embryo at one cell stage (near the animal pole) or at high stage (into the YSL). For experiments involving keratin 18 and FOXH1 knockdown 3ng of MO was injected at one cell stage. The same concentration as the keratin MO of human beta-globin MO was injected as a control. For this thesis, keratin 8, keratin 4, keratin 18, and dn-keratin 18 constructs were made from zebrafish cDNA. cDNA was prepared using Trizol (Invitrogen) based total RNA extractions from 20 WT embryos at 4 and 8 hpf after dechorionation. 750 μ l of Trizol per 20 embryos was used for extraction. Luna RT Supermix was used to generate cDNA libraries from the total RNA extracted. The primers used for cloning the cDNA of splice zebrafish transcripts are:

krt18 forward: 5'GGGGACAAGTTTGTACAAAAAAGCAGGCTTAATGAGTCTGAGAACAAGCTACAGCG3'

krt18 reverse: 5'GGGGACCACTTTGTACAAAGAAAGCTGGGTTTTAAAGTTTCCTCCTTGGTTTCTGTGC3'

krt8 forward: 5'GCATGGACGAGCTGTACAAGAAGACAGAAAACACACAAGGCAGGATGAG

krt8 reverse: 5'GCTGGTTTTCTTACTATACGTACTCATCCTGCCTTGTGTGTTTTCTGTC TTCTTG3'

krt4 forward: 5'GGCATGGACGAGCTGTACAAGCTCAAAGACACGGGGATCATGTCGACGC GCTCTATCTCT3'

krt4 reverse: 5'GTAATACGACTCACTATAGTTCTAGAGGCTTAATAGCGTTTACTGCTGA CGGTGG3'

The dominant negative construct for keratin 18 was created from the cDNA for keratin 18 by mutating the arginine at the 93rd position to cysteine. The mutagensis was confirmed by sequencing the construct. Primers used:

dnkrt18 forward: 5'CATGCAGAACTTGAACGACTGTCTGGCCTCCTATCTGGAG3' dnkrt18 reverse: 5'CTCCAGATAGGAGGCCAGACAGTCGTTCAAGTTCTGCATG3'

The PCR products were then integrated to generate entry vectors via recombining with pDONR(P1-P2) (Lawson #208) and the entry clone was further recombined with pCS-N-term-

mEmerald (Lawson #223) or pCS-N-term-mCherry (Lawson #362) destination vector (krt4-mcherry, krt8-mcherrry, krt4-mEmerald, krt8-mEmerald) or p3E mNeonGreen, pCS2-Dest (Lawson #444) for C-terminal tagging (DNkrt18). Expression constructs were created using the pCS2 such that RNA could be produced using the sp6 promoter in the plasmid. RNA for injection was made using the SP6 mMessage mMachine Kit (Ambion).

Both mRNA and MO were injected using needles pulled from glass capillaries (30-0020, Harvard Apparatus) pulled using a needle puller (P-97, Sutter Instruments). Microinjection system (PV820, World Precision Instruments) was used to inject according to the method described before [106]. For YSL injections, injections were done directly into the newly formed YSL at high-stage (3.3 hpf) through the yolk. For keratin 4 and keratin 8 mRNA injection concentration of mRNA was limited to 25 pg each as anything over 50 pg lead to abnormal keratin network formation with thicker than WT filaments and incomplete divisions being seen. For CARhoA injections, 0.5-1pg CARhoA together with 2pg H2A-mCherry mRNA were injected into marginal blastomeres at the 128-cell stage. For CAMypt injections, 100pg CAMypt mRNA together with 0.2% phenol red was injected into the YSL at high-stage (3.3 hpf). For CARhoA injections analysis was restricted to the region where mCherry labelled nuclei were clearly seen.

2.6 Sample preparation and fluorescence imaging

For this thesis, imaging was done on the Leica TCS sp5 (upright and inverted), Leica TCS SP8 (upright and inverted), Andor laser cutter (inverted), Nikon CSU-W1 (inverted) and Leica Stellaris 5 (inverted) systems. Before imaging the embryos were dechorionated and incubated at $28^{\circ}C$ until they were imaged. The embryos were mounted laterally or animally in 0.3%–0.5% low melting point (LMP) agarose in E3 (Invitrogen) on glass bottom dishes (MatTek) for inverted imaging. For upright imaging, the embryos were embedded in wells made from moulds made from 3% agarose and covered with 0.5%-0.6% low-melting point agarose. Fixed samples were used for imaging immunostaining and FISH. Images were acquried with upright microscopes mentioned above using HyD S detectors (410 – 850 nm, tunable detection with 1 nm step, min. range = 5nm).

2.7 UV ablation/cutting

Two types of cuts were made using the UV ablation set up: UV cortical laser ablation to measure the recoil and UV ablations to study the tissue wound recovery after ablation of a set number of cells. UV cortical laser ablations were performed on the YSL actomyosin ring, EVL cell-cell/cell-YSL junction ($<30\mu m$) and EVL tissue ($>50\mu m$) at $28.5^{\circ}C$ maintained by a stage incubator. UV cortical laser ablation were performed on a Andor SD laser cutter system with a 63x 1.2 NA water immersion lens on Tg(actb1:GFP-utrCH), Tg(actb1:myl12.1-eGFP/mCherry) and Tg(actb1:Utr-mCherry) emrbyos. Cortical laser ablations were carried by applying 25 ultraviolet pulses at 100 Hz at 2 $shots/\mu m$ along a line parallel and perpendicular to the EVL margin. Fluorescent images were acquired with a iXon DU-897-BV camera (Andor Technology) at frame rate of 0.5 sec/frame. Recoil velocity of the cortex after laser ablations was measured using particle image velocimetry (PIV) and kymographs made on a linear roi with $10\mu m$ thickness at the centre of the ablation. To asses the initial recoil the temporal average recoil was measured as an average of the PIV flow in a rectangular roi over the length of the wound with a thickness of half the wound length was measured. Under these parameters

as observed previously on this setup [71], about 60 % of the cuts were clean cortical openings with minimal changes in the actin/myosin accumulation around the wound while another 40 % showed an apparent accumulation of actin/myosin or a what is observed as a sinking of the wounded area immediately upon ablation.

For EVL tissue $>50 \mu m$ ablation, it was also observed that the wound response was localized to specific cells/cell junctions along the wound length. Junctions showed a higher incidence of wound-responsive actin accumulation, while the surrounding cortex recoiled relatively uniformly. Recoils upon tissue ablations were measured using PIV tissue flow.

EVI cell extrusion upon wound healing was used to induce an anisotropic tension actin ring similar to the YSL locally. Line cuts over 3/4 cells were performed at higher than cortical laser ablation UV laser intensities to cause extrusion out of the epithelial layer. The cuts were $80-100\mu m$ long and led to the simultaneous extrusion of 5-7 EVL cells. Experiments were performed on the lateral side of the embryo between the EVL margin and the animal pole of Tg(krt18:krt18-GFP, actb2:Utr-mCherry) injected with control MO or Keratin MO at one cell stage. The cuts lasted a total of 2 sec while acquisition was stopped. Actin ring was observed as soon as the acquisition started and up to 3 seconds after the cut the actin ring continued to accumulate. The tissue flow was measured using PIV over the un-ablated region. Cell orientations were measured using the orientation of the longest axis of the cells segmented using Cellpose and Fiji [107]. A cellpose model was trained using the pre-trained CPx model on the first frame after the ablation of 10 movies and used to segment the movies.

2.8 Pipette aspiration

Pipette aspirations were used to measure the mechanosensitive properties of the keratin network and the material properties of the EVL. Pipette aspirations were carried out on embryos mounted in 3% methylcellulose in E3 on an inverted Leica SP5 or a Leica Stellaris 5 confocal microscope equipped with the micropipette aspiration system. Micromanipulators(TransferMan Nk2, Eppendorf) were used to control the micropipette position, and a pump controlled by Microfluidic Flow Control System pump (Fluiwell, Fluigent) and the Dikeria micromanipulation software the pressure applied at the end of the pipette. Fire-polished and heat-inactivated FBS passivated micropipettes (Biomedical Instruments) with an inner diameter of $60\mu m$, 30° bent positioned by micromanipulators (TransferMan Nk2, Eppendorf), and with a blunt end were placed on the EVL around 3-4 cells away from the EVL margin. For creep-recovery experiments, negative pressure of 200 mbar was applied until the aspirated tissue flowed in the pipette with constant velocity for 5 mins, followed by pressure release until the tissue reached the end of the pipette. A single z-plane was acquired in the central plane of the pipette every second. The leftmost dark pixel was tracked with a line ROI in Fiji and a custom-made macro script and the length of the aspirated tissue was plotted as a function of time to measure the aspiration and retraction speed [108].

Aspirations were performed under constant pressure to measure the mechanosensitive keratin response in Tg(krt18:krt18-GFP) injected with CAAX-mCherry and Tg(krt18:krt18-GFP, actb2:Utr-mCherry). The mean intensity of keratin at the midplane of the pipette and a region of $30\mu m$ around the aspiration site were measured through fluorescence using an ROI defined in Fiji. Intensities before aspiration and upon aspiration were measured for keratin, actin, and membrane intensities. A membrane labeled with CAAX was used as a nonresponsive control for the aspiration, whereas actin was visualized with Utrophin-mCherry.

For YSL aspirations, a z-stack of $50\mu m$ was acquired from the pipette mid-plane towards the objective. The intensity of Utrophin as a measure of actin recruitment was measured in an ROI next to the pipette in Tg(krt18:krt18GFP, actb2:Utr-mCherry) injected with control MO or keratin MO at high stage into the YSL.

2.9 Analysis of actomyosin flows

For high-resolution confocal imaging of YSL actomyosin flows within the YSL Tg(krt18:krt18-GFP,actb2: Utr-mCherry) and Tg(actb1:GFP-utrCH). Imaging of keratin filaments together with F-actin was done on Tg(krt18:krt18-GFP,actb2: Utr-mCherry) at 7 hpf when the keratin network in the YSL was least dense. Imaging was done Nikon CSU W1 spinning disc microscope with a 63x objective at a frame rate of 30 seconds. A 500×500 -pixel region of interest (ROI) within the YSL was selected with maximum intensity projections centered along the AV axis close to the margin of the EVL. Due to the radial symmetry of epiboly, the 2D flows were reduced to 1D for speed measurement. The flows were measured in this ROI using PIVlab [109]. The alignment of these flows was analyzed by measuring the angular mean of the flow vectors using a custom Python script.

2.10 EVL cell tracking automation

EVL cells were tracked by using Tg(actb2: Utrophin-mCherry) or Tg(acbt2:Utrophin-mCherry, krt18:Krt18-GFP) transgenic embryos. Maximum intensity projections of Z-stacks approximately $150\mu m$ depth (for imaging with sp8 25x) or $30\mu m$ depth (for imaging with Nikon spinning disc microscope) were used to segment apical cell junctions of the EVL cells. Segmentation of the EVL cells were performed using the Cellpose segmentation software using "human in the loop" pipeline described in [107].

Segmentations obtained from cellpose were verified by visually correcting any mis-segmentations. These 2D segmentations were corrected for their 3D projection artifacts using 3D height maps made with local Z-projector in Fiji. The cell orientations were measured on corrected segmentation using Deproj software in Matlab [110]. Data analysis and plots were made in custom Python scripts.

2.11 Keratin network segmentation

For measuring the network of the keratin cytoskeleton in EVL cells, Tg(krt18:Krt18GFP,actb2:UtrmCherry) embryos were imaged on a Nikon CSU-W1 system with a 63x objective. The keratin network distribution was approximated to the apical distribution in z-projected images. The z-projected images were denoised with a gaussain filter and Python-based denoising to obtain a better signal-to-noise ratio for the filaments. These images were thresholded using an adaptive median threshold (Otsu) and the area fraction in Fiji covered by the network was used as an estimate for the network density inside the cell.

Junctional keratin accumulation was measured on the cell margins using the cell outlines with a thickness of 3 pixels obtained from cell segmentations described above. The apical intensity was measured as the intensity of keratin inside the cell outline, excluding the junctional intensity.

2.12 EVL primary cell culture

EVL primary cell cultures were performed as described in two different stages of keratin maturation at 3.5 hpf and at 6hpf [111]. Tg(acbt2:Utrophin-mcherry,krt18:Krt18GFP) or Tg(krt18:Krt18GFP) embryos were transferred to pre-warmed (28.5–31°C) 0.9x DMEM/F12 medium supplemented with GlutaMAX and Penicillin-Streptavidin. The blastoderm caps were dissected from the yolk cells with forceps and transferred to 1.5 ml Eppendorf tubes using glass pipettes.

These explants were dissociated by gentle tapping, seeded at 29° C and imaged for at least 4 hours after seeding. EVL cells were identified by their shape and the presence of keratin fluorescence.

CHAPTER 3

Results

This thesis section summarizes the developmental, mechanosensitive, and intercytoskeltal interactions that the keratin network shows during zebrafish early development. Chapter 3.1 contains the publication titled "Keratins coordinate tissue spreading by balancing spreading forces with tissue material properties"

3.1 Mechanosensitive regulation of keratin organization co-ordinate tissue spreading

This section Chapter 3 section 1 appears in full in the reference [1] and is covered by the CC BY ND 4.0 copyright.

Author Contributions: S.N., E.H. and C.-P.H. designed the research. S.N. performed the experiments and analyzed the experimental data. S.H. and Y.E.K. performed numerical simulations and modeling. K.P. provided help with reagents, and support with experiments. S.N., Y.E.K, S.H. and C.-P.H. wrote the manuscript. All authors edited the manuscript.

Suyash Naik, Yann-Edwin Keta, Kornelija Pranjic-Ferscha, Édouard Hannezo, Silke Henkes, and Carl-Philipp Heisenberg. Keratins coordinate tissue spreading by balancing spreading forces with tissue material properties. *bioRxiv*, 2025

3.1.1 Keratins coordinate tissue spreading by balancing spreading forces with tissue material properties.

Suyash Naik1, Yann-Edwin Keta2, Kornelija Pranjic-Ferscha1, Édouard Hannezo1, Silke Henkes2,* and Carl-Philipp Heisenberg1,*

1 Institute of Science and Technology (ISTA), Am Campus 1, 3400 Klosterneuburg, Austria 2 Lorentz Institute for Theoretical Physics, LION, Leiden University, P.O. Box 9504, 2300 RA Leiden, The Netherlands * email: shenkes@lorentz.leidenuniv.nl and heisenberg@ist.ac.at

Abstract

For tissues to spread, they must be deformable while maintaining their structural integrity. How these opposing requirements are balanced within spreading tissues is not yet well understood. Here, we show that keratin intermediate filaments function in epithelial spreading by adapting tissue mechanical resilience to the stresses arising in the tissue during the spreading process. By analysing the expansion of the enveloping cell layer (EVL) over the large yolk cell in early zebrafish embryos in vivo, we found that keratin network maturation in EVL cells is promoted by stresses building up within the spreading tissue. Through genetic interference and tissue rheology experiments, complemented by a vertex model with mechanochemical feedback, we demonstrate that stress-induced keratin network maturation in the EVL increases tissue viscosity, which is essential for preventing tissue rupture. Interestingly, keratins are also required in the yolk cell for mechanosensitive actomyosin network contraction and flow, the force-generating processes pulling the EVL. These dual mechanosensitive functions of keratins enable a balance between pulling force production in the yolk cell and the mechanical resilience of the EVL against stresses generated by these pulling forces, thereby ensuring uniform and robust tissue spreading.

Introduction

Epithelial cell layer spreading is a core feature of multiple developmental and disease-related processes. In *Drosophila* development, for instance, the spreading of the epidermis leads to the closure of an opening at the dorsal side of the embryo [112, 113]. Likewise, in wound healing, the epidermal cell layer spreading and fusion close the wound [114, 115]. Various cellular processes have been proposed to contribute to epithelial cell layer spreading, including cell spreading, cell migration, oriented cell division, and cell intercalation [116, 117]. These processes can generate the mechanical forces driving active tissue expansion and determine the aptitude of tissues to undergo spreading.

Zebrafish embryo morphogenesis is initiated by the spreading of the blastoderm over the large yolk cell in a process named epiboly [118]. During epiboly, the EVL, a simple squamous epithelial cell layer formed at the surface of the blastoderm, undergoes massive spreading to eventually engulf the entire yolk cell at the end of epiboly (Figure1A) [119, 120]. EVL spreading has been shown to depend on the formation and contraction of a large actomyosin band positioned within a thin cytoplasmic layer at the surface of the yolk cell, the yolk syncytial layer (YSL) [121]. This actomyosin band within the YSL forms around the entire circumference of the yolk cell close to where the leading edge of the EVL contacts the YSL, and its contraction and flow are thought to generate the mechanical forces pulling the EVL over the yolk cell (Figure 1A) [121, 122]. Both active spreading of EVL cells and oriented EVL cell divisions have been implicated in facilitating EVL spreading by modulating EVL surface tension [123, 124]. However, EVL morphogenesis not only relies on the generation and transmission of active

forces within the EVL and YSL, but also on changes in the material properties of the tissue resisting such forces [125]. Yet, the molecular and cellular mechanisms that determine EVL material properties and how they are spatiotemporally coupled to changes in active force production remain unclear. Understanding these mechanisms requires a closer examination of the cytoskeletal components within epithelial cells, particularly those that have been implicated in modulating tissue material properties.

Keratin intermediate filaments are the most abundant and diverse cytoskeletal components in epithelial cells [126, 127]. They form bundled filaments from keratin type I and type II heterodimers laterally associating in an antiparallel fashion into apolar tetramers that again align and anneal longitudinally into unit-length filaments [128, 129]. Keratin filaments are semiflexible, stable and highly elastic, different from the rather stiff and rigid actin and microtubule filaments [130, 131]. They can self-assemble into intricate subcellular networks, the precise organisation of which depends on their functional adaptation in different cell types [132]. Generally, the intracellular keratin network can organise into a rim network, supporting plasma membrane integrity and connecting desmosomal contacts, and a spoke network, surrounding the nucleus and transferring information from the cell exterior to the nucleus [133, 134, 135]. In polarised simple epithelia, such as the EVL, keratin networks are typically positioned near the apex where they are thought to function in resisting mechanical and chemical stresses and maintaining epithelial apicobasal polarity [136, 137, 138]. Keratins have been shown to be sensitive to mechanical forces by reorganizing and changing their mechanical properties upon stress application [130, 139, 140]. Yet, how keratin network mechanosensitivity functions in epithelial tissue morphogenesis remains unsettled [141, 142].

The role of epithelial keratins in development and disease is only beginning to be understood [143, 144]. Keratin mutations can cause diseases that lower the resilience of epidermal tissues to mechanical stress [145]. Moreover, studies in mouse embryos have shown that keratins are required for trophectoderm specification and extra-embryonic tissue growth and expansion [141, 142]. Here we show that keratin intermediate filaments are required for EVL spreading during zebrafish epiboly. They function in this process by balancing EVL tissue viscosity with the external pulling forces mediating EVL spreading. This balancing function of keratins enables the EVL to undergo uniform spreading without rupturing.

Results

Keratins are specifically expressed within the EVL and YSL during gastrulation.

To explore the function of keratins during early zebrafish embryogenesis, we analysed the expression of different keratins in embryos from early blastula to late gastrula stages (4.5–8.5 hpf). Previous studies have shown that 13 type I keratins and 3 type II keratins are specifically expressed within the developing EVL during this period [146, 147]. To identify the temporal keratin expression profiles within the EVL during epiboly, we used RT-qPCR to map the expression of three keratin type II (keratin 4, 5, 8) and one keratin type I (keratin 18), abundantly expressed within the EVL [147, 148]. We found all of these keratins to be expressed already at early blastula stages, with their expression continuously increasing until the end of gastrulation (Figure Supplement 1A). The expression was restricted to the epithelial cells as evidenced by fluorescence *in situ* hybridization for keratin 8 mRNA (Figure Supplement 1B). To determine the spatial distribution of keratins within the epibolizing embryo, we took advantage of Tg(krt18krt18-GFP) embryos expressing GFP-tagged keratin 18 under its endogenous promoter. Keratin 18 expression was first detected in EVL progenitor cells within the early gastrula (4.0 hpf) arranged in short, bundled and unconnected filaments located predominantly at the apical

surface of these cells (Figure 1B, Video 1 and Figure Supplement 1C). Keratin 18 continued to be selectively expressed within EVL cells until mid-gastrulation (5.5 hpf), when some additional expression was also detected within the forming YSL directly adjacent to the place where the leading edge of the EVL contacts the YSL (Figure 1B and Figure Supplement 7A). During this period and continuing until the end of gastrulation, the apical network of keratin 18 filaments within EVL cells became increasingly dense and interconnected (Figure 1B), as evidenced by a continuous increase in keratin 18-GFP intensity and network density between 4.5 and 8.5 hpf (Figure 1C and D, and Video 1). This increase in keratin network intensity and density was accompanied by EVL cells increasing the apical area during epiboly (Figure 1E), suggesting a close temporal correlation between keratin network maturation and EVL cell spreading (Figure 1F). Initially, keratin filaments were predominantly localized to the apical surface of the EVL cells (Figure 1B and Supplement 1C), but from 6 hpf onwards, additional keratin 18 expression was detected in a bundle-like configuration along the apical junction of EVL cells (Figure 1B and G), consistent with previous observation of keratins showing both junctional ("rim") and apical ("spoke") localization [133, 141, 142].

Keratin network maturation is mechanosensitive.

EVL epiboly movements are driven by a large actomyosin cable forming within the YSL and pulling the margin of the EVL over the yolk cell [121]. Given that keratin networks can reorganise under stress [140, 149], we speculated that the observed maturation of the keratin network within EVL cells might be facilitated by EVL tissue tension building up during the course of epiboly [121, 150]. To test this possibility, we analysed whether and how EVL network maturation is affected in embryos where EVL tension is either increased or decreased. To modulate EVL tension, we expressed a constitutively active form of RhoA (CA RhoA) specifically within the YSL, promoting YSL actomyosin contractility and pulling, or a constitutively active form of myosin phosphatase (CA Mypt) leading to reduced YSL contractility and pulling [122, 151]. In CA RhoA-expressing embryos, keratin 18 expression intensity and network density in EVL cells prematurely increased during the course of epiboly, while in CA Mypt-expressing embryos, keratin expression and network maturation were delayed (Figure 2A–D, Video 2–5 and Figure Supplement 2B). This keratin mechanosensitivity was detectable both when network maturation was analysed as a function of developmental time or degree of epiboly progression (Figure 2A-D and Figure Supplement 2B-C), suggesting that the effect of EVL tension on keratin network maturation is not just a secondary consequence of changes in EVL epiboly movements (Figure Supplement 2D).

To more directly assess the effect of EVL tension on keratin network maturation, we locally increased EVL tension in 5 and 7 hpf embryos by aspirating the EVL using a micropipette and analysing resultant changes in EVL network maturation. We found that keratin filaments showed increased accumulation in EVL cells upon aspiration (Figure 2F–H, Video 8), further supporting the notion that keratin network maturation within the EVL cells is promoted by EVL tension building up during the course of epiboly.

To investigate the mechanisms underlying keratin network mechanosensitivity, we examined whether keratin mRNA expression within the EVL is responsive to reduced pulling forces from the YSL. Using qPCR, we compared keratin 4, 5, 8 and 18 expression levels in control embryos and embryos expressing *CA* Mypt within the YSL, which attenuates actomyosin contraction-mediated pulling on the EVL. Notably, this comparison revealed no significant differences in keratin 4, 5, 8 and 18 expression (Figure Supplement 2I), arguing against a force-dependent transcriptional regulation of keratin within the EVL.

Interestingly, in our micropipette aspiration assay, increased keratin expression in the EVL

was spatiotemporally accompanied by a marked enhancement of actin network assembly (Figure Supplement 2F). Given the well-established mechanosensitivity of the actomyosin cytoskeleton [152, 153] and its known physical interactions with the keratin network [132, 154, 155], this observation raises the possibility that keratin mechanosensitivity in the EVL may depend on actin network dynamics.

To test this hypothesis, we treated embryos with low concentrations of Cytochalasin D (CytoD) to impair actin network assembly in EVL cells and assessed keratin upregulation upon micropipette aspiration. Strikingly, CytoD-treated embryos showed a markedly reduced keratin response to aspiration (Figure 2H), suggesting that proper actin network assembly is required for keratin mechanosensitivity in the EVL.

To more directly assess whether actomyosin contractility affects keratin network assembly, we injected *CA* Mypt mRNA into a single blastomere at the 64-cell stage to generate EVL clones with reduced contractility. We found that downregulation of actomyosin contractility resulted in a corresponding decrease in keratin network assembly within these clones (Figure 2A–D and Figure Supplement 2G–H), supporting a causal role of actomyosin tension in promoting keratin assembly.

Together, these findings demonstrate that the keratin cytoskeleton in EVL cells is mechanosensitive and that this mechanosensitivity is dependent on the mechanosensitive assembly of the actin network.

Keratins regulate EVL tissue properties.

Keratins have previously been implicated in resisting mechanical stresses in epithelial cells. Thus, the mechanosensitive coupling between EVL keratin network maturation and pulling force generation within the YSL might constitute a mechanism to protect the EVL tissue against excessive deformations by mechanically strengthening it proportionally to the force exerted on it.

To test this possibility, we knocked down/out the expression of the two keratin type II genes (keratin 4 and 8) primarily expressed within EVL cells [147], reasoning that in the absence of keratin type II expression, no keratin dimers can be formed within the EVL and thus keratin network formation should be defective. Ubiquitous knock-down/out of keratin 4 and 8 expression by using morpholinos and CRISPR-Cas9 or interference with keratin network formation by overexpressing a dominant-negative version of keratin 18 (DNkrt18) [156], led to strongly diminished keratin 18 expression and network formation within EVL cells (Figure 3A–C, Video 6–7 and Figure Supplement 3A–B). Loss of the keratin network in all these perturbations led to delayed EVL epiboly movements (Figure 3D, Video 6 and 7 and Figure Supplement 3C) and frequent rupturing of the EVL towards the end of gastrulation, causing embryo lethality (Figure Supplement 3D–E). Rupture of the EVL was typically preceded by a reduction in junctional localization of E-cadherin (adherens junctions), Occludin-B (tight junctions), and plakoglobin-A (desmosomal junctions) (Figure Supplement 3F–H), suggesting that keratins are essential for maintaining EVL tissue integrity by enabling proper formation and stabilization of cell-cell junctions between EVL cells.

To understand how keratins function in EVL epiboly movements, we analysed changes in EVL cell shapes and rearrangement in response to the pulling forces from the YSL during epiboly. Comparing wild-type with keratin 4/8 morphant embryos revealed that EVL cells in wild-type embryos coordinately elongated along the animal—vegetal (AV) axis of the gastrula, the axis of EVL spreading, while no such coordinated cell elongation was detectable in morphant embryos

(Figure 4A–B). This points at the possibility that tissue material properties, determining force transduction and mechanical resilience, might be altered by keratin network formation.

To investigate this possibility, we measured the material properties of EVL tissue at early and mid-gastrulation (5 and 7 hpf) using micropipette aspiration. Analysis of the flow profile of the EVL into the pipette revealed a linear response, consistent with viscous properties, which allowed us to assess the viscosity of EVL tissue. Comparing the viscosity of EVL tissue between early and mid-gastrulation stages showed a significant increase in viscosity at mid-gastrulation, coinciding with the maturation of the keratin network (Figure 4C). This suggests that keratin network maturation during epiboly contributes to the increase in EVL tissue viscosity. To test this function of keratins more directly, we performed EVL micropipette aspiration experiments in wild-type and keratin 4/8 morphant embryos. At early gastrulation, when differences in keratin network formation between wild-type and morphant embryos were still relatively small (Figure 1B), we observed a slight reduction in viscosity in keratin 4/8 morphant embryos compared to wild-type (Figure 4C). In contrast, at mid-gastrulation (Figure 4C, Video 8), when the differences in keratin network organization between morphant and wild-type embryos became more pronounced (Figure 1B), viscosity was significantly reduced in the morphant embryos. This supports the idea that keratin network maturation enhances EVL tissue viscosity.

To test whether this effect is due to keratin expression specifically within EVL cells, we knocked down keratin 4/8 expression within the YSL by injection of keratin 4/8 morpholinos directly into the forming YSL at the 512-cell stage. Interestingly, this did not cause any detectable changes in coordinated EVL cell elongation along the AV axis, suggesting that keratins control EVL cell shape changes in a tissue-autonomous manner (Figure Supplement 4A–B). To further challenge this conclusion, we developed an EVL wound-healing assay, allowing us to monitor autonomous EVL spreading during wound closure [157, 158]. For wounding the EVL, we ablated 3-5 neighbouring cells at random positions within the EVL in mid-gastrulation stage embryos (7 hpf) and observed how the coordinated spreading of the neighbouring cells extruded the ablated cells. In control embryos upon ablation, a supracellular actin cable formed at the leading edge of EVL cells neighbouring the ablated cells (Figure 4D, Video 9–10). This was accompanied by the highly coordinated movement and spreading of EVL cells towards the site of cell ablation, eventually leading to the extrusion of the ablated cells and closure of the wounding site (Figure 4G). During this process, not only the leading edge EVL cells elongated towards the wounding site, but also cells further away from the ablation site, resulting in a highly coordinated long-range tissue spreading detected by tissue flow and cell alignment analysis (Figure 4D-G). In contrast, EVL oriented cell elongation and tissue spreading were largely restricted to EVL cells directly neighbouring the wounding site in keratin 4/8 morphant and crispant embryos (Figure 4D–G and Figure Supplement 4C–E). This supports the notion that keratin expression within the EVL promotes tissue viscosity, leading to an increased length (hydrodynamic length) by which the tissue deforms in response to forces pulling at its margin.

Keratins are required for mechanosensitive actomyosin contraction within the YSL. Given that keratin expression within the EVL is mechanosensitive, we hypothesised that this behaviour might constitute a feedback mechanism balancing EVL tissue viscosity with the forces pulling on its margin, thereby setting the rate of EVL epiboly movements. To address this hypothesis, we developed a vertex model [159, 160] of the EVL, enabling us to relate EVL tissue spreading dynamics to mechanosensitive keratin expression. To this end, we wrote the energy, which penalises deviations of the areas A_i and perimeters P_i of the cells i from their

target values $A_{i,0}$ and $P_{i,0}$, respectively, as

$$U = \sum_{i} \left[\frac{\Gamma_{i}}{2A_{0}} \left(A_{i} - A_{i,0} \right)^{2} + \frac{\Gamma_{i}}{2} \left(P_{i} - P_{i,0} \right)^{2} \right],$$

where Γ_i is the cell stiffness constant. In order to make the tissue viscoelastic, we relaxed the target area $A_{i,0}$ over a characteristic viscous relaxation timescale τ_i following

$$\tau_i \frac{dA_{i,0}}{dt} = -(A_{i,0} - A_i),$$

while enforcing a minimum area A_0 , and scaled $P_{i,0}$ to work at a constant shape parameter $s_0 = P_{i,0}/\sqrt{A_{i,0}} = 3.72$, a value where the tissue is predicted to be still rigid [159].

We next incorporated keratin into our model (Figure 5D). As illustrated in Figure 1B, keratin forms an intracellular network that is initially floppy, but reaches a percolation threshold at approximately $K_{\rm th}=150$. Capturing the full complexity of its behavior would require simulating the coupled dynamics of actin and keratin networks, including keratin polymerization and depolymerization as well as actomyosin contractility. To simplify the analysis, we instead implemented a mesoscale approximation in which the keratin network acts in parallel with other mechanical components of the cell. Above the percolation threshold, keratin contributes proportionally to both the cell's effective stiffness and relaxation time with

$$\Gamma_i = \Gamma(1 + \beta \Delta K_i), \qquad \tau_i = \tau(1 + \beta \Delta K_i),$$

where $\Delta K_i = \max(0, K_i - K_{\rm th})$ and β is the mechanical feedback constant that determines the mechanical effect of the keratin concentration above the threshold ΔK_i .

To include keratin mechanosensitivity, we further assumed that its assembly from the cytosol increases with the stress applied on the tissue. To account for this, we used a simple, linear model of the evolution of the keratin concentration,

$$\tau_K \frac{dK_i}{dt} = \alpha \, \max(0, \, p_i) - K_i,$$

where keratin dissociates with timescale τ_K and α is a coupling constant (note that other non-linear rheology models have also been used to model the effect of keratin [140]). Mechanosensitivity in our model arises through biaxial stress, or equivalently, the in-plane pressure p_i defined as

$$p_{i} = \frac{1}{V_{0}} \left(\frac{\Gamma_{i}}{A_{0}} (A_{i} - A_{i,0}) A_{i} + \Gamma_{i} (P_{i} - s_{0} \sqrt{A_{i,0}}) P_{i} \right),$$

where V_0 is the conserved 3D cell volume (see SI, Section 2). This formulation captures the pressure response arising from deviations in both cell area and perimeter relative to their preferred values. In this framework, EVL spreading corresponds to a substantial increase in cell area A_i , accompanied by dramatic thinning of individual cells. At steady state, this mechanosensitive feedback yields a linear relationship between keratin concentration and pressure, expressed as $K_i = \alpha P_i$ under the assumption of positive pressure. A summary of this mechanochemical feedback loop is presented in Figure 5E.

To estimate the parameters for simulating EVL spreading, we used the EVL aspiration experiments described above (Figure 5A–B, Figure 2F–H and 4C). First, we separately fitted the low-keratin initial response and the high-keratin release curve in the aspiration experiments

using a modified viscoelastic Maxwell model to obtain estimates of dissociation timescale τ_K , pressure coupling α , cell stiffness constant Γ , and relaxation timescale τ (Figure 5C, Figure Supplement 5A–D and SI Section 1). Then we used these values together with a mean-field version of the mechanical model (see SI Section 4) to compute tissue height and keratin expression in the aspirated tissue (Figure 5F–G and Figure Supplement 6A–D). We chose $\beta=0.005$ for the wild-type model tissue such that the increase of keratin levels from $K_i=0$ to $K_i=550$ with a percolation threshold $K_{\rm th}=150$ leads to a 2-fold increase of Γ and τ (Figure Supplement 5E–F). Please see Table S1 for the full list of fitted parameters.

Using these parameters in our extended vertex model (see simulation library [159]), we first simulated the EVL wound-closure behaviour in wild-type and keratin-deficient embryos. For this, we initialised a disordered tissue patch under tension, and then created a model wound by deleting several cells and adding a contractile cable to the wound perimeter (Figure 5H–J, Video 14; for details see SI Section 3). We observed that junction tension

$$t_i = \Gamma_i \left(P_i - P_{i,0} \right)$$

was higher and more widely distributed around the wound in wild-type ($\beta=0.005$) compared to keratin-deficient ($\beta=0$) tissues (Figure 5I), while the time required to close the wound remained largely unchanged between these conditions (Figure 5J). This closely matched our experimental observations where keratin-deficient embryos exhibited a more localized distribution of junctional tension near the wound site (Figure 4D–G), while the wound-closure rates were indistinguishable between wild-type and keratin-deficient embryos (Figure 4H). These results support the hypothesis that keratin contributes to a mechanochemical feedback loop within the EVL, modulating tension propagation without significantly altering the kinetics of wound closure.

To test whether we can also simulate the behaviour observed for EVL spreading during epiboly, we simulated epiboly by representing the EVL tissue as a disordered circular packing of N=529 cells, where the outer vertices are pulled outwards (Figure 5K and Video 15). As the actual embryo is spherical, we defined the effective height of the model tissue as

$$z = \frac{\sum_{i} A_i}{2\pi R},$$

which is the height of its projection on a sphere of radius $R=350~\mu\mathrm{m}$, and we defined the tissue's velocity v_z as the time derivative of this height. To mimic the pulling of the EVL margin by actomyosin contraction and flow within the YSL, we applied an outward force F_{YSL} on the edge of the simulated tissue with an amplitude which increases linearly with time, following the experimentally determined pulling-force evolution within the YSL [121]. We then measured the mean keratin expression K and edge velocity v_z as a function of time and pulling forces (Figure 5N–P). By ramping the pulling force from 0 at the beginning to $0.57~\mu\mathrm{N}$ (a value equivalent to the pulling force used in the aspiration experiments) at the end of the simulation, we obtained keratin expression values and tissue edge velocities matching our experimental observations (Figure 1C, 3D and 5O). Interestingly, we also found, similar to our experimental observations (Figure 5M), that keratin expression increased to heterogeneous levels in individual EVL cells in our simulations (Figure 5L), suggesting that this heterogeneous keratin expression is mechanically regulated.

To determine whether our model can also account for the experimentally observed changes in EVL dynamics when pulling forces within the YSL were either increased or decreased, we analysed the response of keratin expression and tissue edge velocity to variations in pulling

forces (F_{YSL}) in our simulations (Figure 5N, P). Consistent with experimental observations, mean keratin expression increased when F_{YSL} was upregulated and decreased when F_{YSL} was downregulated (Figure 5N). Moreover, in line with the observed scaling of keratin expression, and thus tissue viscosity, edge velocity in our simulations was not significantly affected by changes in F_{YSL} (Figure 5P). The origin of this rheostat-like behaviour is that the fixed point of the nonlinear keratin-strain-rate dynamics is nearly independent of the strain rate (see SI Section 4). However, these predictions did not align with our experimental findings at later stages of gastrulation, where both increasing and decreasing $F_{\rm YSL}$ —by modulating actomyosin contractility within the YSL—slowed EVL epiboly movements (Figure Supplement 2D). This suggests that changes in keratin expression, and consequently EVL tissue viscosity, cannot fully compensate for alterations in F_{YSL} throughout gastrulation. A similar discrepancy between model predictions and experimental results emerged when comparing tissue edge velocity between wild-type and keratin-deficient embryos. While our simulations predicted a significant increase in edge velocity in keratin-deficient embryos compared to wild-type (Figure 50)—as expected for a less viscous and more deformable EVL—experimental data showed a decrease in edge velocity in keratin-deficient embryos (Figure 3D).

Interestingly, in our simulations, the reduction in EVL tissue edge velocity observed in keratin-deficient embryos could only be explained by a decrease in the pulling force $F_{\rm YSL}$ (Figure 5P). This led us to speculate that keratins may have additional functions within the YSL in regulating $F_{\rm YSL}$, a possibility supported by previous findings that have implicated keratins in actomyosin network organization and mechanosensation [161, 162]. To test this possibility, we analysed dynamic actomyosin reorganization within the YSL in the presence and absence of keratins. In wild-type embryos, retrograde flows of actin and myosin within the YSL led to the formation of a contractile actomyosin band, previously shown to generate the pulling forces that drive EVL spreading [121]. However, in embryos where keratin 4/8 was specifically knocked down within the YSL, these actomyosin flows were severely diminished and less aligned (Figure 6A, D, F).

To investigate the functional interaction between keratins and the actomyosin network within the YSL, we analyzed the coordination of YSL actin and keratin network dynamics during EVL epiboly movements. Using particle image velocimetry (PIV) analysis, we observed both actin and keratin retrograde flows within the YSL, with keratin flows being more spatially confined to the EVL–YSL boundary where the keratin network was predominantly localized (Figure Supplement 7C–C'). Moreover, actin flows further away from the EVL–YSL boundary were strongly reduced when reaching the region of keratin localization close to the boundary, suggesting that actomyosin contraction-driven flows compress the keratin network by physically interacting with it as previously reported [163].

To assess whether this interaction impacts force transmission within the actin network—potentially by keratins providing a rigid scaffold that enhances actin network crosslinking—we performed UV-laser ablation of the YSL actin network in embryos with or without keratin expression in the YSL. Strikingly, the actin recoil velocity and hydrodynamic length following laser cuts was significantly reduced in krt4/8 morphants compared to controls (Figure Supplement 7D–F), indicating decreased force transmission within the actin network in the absence of keratin.

Given this keratin-dependent effect on actin network rheology, and previous reports linking keratins to actomyosin mechanosensation [161, 162], we next asked whether keratin within the YSL might be required for the YSL actin network responding to tension generated at the EVL–YSL boundary. To address this, we performed micropipette aspiration of the YSL

and monitored mechanosensitive changes in the actomyosin network in both wild-type and keratin loss-of-function embryos. In wild-type embryos, pulling on the YSL induced a local increase in actin intensity near the site of aspiration (Figure 6B, E), suggesting that YSL actomyosin contraction and flow is upregulated by tension generated at the EVL-YSL boundary. In contrast, embryos with specific knockdown of keratin 4/8 in the YSL failed to show this upregulation (Figure 6B, E), suggesting that this mechanosensitive response of the actomyosin network depends on keratin network formation within the YSL.

Collectively, these findings suggest that keratins are required for the generation of tension within the YSL that drives EVL epiboly movements, likely by supporting actin network crosslinking and its mechanosensitive response to applied forces.

Discussion

Our findings suggest that keratins function in EVL spreading during epiboly by coupling tissue contractility and tension to tissue viscosity and connectivity. During epiboly, actomyosin contraction and flow within the YSL generate the forces pulling the margin of the EVL towards the vegetal pole of the gastrula. These pulling forces not only induce stress within the EVL, but also within the YSL to which the EVL is mechanically coupled at its margin. In the EVL, build-up of stress triggers keratin network maturation, which again increases EVL tissue viscosity and promotes cell-cell junction formation and maintenance, thereby ensuring that the tissue remains intact when stress rises during epiboly. In the YSL, keratins are essential for transmitting forces within the actin network, promoting stress-dependent actin accumulation, and enabling efficient contractions required to pull the EVL over the yolk cell. By fulfilling this dual mechanosensitive role — linking EVL viscosity to YSL contractility — keratins ensure robust and efficient EVL spreading during epiboly.

Keratins have previously been shown to be stress-responsive and display important functions in mechanical tissue resilience and spreading [142, 129, 161, 162]. While spreading necessitates malleability, mechanical resilience is facilitated through properties such as tensile strength. Various studies have linked keratins to both these functions in culture cells and mouse embryos [142, 163]; however, it remains unclear exactly how keratins could mediate these contrasting roles in a systemic manner. Our findings suggest a mechanism by which to reconcile the functions of keratins in ensuring tissue integrity [144, 161, 164] and promoting tissue spreading [142, 165]. The ability of keratins to resist mechanical stress increases as their organisation progressively transforms from an immature, disconnected form into a dense, interconnected cellular network, which ultimately develops into a supracellular, tissue-scale network through the association of keratins with desmosomal junctions [133]. This process links cellular keratin networks and stabilises desmosomal proteins [134, 166, 167]. To ensure that this increasing resistance against deformation of the EVL does not stall EVL spreading and epiboly movements, keratins also facilitate tension-dependent actin network accumulation within the YSL, thereby adapting mechanical pulling force production within the YSL to EVL tissue viscosity resisting its deformation.

Previous studies have suggested that keratins can interact with the actomyosin cytoskeleton [129, 168], although the biochemical basis and functional significance of this interaction during early development remain poorly understood. Keratin—actin interactions are thought to occur either directly [154, 129] or indirectly via large cytolinker proteins such as plakins and plectin [169, 170]. Disruption of the actin cytoskeleton has been shown to impair keratin network organization and stability [155]. Conversely, keratin loss can perturb actin network architecture during wound healing [163], as well as impair actin stress fiber formation and cell

polarization in response to local mechanical forces acting on C-cadherins [171]. Our results provide direct evidence that keratin and actin networks interact functionally: keratins are required for actin mechanosensation within the YSL, and conversely, actin is necessary for keratin mechanosensation within the EVL. Whether these interactions are purely mechanical — for example, providing structural support for network assembly and remodeling — or also involve biochemical signaling pathways that regulate polymerization and architecture remains to be determined.

Notably, keratin intermediate filaments are thought to be absent in insects [172], suggesting that tissue morphogenesis and spreading in these animals can occur in the absence of keratin function. In embryogenesis of the insect *Tribolium castaneum*, for instance, the extraembryonic serosa, a simple squamous epithelial cell layer, undergoes massive spreading during epiboly [173]. Similar to EVL epiboly movements in zebrafish, serosa spreading is mediated by forces pulling on its leading edge [173]. Interestingly, this pulling leads to a regionalization of the serosa tissue into a solid-like dorsal portion with little cell rearrangements and a fluid-like ventral portion consisting of cells undergoing intercalations [173]. In contrast, no such clear regionalization can be observed in the zebrafish EVL with very little cell intercalations occurring throughout the tissue except some cells at the EVL margin withdrawing from the leading edge at very late stages of EVL epiboly. This different response of the EVL and serosa tissues to pulling forces might be due to the presence and absence of keratin expression within the respective tissues, pointing to the intriguing possibility that the function of keratins for homogeneous tissue spreading has become dispensable in insects. How this function of keratins in epithelial tissues has been adapted to specific organismal settings, and why keratins became expendable in many insect species remains to be explored.

While keratins belong to the most abundant and diverse cytoskeletal components in epithelial cells, remarkably little is yet known about the mechanisms by which they function in epithelial tissues. Our findings identify a critical role of keratins in promoting tissue viscosity and contractility in response to tissue tension. This ensures robust tissue spreading by balancing tissue integrity and expansion.

Figures

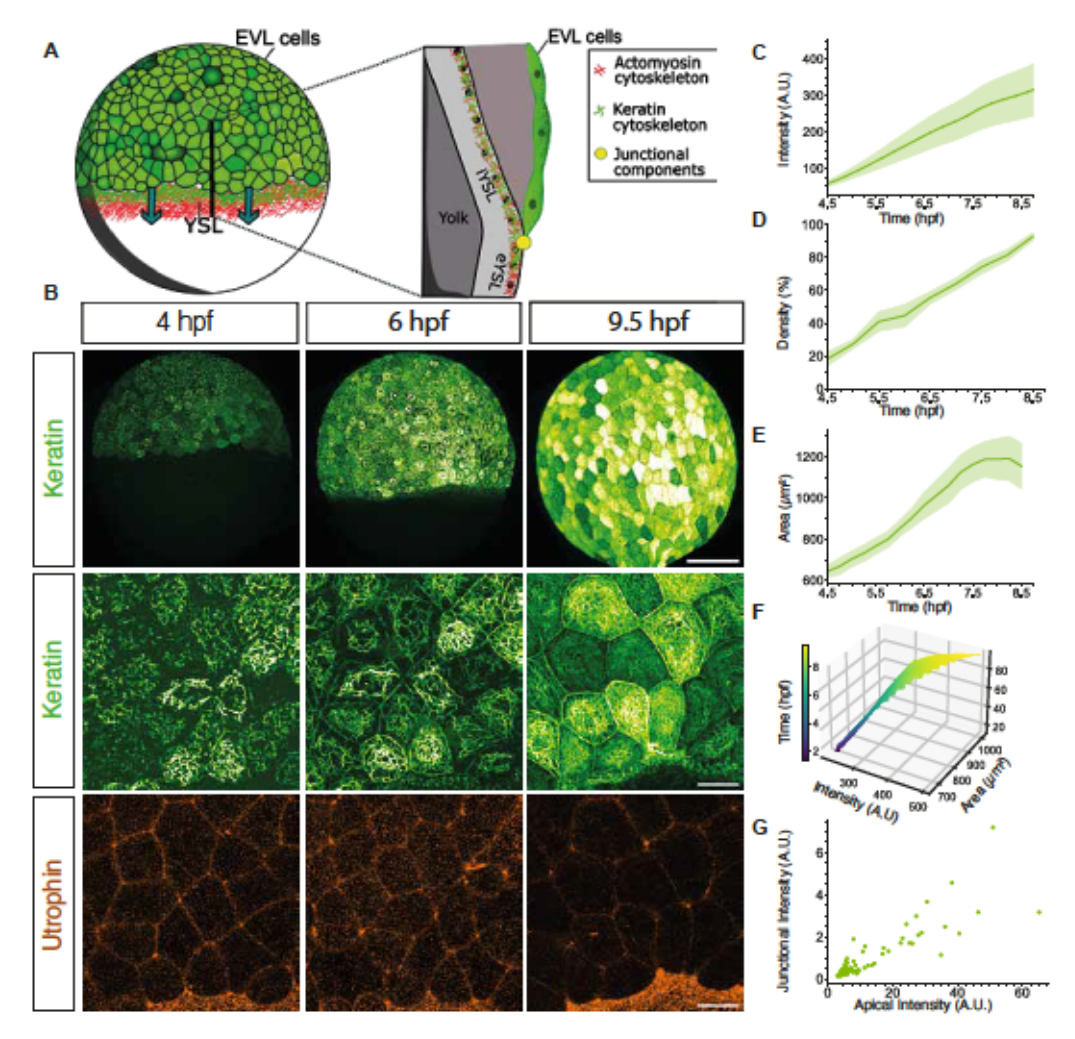


Figure 3.1: Keratin network maturation in the EVL.

Figure 3.1 Keratin network maturation in the EVL.

- (A) Left: schematic representation of a zebrafish embryo at 60% epiboly stage (6 hpf) showing the expression and localization of keratin within the EVL and YSL (together with actin). Arrows mark the direction of EVL epiboly movements. Right: cross-section of the region outlined in the left panel marking the expression and localization of keratin, actin (within the YSL) and junctional components linking the margin of the EVL to the YSL.
- (B) Maximum intensity projection images of keratin (top and middle rows) and actin (Utrophin; bottom row)) expression in Tg(krt18:krt18-GFP) (keratin) and Tg(acbt2:utr-mCherry) (actin) embryos showing the progression of keratin expression within the EVL and YSL during epiboly (4 9.5 hpf).
- (C) Averaged keratin intensity within the EVL in Tg(krt18:krt18-GFP) embryos as a function of time during epiboly (4 9.5 hpf). N = 3 experiments, n = 5 embryos. Error bars as ribbons SD of mean.
- (D) Averaged density of the keratin network in Tg(acbt2:utr-mCherry, krt18:krt18-GFP) embryos as a function of time during epiboly (4 9.5 hpf). N = 3, n = 6 embryos. Error bars as ribbons SD of mean.

- (E) Average apical cell area of individual EVL cells in Tg(acbt2:utr-mCherry, krt18:krt18-GFP) embryos as a function of time during epiboly (4 hpf-8.5 hpf). N=3, n=4 embryos. Error bars as ribbons SD of mean.
- (F) 3-dimensional (3D) plot of keratin intensity, network density, and EVL cell area as a function of time during epiboly. N=3, n=4 embryos. Spread of the surface (width) represents data spread, indicating their variability (SD of intensity and area).
- (G) Correlation of junctional and apical keratin intensity measured in individual EVL cells in Tg(acbt2:utr-mCherry, krt18:krt18-GFP) embryos at 60% epiboly stage (6 hpf) N = 3, n = 3 embryos.

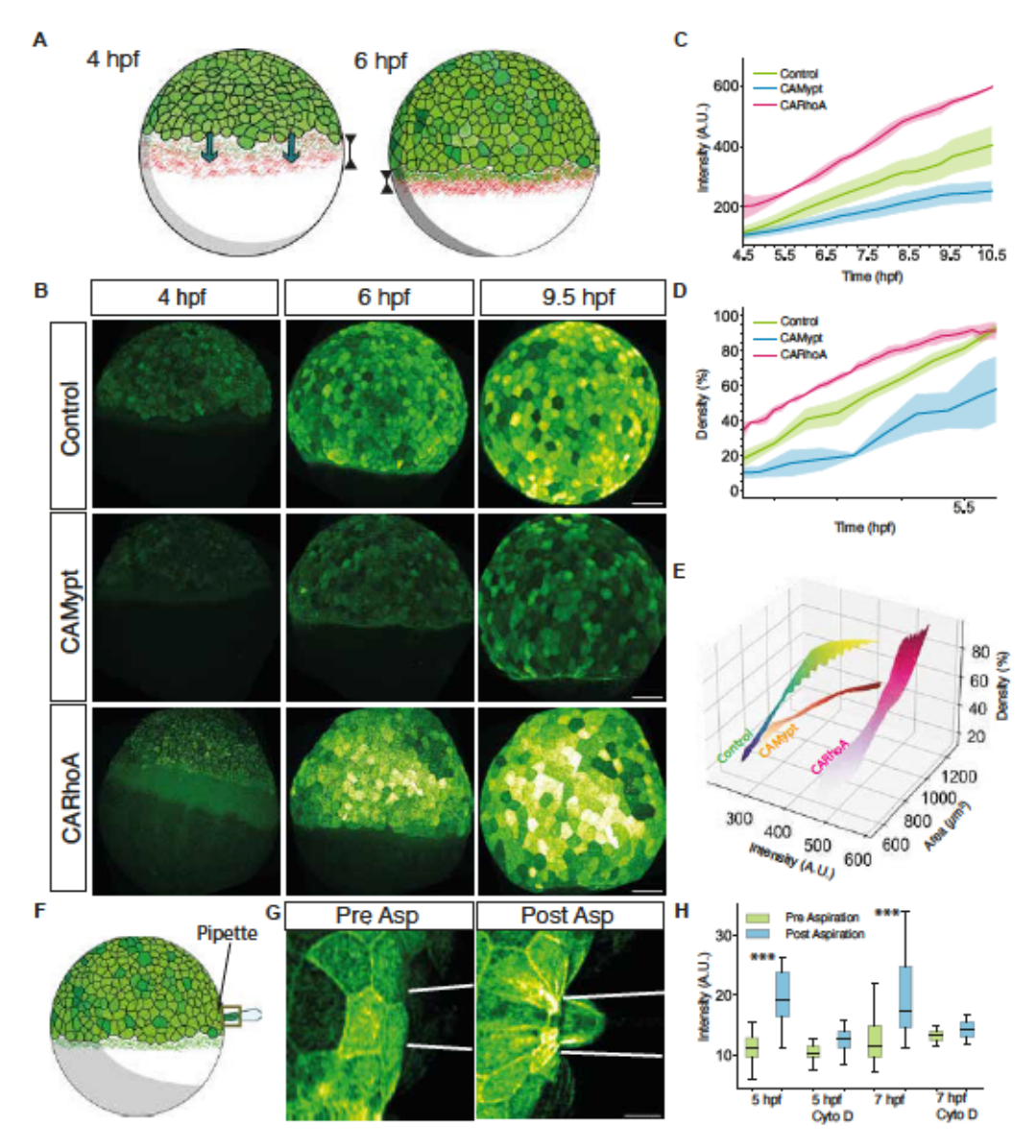


Figure 3.2: Pulling forces promote keratin expression within the EVL.

Figure 3.2 Pulling forces promote keratin expression within the EVL

- (A) Schematic showing actomyosin contraction and flows within the YSL providing the mechanical forces pulling the EVL over the yolk cell during epiboly (for details see10) in a zebrafish embryo at 4 hpf (left) and 6 hpf (right). Green arrows, EVL epiboly movements; black arrows, actomyosin contraction within the YSL.
- (B) Maximum intensity projection images of keratin expression in representative Tg(acbt2:utrmCherry, krt18:krt18-GFP) control embryos (YSL injection of 0.2% phenol red, top row) and embryos injected with 100 pg CAMypt (middle row) and 50 pg CARhoA (bottom row) into either the YSL at 3.3 hpf (CAMypt) or marginal cells at 3.3 hpf (CARhoA) at sphere stage (4 hpf, left column), shield stage (6 hpf, right column), and 90% epiboly stage (9.5hpf, right column). Scale bar: $100 \, \mu m$.
- (C) Plot of average keratin intensity as a function of time (hpf) in Tg(krt18:krt18-GFP) control (green, N=3, n=5 embryos), CAMypt (orange, N=3, n=5 embryos) and CARhoA mRNA injected embryos (pink, N=3, n=4 embryos) as described in (B). Error bars as ribbons SD of mean.

- (D) Plot of average density of keratin network as a function of time (hpf) in Tg(actb2:utr-mCherry, krt18:krt18-GFP) control (green, N=3, n=6 embryos), CAMypt (orange, N=3, n=4 embryos) and CARhoA mRNA injected embryos (pink, N=3, n=3 embryos) as described in (B). Error bars as ribbon SD of mean of individual cells per replicate.
- (E) 3-dimensional (3D) plot of keratin intensity, network density and EVL cell area as a function of time (hpf) in Tg(actb2:utr-mCherry, krt18:krt18-GFP) control (viridis, N = 3, n = 3 embryos), caMypt (orange, N = 3, n = 3 embryos) and caRhoA mRNA injected embryos (White to Pink, N = 3, n = 3 embryos) as described in (B). Spread of the surface (width) represents data spread, indicating their variability (SD of intensity and area).
- (F) Schematic showing pipette aspirations of the EVL of a 70% epiboly (7 hpf) stage embryo where the regions of interest within the pipette and outside of it are marked as yellow boxes.
- (G) Maximum intensity projection images of keratin localization and intensity within the EVL before (left) and after (right) aspiration with a pipette in a representative Tg(krt18:krt18-GFP) embryo. White lines outline the boundary of the pipette. Scale bar: 10 μ m.
- (H) Box plot of keratin intensity within the pipette before (green) and after (orange) EVL aspiration in control (N = 4, n = 33 embryos), and Cytochalasin D (CytoD; 25 nM)-treated Tg(actb2:utr-mCherry, krt18:krt18-GFP) embryos at 5 and 7 hpf (N = 3, n = 25 embryos). Boxes represent quartiles for the data, dots outliers (pvalues: ***<0.001 Wilocoxon test).

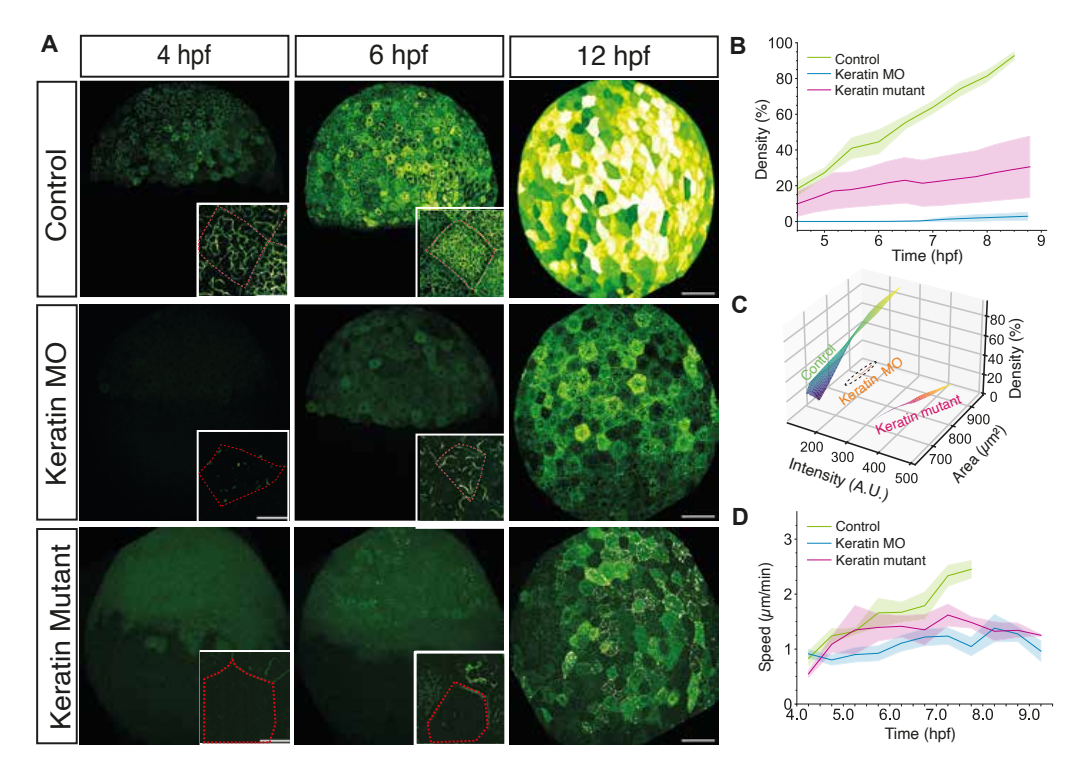


Figure 3.3: Loss of keratin expression diminishes EVL epiboly movements.

Figure 3.3 Loss of keratin expression diminishes EVL epiboly movements

- (A) Maximum intensity projection images of keratin expression in representative Tg(krt18: krt18-GFP) embryos at sphere stage (4 hpf, left column), shield stage(6phf, middle column) and bud stage (10 hpf, right column) with insets on the right lower corner showing single cells with their boundary marked by a red line injected at the one-cell stage with 2 ng control MO (top row), 1 ng krt4 plus 1 ng krt8 MO (middle row), or with TraCr krt4 and krt8 gRNA (krt4/8 crispant F0; bottom row). Scale bar: $100 \mu m$.
- (B) Plot of averaged density of keratin network in individual EVL cells as a function of time (hpf) during epiboly in Tg(actb2:utr-mCherry, krt18:krt18-GFP) embryos injected at the one-cell stage with 2 ng control MO (top row; green, N=4, n=4 embryos), 1 ng krt4 plus 1 ng krt8 MO (middle row; orange, N=4, n=4 embryos), or with TraCr krt4 and krt8 gRNA (krt4/8 crispant F0; bottom row; pink, N=2, n=6 embryos). Error bars as ribbon SD of the mean of individual cells per replicate.
- (C) 3-dimensional (3D) plot of keratin intensity, network density and area of EVL cells as a function of time (hpf) during epiboly in Tg(actb2:utr-mCherry, krt18:krt18-GFP) embryos injected at the one-cell stage with 2 ng control MO (top row; green, N=4, n=4 embryos), 1 ng krt4 plus 1 ng krt8 MO (middle row; orange, N=4, n=4 embryos), or with TraCr krt4 and krt8 gRNA (krt4/8 crispant F0; bottom row; pink, N=2, n=6 embryos). Spread of the surface (width) represents data spread, indicating their variability (SD of intensity and area).
- (D) Plot of EVL epiboly movement speed as a function of time (hpf) during epiboly starting at sphere stage (4 hpf) until late epiboly stages (9 hpf) in Tg(actb2:utr-mCherry, krt18:krt18-GFP) embryos injected at the one-cell stage with 2 ng control MO (top row; green, N=3, n=4 embryos), 1 ng krt4 plus 1 ng krt8 MO (middle row; orange, N=3, n=4 embryos), or with TraCr krt4 and krt8 gRNA (krt4/8 crispant F0; bottom row; yellow, N=2, n=4 embryos). Error bars as SD of the mean of replicates.

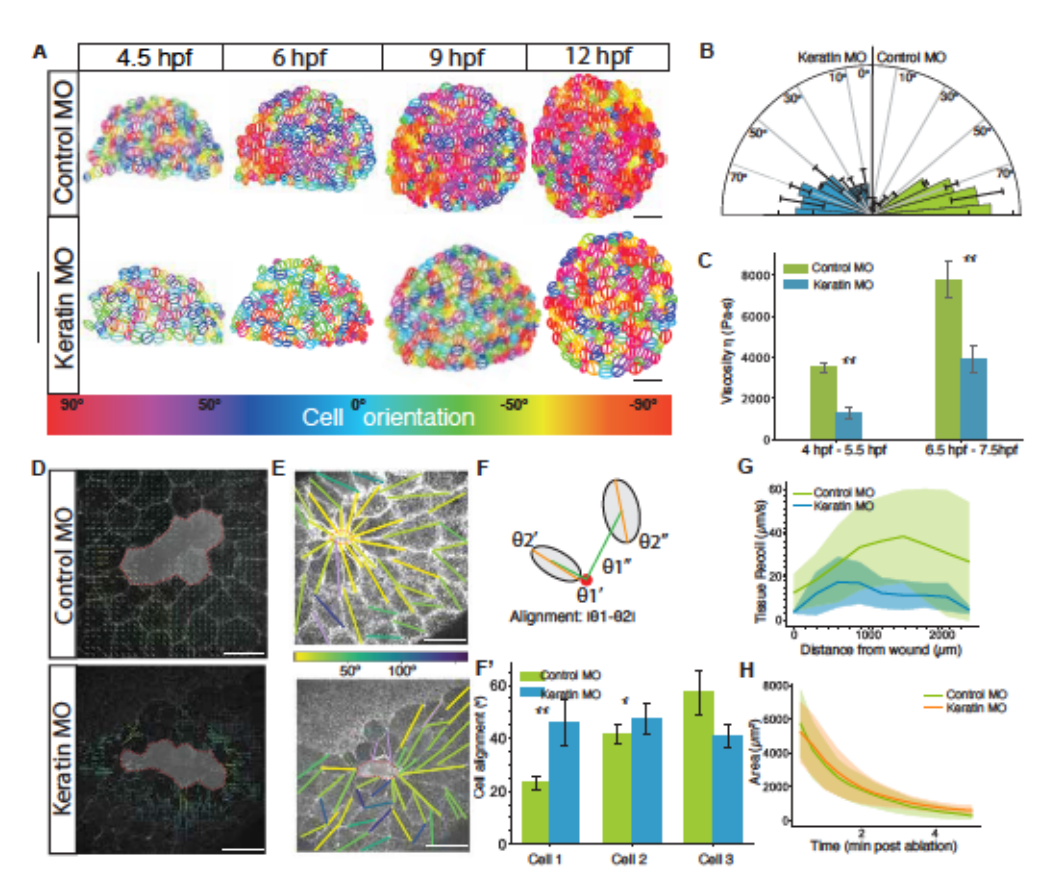


Figure 3.4: Mechanical force percolation within the EVL is dependent on keratin expression.

Figure 3.4 Mechanical force percolation within the EVL is dependent on keratin expression

- (A) Plots of EVL cell orientations with ellipses representing shape descriptors (long and short axis) of individual EVL cells with the line in the middle marking the orientation of the long axis at consecutive stages during epiboly (4.5, 6, 9, 12 hpf) in curvature corrected Tg(actb2:utr-mCherry, krt18:krt18-GFP) embryos injected at the one-cell stage with 2 ng control MO (top row) or 1 ng krt4 plus 1 ng krt8 MO (middle row). Each cell is colour-coded according to the orientation of the axis (hsv) as shown in the colour bar at the bottom (Red: AV axis orientation, blue: dorsoventral/DV orientation).
- (B) Rose plot of EVL cell orientations in curvature corrected Tg(actb2:utr-mCherry,krt18:krt18-GFP) embryos at 6 hpf injected at the one-cell stage with 2 ng control MO (B; N=4, n=93 cells) or 1 ng krt4 plus 1 ng krt8 MO (C; N=4, n=84 cells).
- (C) Bar plots of tissue viscosity measured at the EVL margin using micropipette aspiration at 4-6 hpf and 6-7.5 hpf in Tg(actb2:utr-mCherry, krt18:krt18-GFP) injected at the one-cell stage with 2 ng control MO (B; N=5, n=37 embryos) or 1 ng krt4 plus 1 ng krt8 MO (C; N=5, n=37 embryos).
- (D) Representative quiver plots of EVL tissue recoil flow velocities after cell ablation/wounding (wound centre marked by a red dot) in Tg(actb2:utr-mCherry) embryos at 6 hpf injected with 2 ng control MO (top) or 1 ng krt4 plus 1 ng krt8 MO (bottom). The arrows show the local velocity coloured according to the magnitude (viridis).

- (E) Average radial recoil velocity of the tissue flow plotted as a function of distance from the wound centre (0 μ m) in Tg(actb2:utr-mCherry) embryos injected with 2 ng control MO (top) or 1ng krt4 plus 1 ng krt8 MO (bottom) at successive time points after cell ablation (from yellow to blue; N = 4, n = 23 embryos).
- (F) Left panels: Max intensity projection images of EVL cells in Tg(actb2:utr-mCherry) embryos injected with 2 ng control MO (top) or 1 ng krt4 plus 1 ng krt8 MO (bottom) at 6.5 hpf. Images were overlaid with lines representing their orientation (line angle) and alignment (colour-coded according to the alignment angle; reversed viridis). Right upper panel: schematic showing how cell alignment was determined by measuring the angle from the wound centre (θ 1, green lines) and the cell longest cell axis (θ 2, blue lines). The alignment was calculated by determining the magnitude of the difference between the angle from the wound centre and the cell longest cell axis ($|\theta$ 1- θ 2|) in successive rows of cells around the wound centre. Right lower panel: bar plot (bottom) of EVL cell alignment in Tg(actb2:utr-mCherry) embryos injected with 2 ng control MO (green) or 1 ng krt4 plus 1 ng krt8 MO (blue) upon control MO injection (green) in successive cell rows (cell 1 cell 3) around the wound center. (N = 4, n = 23 embryos).
- (G) Plot of tissue recoil velocity as a function of distance from the wound center in Tg(actb2:utrmCherry) embryos injected with 2 ng control MO (green) or 1 ng krt4 plus 1 ng krt8 MO (blue). N = 4, n = 23 embryos.
- (H) Plot of wound area as a function of time upon ablation of EVL cells in Tg(actb2:utrmCherry) embryos injected with 2 ng control MO (green) or 1 ng krt4 plus 1 ng krt8 MO (orange). N=4, n=23 embryos.

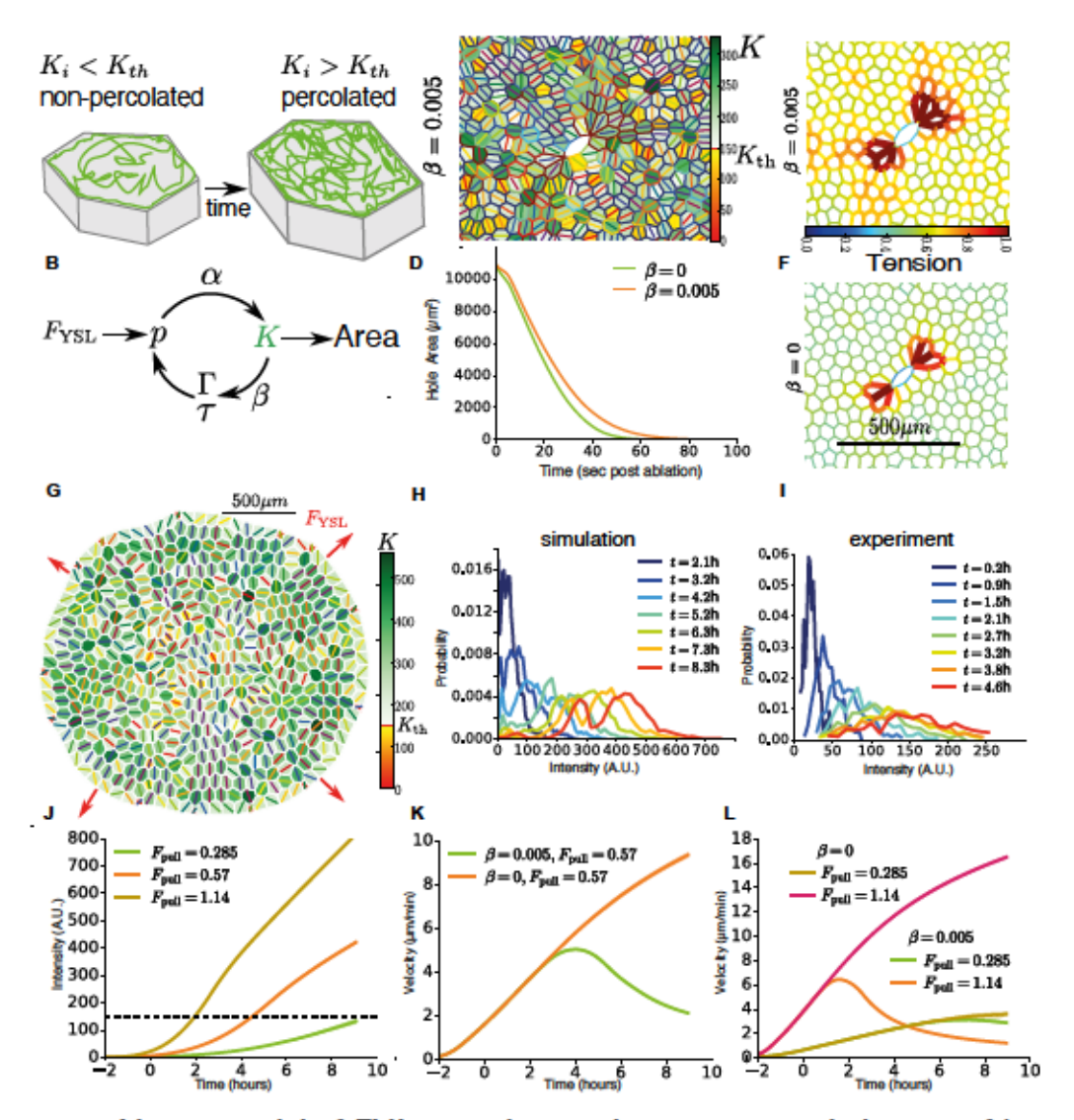


Figure 3.5: Vertex model of EVL spreading in the presence and absence of keratin expression.

Figure 3.5 Vertex model of EVL spreading in the presence and absence of keratin expression

- (A) Plot of extension length of the aspirated EVL tissue in Tg(krt18:Krt18GFP) embryos as a function of time upon micropipette aspiration. Colormap represents developmental time starting at the beginning of epiboly (4 hpf, blue) to later stages (8 hpf, orange).
- (B) Plot of keratin intensity measured inside the pipette in the aspirated EVL tissue in Tg(krt18:Krt18GFP) embryos as a function of time upon micropipette aspiration. Colormap represents developmental time starting at the beginning of epiboly (4 hpf, blue) to later stages (8 hpf, orange).
- (C) Representative plot of extension length as a function of time fit to the modified viscoelastic Maxwell model (inset, schematic representing the model) used to measure parameters for the vertex model.
- (D) Schematic representing a singular model EVL cell showing keratin filaments (green) at two distinct states of the network activity, dependent on the keratin K_i formation: unpercoalted (left, $K_i < K_{th}$, mechanically inactive) and percolated (right, $K_i > K_{th}$, mechanically active)

with K_{th} being the threshold value of K above which the keratin mechanochemical feedback loop becomes activated.

- (E) Schematic diagram of the mechanochemical feedback loop built into the model representing the feedback from pulling forces from the YSL (F_{YSL}) stretching the tissue leading to increased pressure p in the tissue that enhances keratin K formation. This increase in keratin K feedsback into the area A of the cells and increases tissue stiffness Γ and relaxation time τ . This increase in tissue stiffness Γ and relaxation time τ , in turn, feeds back on the pressure p in the tissue.
- (F) Plot of model aspirated tissues heights as a function of time measured in the mean field model. Mean tissue height (dark red line) is represented as solid line over curves representing estimated parameter variability shown as lines with higher transparency (light red lines).
- (G) Plot of model keratin intensities in aspirated tissues as a function of time in the mean field model. Mean keratin intensity (dark green line) is represented as a solid line over curves representing estimated parameter variability shown as lines with higher transparency (light green lines).
- (H) Representative model tissue ablations showing keratin expression at t=30s in a EVL model tissue with periodic boundary conditions and mechanochemical feedback model parameter β =0.05. At t=0s 6 cells are removed to create a hole at the center of the tissue. A tension of 3 μ N is applied on the edges surrounding the removal site to simulate a wound healing process. Colormap on the side represents the keratin intensities of the cells as a function of keratin K with percolated keratin network ($K_i > K_{th}$) appearing in green and unpercoalted ($K_i < K_{th}$) in red-yellow.
- (I) Plot of edge tension at t=30s around the ablated wound site in keratin-deficient (below; β =0) and in wild-type (top; β =0.005) EVL model tissues. Colormap on the right represents the edge tension. Rainbow: 1.0 μ N to 0.0 μ N).
- (J) Plot of wound area (shown in I) as a function of time after ablation in keratin-deficient (β =0; green) and wild-type with (β =0.005; orange) EVL model tissues.
- (K) Representative vertex model of the EVL tissue at mid epiboly depicting intensity of keratin K (green, percolated and red-yellow, unpercolated) and the orientation of the cell elongation shown as a line in the cell centre (red line). The pulling force by the YSL applied at the edge is represented as red arrows pointing outwards. Stage of pulling corresponds to approximately 7.3 hpf in the zebrafish developing embryo.
- (L) Histograms of keratin intensity distributions in simulated tissues as a function of simulated developmental time shown as a colormap of the lines (2.1h violet to 8.3h red.
- (M) Histograms of keratin intensity distributions observed within the individual EVL cells in a representative Tg(krt18: Krt18GFP) embryo as a function of development time during epiboly shown as a colormap of the lines (4.7 hpf violet to 9.1 hpf red).
- (N) Plot of mean keratin intensity in the model EVL tissue as a function of time at increasing pulling forces from the YSL F_{YSL} (color-coded). The threshold level of keratin K_{th} is represented as dotted line above which the mechanochemical feedback becomes active in the model.
- (O) Plot of mean tissue edge velocity in the presence of wild-type pulling force F_{YSL} as a function of time in keratin-deficient (β =0; orange) and wild-type (β =0.005; green) EVL model tissues.

(P) Plot of mean tissue edge velocity in the presence of three different pulling forces (F_YSL) : wild-type forces (orange and purple lines), and forces lower (green and pink lines) and higher (blue and brown lines) than the wild-type value. Solid lines represent wild-type (β =0.005; green, orange and brown lines) and dotted lines keratin-deficient (β =0; blue, purple and pink lines) EVL model tissues.

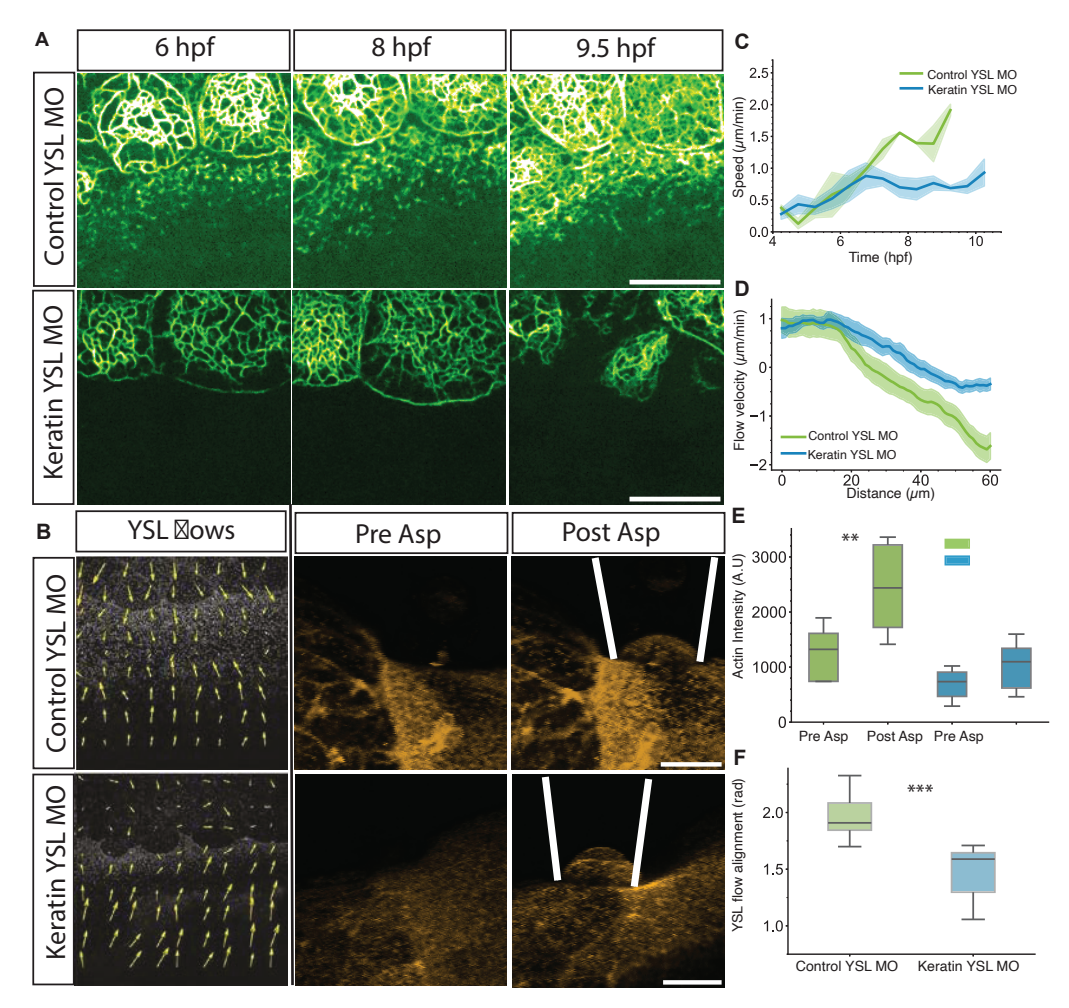


Figure 3.6: Actin flow alignment within the YSL is dependent on keratin expression.

Figure 3.6 Actin flow alignment within the YSL is dependent on keratin expression

- (A) Maximum intensity projections of the keratin network at the EVL-YSL boundary of Tg(krt18:Krt18GFP) embryos at shield (left column), 75% epiboly (middle column) and 95% epiboly (right column) injected with 2 ng control MO (top row) or 1 ng krt4 plus 1 ng krt8 MO (bottom row) into the YSL at sphere stage (3.3 hpf). Scale bar: 25 μ m.
- (B) Maximum intensity projections of the actin network at the EVL-YSL boundary of Tg(actb2:Utrophinmcherry,krt18:KeratinGFP) embryos at 6 hpf injected with 2 ng control MO (top row) or 1 ng krt4 plus 1 ng krt8 MO (bottom row) into the YSL at sphere stage (3.3 hpf) before (Pre Asp, left column) and after (Post Asp, middle column) micropipette aspiration. Scale bar: 25 μ m. Right column: Representative maximum intensity projections of actin and keratin in Tg(actb2:Utrophin-mcherry,krt18:Keratin18GFP) at 3.3 hpf injected with 2 ng control MO (top panel) or 1 ng krt4 plus 1 ng krt8 MO (bottom panel). Images are overlaid with quiver plots of retrograde actin flows within the YSL. Scale bar: 50 μ m.
- (C) Plot of EVL epiboly movement speed as a function of time (hpf) during epiboly in Tg(actb2: Utrophin-mcherry, krt18:Krt18GFP) embryos injected with 2ng control MO (green) or 1 ng krt4 plus 1 ng krt8 MO (orange) into the YSL at sphere stage (3.3 hpf). Error bars as ribbon SD of mean. N=4, n=8 embryos.
- (D) Plot of retrograde actin flow velocity in the YSL as a function of distance from the EVL-YSL boundary in Tg(actb2: Utrophin-mcherry, krt18:Krt18GFP) embryos at shield stage

- (6 hpf) injected with 2 ng control MO (green) or 1 ng krt4 plus 1 ng krt8 MO (orange) into the YSL at sphere stage (3.3 hpf). Error bars as ribbon SD of mean. N = 3, n = 6 embryos.
- (E) Box plot of actin intensity in a fixed region of interest (ROI) within the YSL close to the point of micropipette aspiration before (pre Asp) and after (post Asp) aspiration in Tg(actb2: Utrophin-mcherry, krt18:Krt18GFP) embryos at 3.3 hpf injected with 2 ng control MO (green boxes) or 1 ng krt4 plus 1 ng krt8 MO (orange boxes) into the YSL at sphere stage (3.3 hpf). N=4, n=13 embryos. Boxes represent quartiles of the data and error bars the spread (pvalues: ***<0.001, **<00.1 paired t test).
- (F) Box plot of actin flow alignment within the YSL at 6 hpf in Tg(actb2: Utrophin-mcherry, krt18:Krt18GFP) embryos injected with 2 ng control MO (green boxes) or 1 ng krt4 plus 1 ng krt8 MO (orange boxes) into the YSL at sphere stage (3.3 hpf). Boxes represent quartiles of the data and error bars the spread. N=3, n=6 (***<0.001, paired t test).

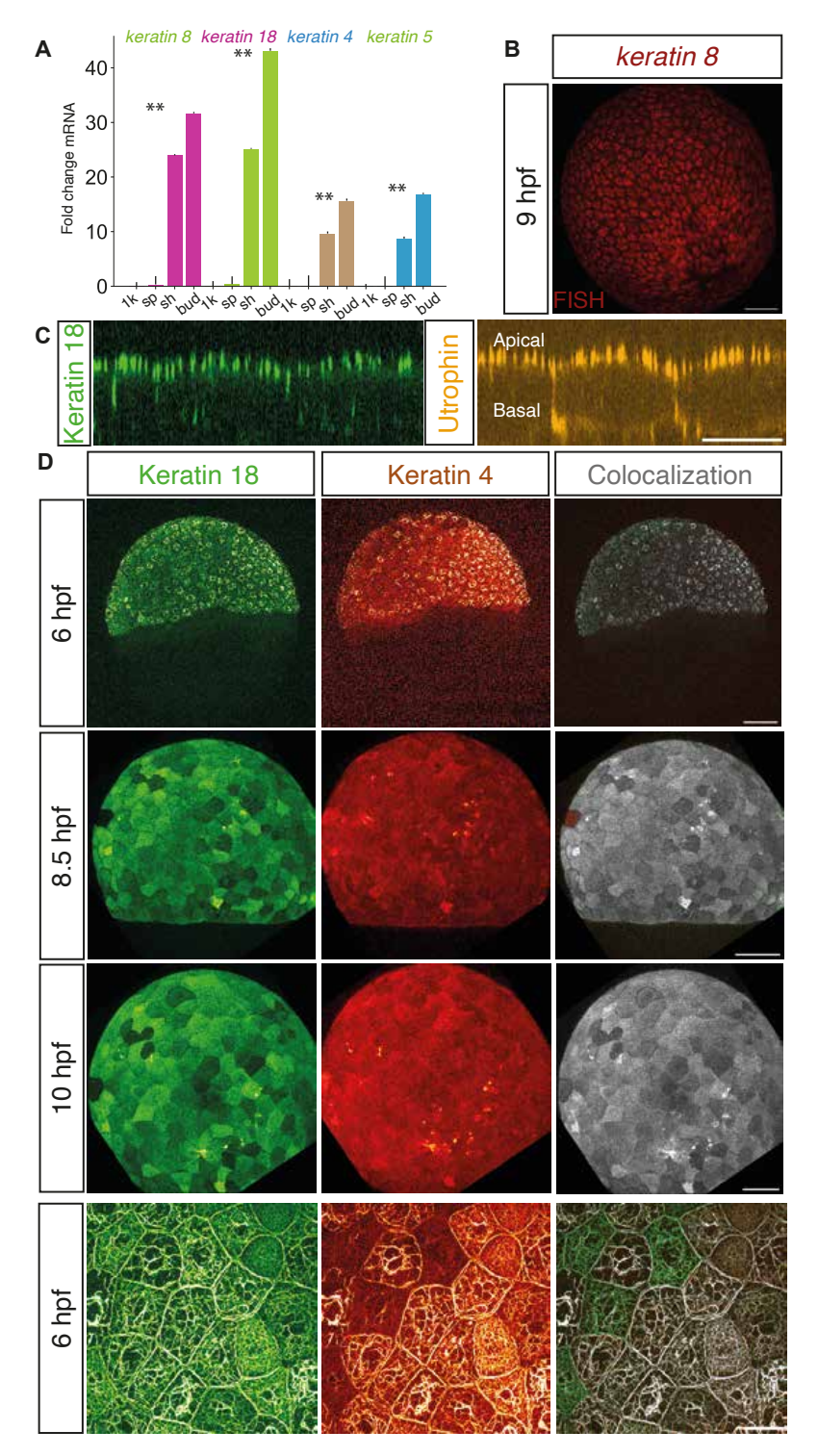


Figure 3.7: Keratin expression and localization during epiboly

Figure 3.7 Supplement 1: Keratin expression and localization during epiboly

- (A) Bar plot of fold change of keratin 18, keratin 8, keratin 4, and keratin 5 expression in embryos at 1K (3.3hpf), 30% epiboly (4.5 hpf), shield (6hpf) and bud (9hpf) stages measured by qPCR.
- (B) Maximum Intensity projections of krt8 mRNA fluorescence via in situ hybridization in WT embryos at 9 hpf. Scale bar: 25 μ m
- (C) Maximum Intensity projections of keratin network in Tg(krt18: Krt18GFP) embryos at

shield (6hpf), 75% epiboly (8.5 hpf) and bud (10 hpf) stages injected of 50pg Krt4-mcherry RNA at the one-cell stage. Left column, keratin 18 (green); middle column, keratin 4 (red); right column, keratin 4 and 18 colocalization (white; co-localization index R below threshold 0.005). Scale bar: 100 μ m

(D) Maximum Intensity projections of keratin network in Tg(krt18: Krt18GFP) embryos at shield (6hpf), 75% epiboly (8.5 hpf) and bud (10 hpf) stages injected of 50pg Krt4-mcherry RNA at the one-cell stage. Scale bar: 25 μ m

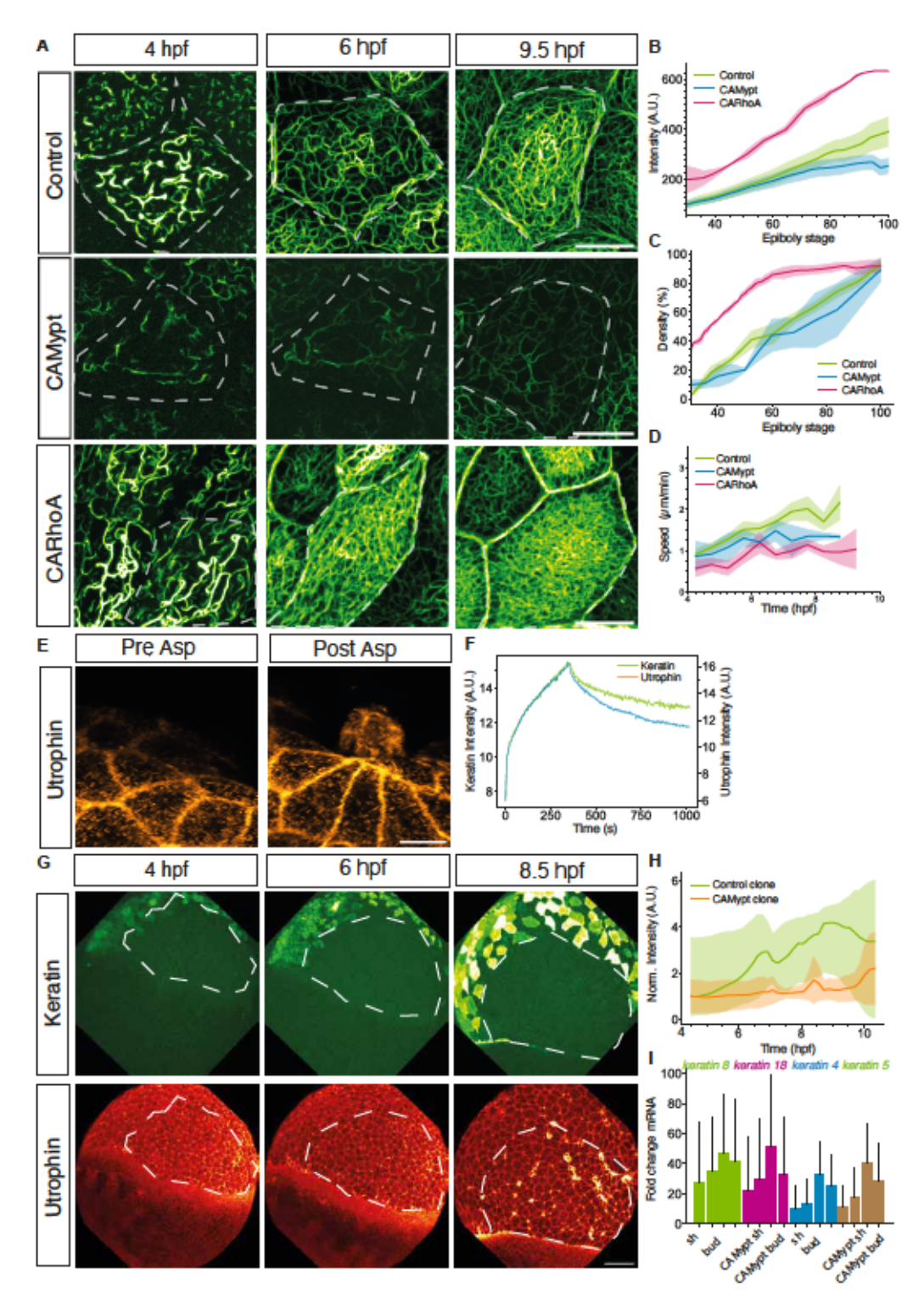


Figure 3.8: Tension-dependent regulation of keratin expression within the EVL

Figure 3.8 Supplement 2: Tension-dependent regulation of keratin expression within the EVL

(A) Maximum intensity projection images of keratin expression in Tg(actb2: Utrophin- mcherry, krt18:Krt18GFP) embryos at sphere (4 hpf, left column), shield (6 hpf, right column), and 90% epiboly (9.5hpf, right column) stages injected with (0.2% phenol red, control, top row), 100pg caMypt (middle row), or 50 pg caRhoA (bottom row) directly into the YSL at 3.3 hpf (control, caMypt) or into marginal cells at 3 hpf (caRhoA) Scale bar: 25 μ m

- (B) Plot of average keratin intensity as a function of epiboly stages in Tg(krt18:KrtGFP) control (green, N=3, n= 5 embryos), caMypt (orange, n=3, n=5 embryos) and caRhoA mRNA injected embryos(pink, N=3, n=4 embryos) at 3.3 hpf into the YSL as described in Figure 2(A- C). Error bars as ribbons SD of mean.
- (C) Plot of average density of keratin network as a function of epiboly stages in Tg(actb2:Utrophin-mcherry, krt18:Krt18-GFP) control (green, N=3, n= 6 embryos), caMypt (orange, n=3, n=4 embryos) and caRhoA mRNA injected embryos (pink, N=3, n=3 embryos) at 3.3 hpf into the YSL as described in (B). Error bars as ribbon SD of mean of individual cells per replicate.
- (D) Plot of EVL epiboly movement speed as a function of time (hpf) during epiboly starting at sphere stage (4hpf) until late epiboly stages (9 hpf) in Tg(actb2: Utrophin-mcherry, krt18:Krt18GFP) embryos injected at 3.3hpf with control (green, N=3, n=6 embryos), caMypt (orange, n=3, n=4 embryos) and caRhoA mRNA (pink, N=3, n=3 embryos). Error bars as ribbon SD of mean of individual cells per replicate.
- (E) Maximum intensity projection images of keratin expression in individual primary cells from Tg(krt18:Krt18GFP) embryos dissociated at 4 hpf (left) and 6.5 hpf (right). The outline of the cell is shown as the red dotted line. Scale bar: 15 μ m

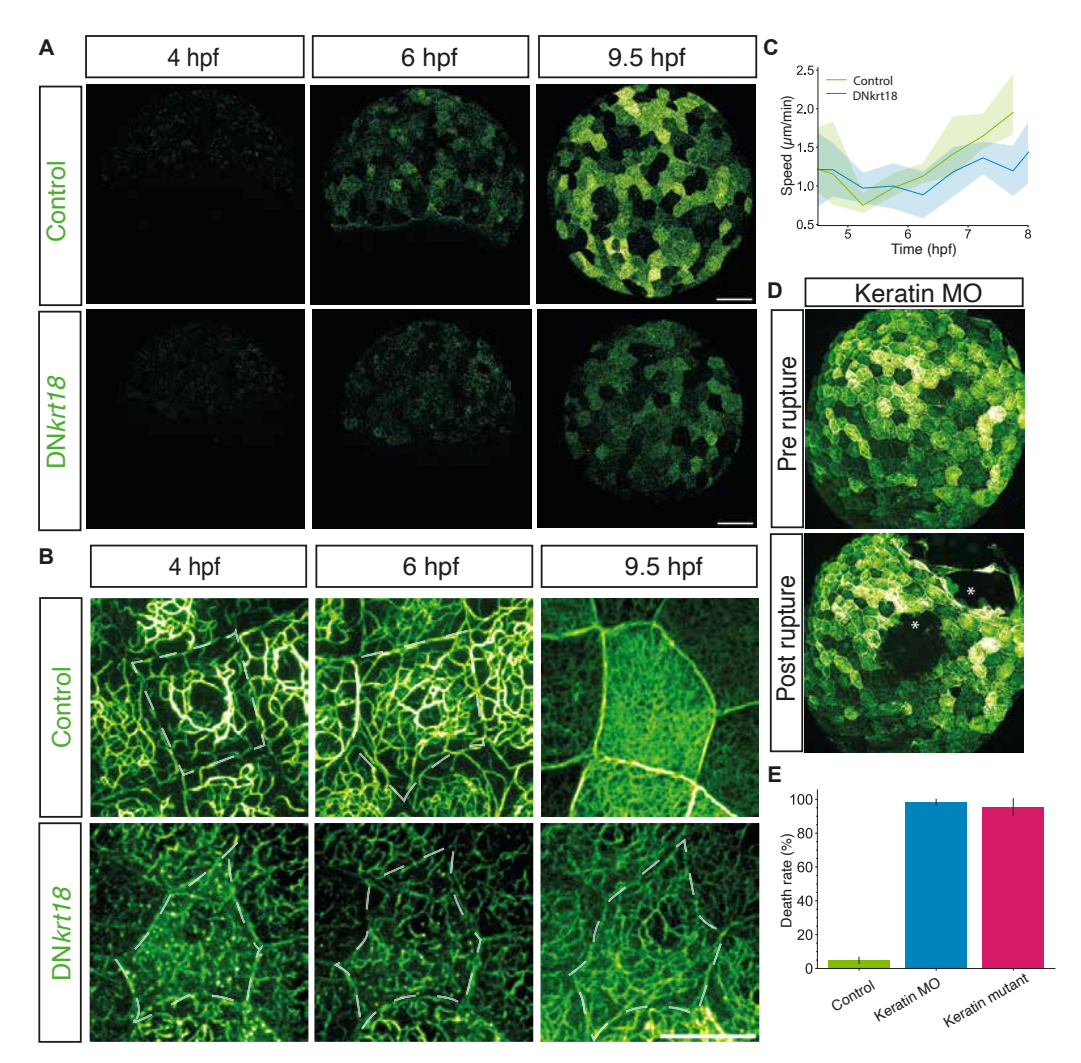


Figure 3.9: Effect of dominant negative keratin 18 expression on keratin network formation and EVL epiboly

Figure 3.9 Supplement 3: Effect of dominant negative keratin 18 expression on keratin network formation and EVL epiboly

- (A) Maximum intensity projection images of keratin expression in Tg(actb2: Utrophin- mcherry, krt18:Krt18GFP) at sphere (4hpf, left column), shield (6phf, middle column) and bud (10 hpf, right column) stages injected with 0.2% phenol red (control, top row) or 150 pg dnKrt18 RNA (bottom row) at one-cell stage. Scale bar: 100 μ m
- (B) Maximum intensity projection images of keratin expression in Tg(actb2: Utrophin- mcherry, krt18:Krt18GFP) at sphere (4hpf, left column), shield (6phf, middle column) and bud (10 hpf, right column) stages injected with 0.2% phenol red (control, top row) or 150 pg dnKrt18 RNA (bottom row) at one-cell stage. Scale bar: 25 μ m
- (C) Plot of EVL epiboly movement speed as a function of time (hpf) during epiboly starting at sphere (4 hpf) until late epiboly (9 hpf) stages in Tg(actb2: Utrophin-mcherry, krt18:Krt18GFP) embryos injected with 0.2% phenol red (control, green) or 150 pg dnKrt18 RNA (orange) at one-cell stage. (N=2, n=6 embryos).
- (D) Maximum intensity projection images of EVL during rupture at 13.5 hpf in Tg(actb2: Utrophin-mcherry, krt18:Krt18GFP) embryos injected with 1ng krt4 plus 1ng krt8 MO at one cell stage showing the EVL before (top) and after the EVL ruptures (bottom).

- (E) Bar plot of quantification of death rate in Tg(actb2:Utrophinmcherry, krt18:Krt18GFP) embryos injected at the one-cell stage with 2ng control MO (top row; green, N=4, n=4 embryos), 1ng krt4 plus 1ng krt8 MO (middle row; orange, N=4, n=4 embryos), or with TraCr krt4 and krt8 gRNA (krt4/8 crispant F0; bottom row; yellow, N=2, n=6 embryos).
- (F) Exemplary plot of tissue extension as a function of EVL tissue aspiration time, displaying a linear response upon aspiration and retraction(green). Plot of fluorescence intensity of keratin as a function of aspiration in the same embryo measured in the medial plane of the pipette in the same embryo (orange)

Figure 3.10: Effect of dominant negative keratin 18 expression on keratin network formation and EVL epiboly

Figure 3.10 Supplement 4: Effect of dominant negative keratin 18 expression on keratin network formation and EVL epiboly

- (A) Exemplary plots of EVL cell orientations with ellipses representing shape descriptors (long and short axis) of individual EVL cells with the line in the middle marking the orientation of the long axis at consecutive stages during epiboly (4.5, 6, 9, 12 hpf) in curvature corrected Tg(actb2:Utrophin-mcherry, krt18:Krt18GFP) embryos injected at high stage (3.3 hpf) directly into the YSL to interfere with keratin network formation within the YSL specifically. Each cell is colour-coded according to the orientation of the axis (hsv) as shown in the colour bar at the bottom (Red: AV axis orientation, blue: dorsoventral/DV orientation).
- (B) Rose plot of EVL cell orientations in curvature corrected Tg(actb2:Utrophinmcherry,krt18:Krt18GFP) embryos at 6 hpf injected at high stage (3.3 hpf) into the YSL with 2 ng control MO (B; N=4, n=93 cells) or 1ng krt4 plus 1ng krt8 MO (C; N=4 n= 84 cells).

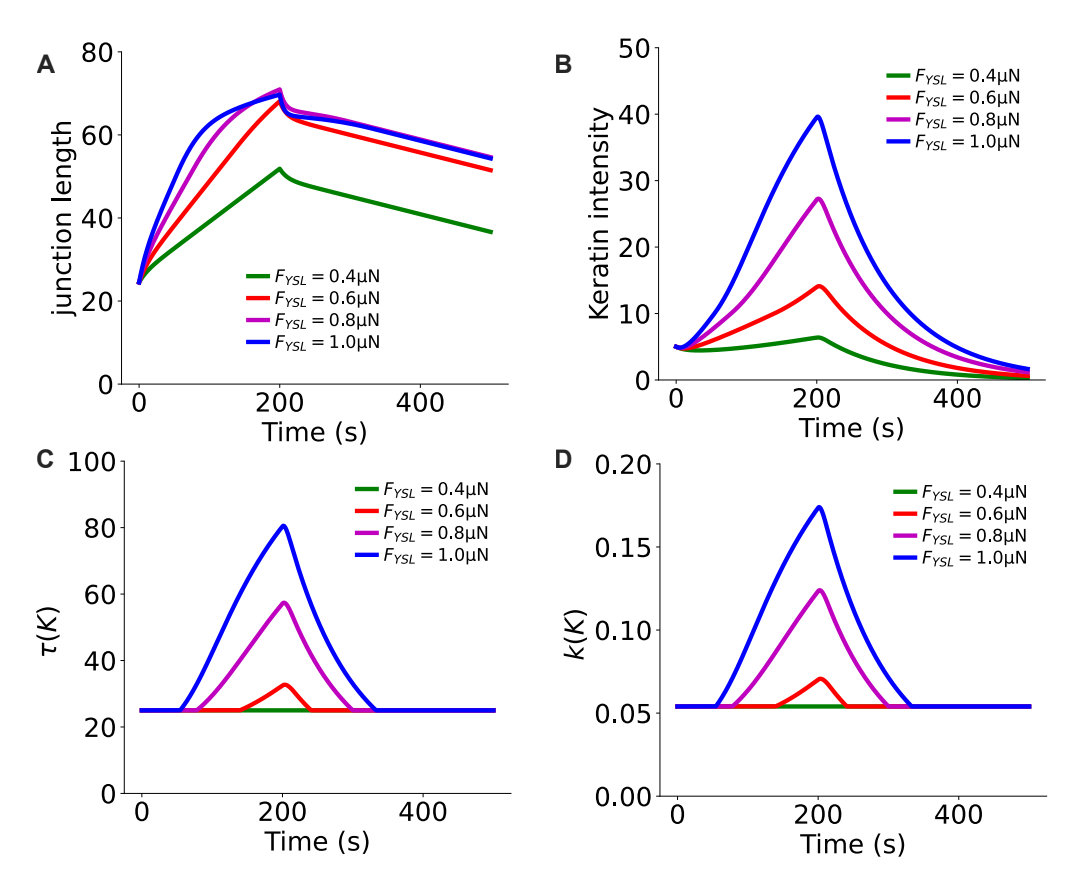


Figure 3.11: Micropipette aspiration experimental data and Maxwell model

Figure 3.11 Supplement 5: Micropipette aspiration experimental data and Maxwell model

- (A) Scatterplot of measured time scales τ_r (blue, square) and τ_r' (green, rhombus) as a function of time during development in the EVL aspiration experiments obtained from fits of the height relaxation to equation (S4) during the aspiration (τ_r , blue) and release phases (τ_r' , green), respectively, using the method described in (Figure 5A-C). Scatter plot of measured time scale τ_κ for the relaxation of the keratin K(T) as a function of time during development as depicted in (Figure 5B) after pipette release (yellow, circle), from a fit to exponential form $e^{-\tau/\tau_\kappa}$. Line plots depict the average with confidence intervals for τ_r (blue), τ_r' (green) and τ_κ (yellow).
- (B) Scatterplot of measured EVL tissue aspiration velocities after aspiration (square, blue), after aspiration but before release (circle, yellow), after release (rhombus, green) as extracted by linear fits to height curves l(t), where $\tau_{release}$ is the time at which the pressure is removed. Line plots depict the average with confidence intervals for l(t>0) (blue), $l\tau_{release}$) (green) and $l(\tau_{release}^-)$ (yellow).
- (C) Scatterplot of tissue relaxation time scales τ during aspiration (square, blue) and τ' during release (circle, yellow) as a function of time during development measured from fits to equation (S4) of the EVL aspiration experiments used to extract Maxwell model parameters (equations (S5)). Line plots over the scatter depict the average with confidence intervals shaded around the line.
- (D) Scatterplot of tissue elastic constant κ_k as a function of time during development, measured from fits to the tissue extension velocities in equation (S5). Line plots over the scatter depict the average with confidence intervals shaded around the line.

3. Results

- (E) Scatterplot of substrate friction coefficient ζ as a function of time during development measured from fits to the tissue extension velocities in equation (S5). Line plots over the scatter depict the average with confidence intervals shaded around the line.
- (F) Scatterplot of internal tissue tension τ as a function of time during development measured from fits to the tissue extension velocities in equation (S5). Line plots over the scatter are the average with confidence intervals shaded around the line.

See SI section 1 for model details.

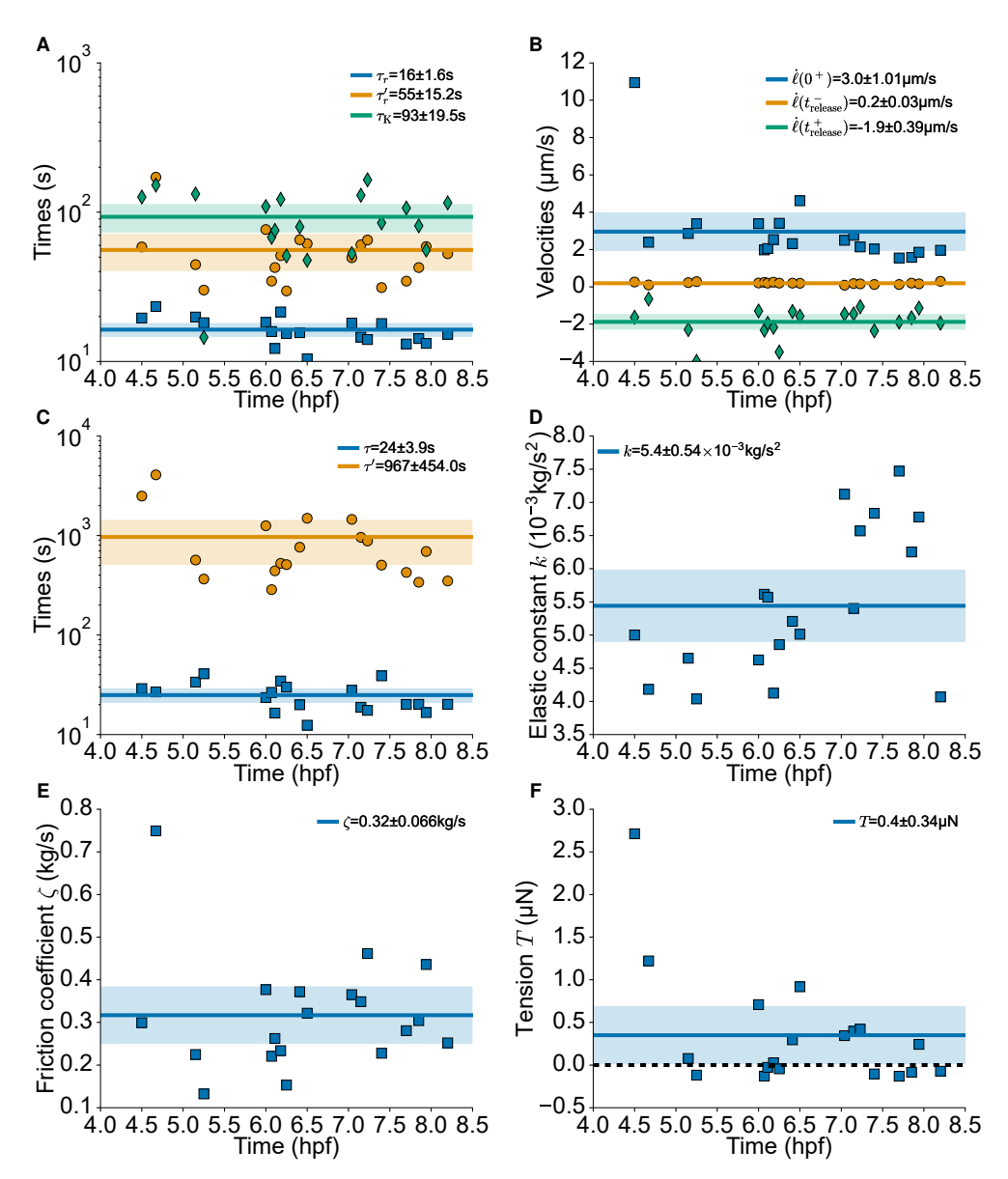


Figure 3.12: Time and velocity scales for the EVL micropipette aspiration experiment and parameters of the Maxwell model

Figure 3.12 Supplement 6: Time and velocity scales for the EVL micropipette aspiration experiment and parameters of the Maxwell model

- (A) Scatter plot of measured time scales τ_r (blue, square) and τ_r' (green, rhombus) in the EVL aspiration experiments from fits of the height relaxation to equation (S4) during the aspiration and release phases, respectively, using the method described in Figure Supplement 5C. Measured time scale τ_{κ} for the relaxation of the keratin $\kappa(T)K(T)$ as depicted in (figure supplement 5B) after pipette release (yellow, circle), from a fit to exponential form $e^{-\tau/\tau_{\kappa}}$. Line plots depict the average with confidence intervals for τ_r (blue), τ_r' (green) and τ_{κ} (yellow).
- (B) Scatter plot of measured velocities in the EVL aspiration experiments as extracted by linear fits to the height curves l(t) (figure supplement 5A) where $\tau_{release}$ is the time where the pressure is removed.
- (C-F) Fits to equation (S4) of the EVL aspiration experiments during aspiration and release inverted to extract Maxwell model parameters (equations (S5)), i.e. tissue relaxation time scales τ during aspiration and τ' during release (C), tissue elastic constant κ (D), substrate

3. Results

friction coefficient γ (E), and internal tissue tension T (F). Line plots over the scatter are the average with confidence intervals shaded.

See SI section 1 for model details.

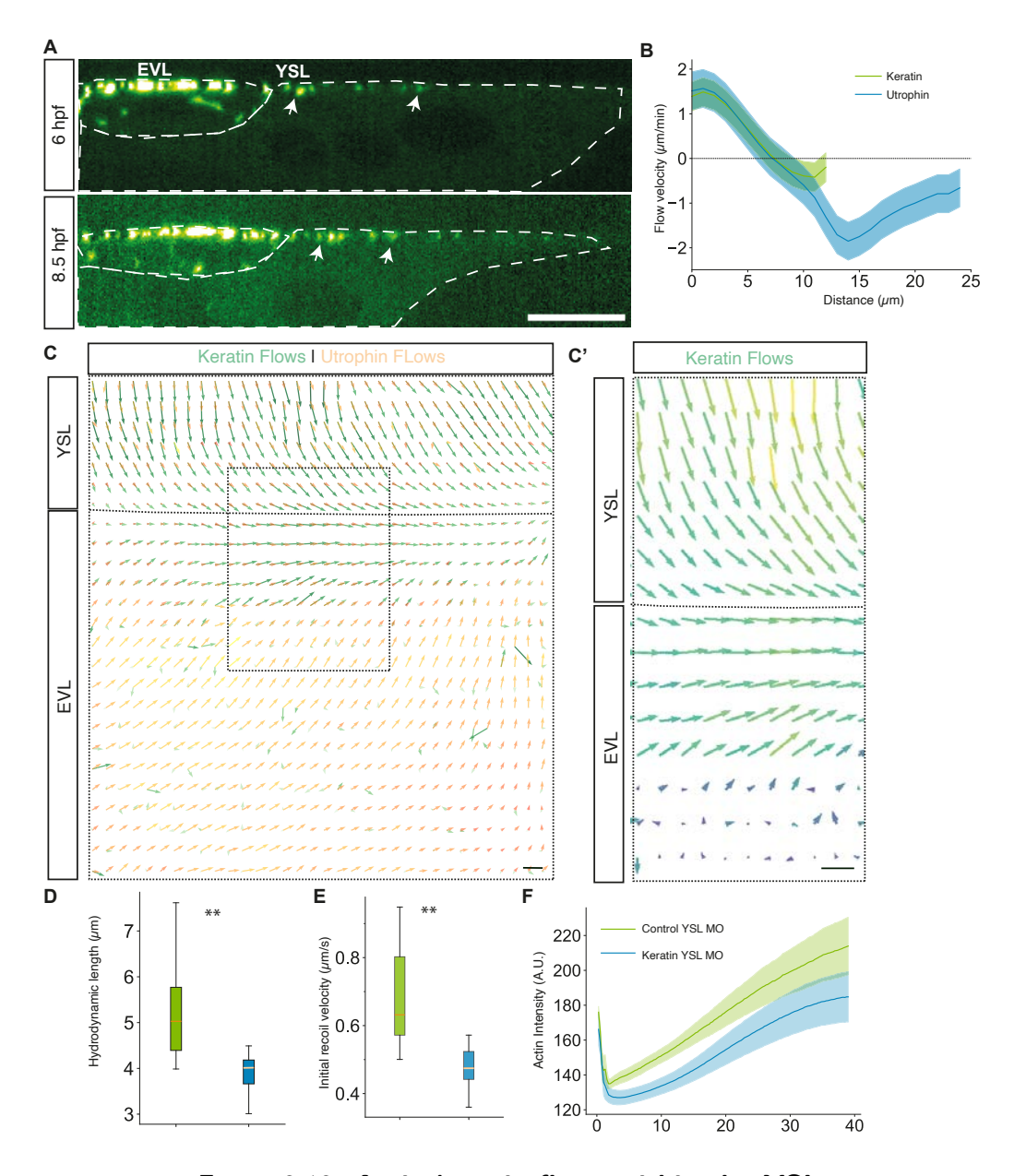


Figure 3.13: Actin-keratin flows within the YSL

Figure 3.13 Supplement 7: Actin-keratin flows within the YSL

- (A) Z-plane reslice image of a cross-sectional view of the YSL at the EVL margin in Tg(actb2:Utrophinmcherry, krt18:Krt18GFP) embryos. EVL and YSL are outlined by a white dotted line, and keratin filaments within the YSL are marked by white arrows. Scale bar: $15~\mu m$.
- (B) Plot of average flow velocity of keratin (green) and actin (orange) within the YSL in Tg(actb2:Utrophinmcherry, krt18:Krt18GFP) embryos measured using PIV as a function of distance from the EVL-YSL boundary.
- (C) Plot of a representative particle image velocimetry flows of keratin filaments (virdis) and actin cortex (plasma) at the EVL-YSL boundary in Tg(actb2:Utrophinmcherry, krt18:Krt18GFP) embryos measured using PIV. The dotted box outlines the region of interest represented in (C') showing a high-magnification view of the keratin flow field (viridis) at the EVL-YSL boundary. Scale bar: $1~\mu m/min$.

3. Results

- (D) Box plot of the hydrodynamic length of the YSL actin network measured by UV-laser cutting of the actin cortex in Tg(actb2:Utrophinmcherry, krt18:Krt18GFP) embryos at shield stage (6.5 hpf) injected with control MO (green, N = 4, n = 15 embryos) or 1 ng krt4 plus 1 ng krt8 MO (orange, N = 4, n = 17 embryos) into the YSL at high stage (**<00.1 paired t test).
- (E) Box plot of initial recoil velocities of the actin cortex after laser ablations in Tg(actb2:Utrophinmcherry, krt18:Krt18GFP) embryos injected with control MO (green, N = 4, n = 15 embryos) or 1 ng krt4 plus 1 ng krt8 MO (orange, N = 4, n = 17 embryos) in the YSL at high stage (**<00.1 paired t test).
- (F) Plot of actin intensity recovery after UV-laser cutting as a function of time measured within a region of interest at the cut within the YSL actin cortex in Tg(actb2:Utrophinmcherry, krt18:Krt18GFP) embryos at shield stage (6.5 hpf) injected with control MO (green, N = 4, n = 15 embryos) or 1 ng krt4 plus 1 ng krt8 MO (orange, N = 4, n = 17 embryos) into the YSL at sphere stage (3.3 hpf).

Video legends

These legends correspond to the movies available as supplementary material that can be downloaded from Videos

Video 1: Keratin expression within the EVL during epiboly Time-lapse of keratin expression (right) and network organization (left) in Tg(krt18:Krt18GFP) embryos during epiboly (4 - 9.5 hpf). Lateral view. Frame rate 11.25 min/frame. Scale bar: 100 (left) and 30 μm (right).

Video 2: Keratin expression within the EVL in embryos with reduced YSL pulling force Time-lapse of keratin expression within the EVL upon reduced pulling forces from the YSL in a representative Tg(krt18:Krt18-GFP) control embryo injected with 0.2% phenol red (left) and an embryo injected with 100 pg CAMypt into the YSL (right) imaged from from 4.5-11 hpf. Lateral view. of the embryos Frame rate 10 min/frame. Scale bar: 100 μm .

Video 3: Keratin network maturation in EVL cells of embryos with reduced YSL pulling force Time-lapse of keratin network maturation in EVL cells upon reduced pulling forces from the YSL in a representative Tg(krt18:Krt18-GFP) control embryo injected with 0.2% phenol red (left) and an embryo injected with 100 pg CAMypt into the YSL (right) imaged from 4.5-7.1 hpf. Lateral view near the EVL-YSL boundary. Frame rate 10 min/frame. Scale bar: 25 μm .

Video 4: Keratin expression within the EVL of embryos with enhanced YSL pulling force Time-lapse of keratin expression upon increased pulling forces from the YSL in representative Tg(krt18:Krt18-GFP) control embryo injected with 0.2% phenol red (left) into the YSL and 50 pg CARhoA into marginal blastomeres at 3.3 hpf (right) imaged from 4.5-10.3 hpf. Lateral view. Frame rate10 min/frame. Scale bar: 100 μm .

Video 5: Keratin network maturation in EVL cells of embryos with enhanced YSL pulling force Time-lapse of keratin network maturation upon increased pulling forces from the YSL in a representative Tg(krt18:Krt18-GFP) control embryo injected with 0.2% phenol red (left) and an embryo injected with 50 pg CARhoA into marginal blastomeres at 3.3 hpf (right) imaged from 4.5-7.5 hpf. Lateral view near the EVL-YSL boundary. Frame rate 10 min/frame. Scale bar: $25~\mu m$.

Video 6: Keratin expression within the EVL of embryos with reduced keratin type II expression Time-lapse of keratin expression in representative Tg(krt18:Krt18-GFP) embryos injected at the one-cell stage either with 2 ng control MO (control, left) or 1 ng krt4 plus 1 ng krt8 MO (right) imaged from 4-15.75 hpf. Lateral view. Frame rate 10.25 min/frame. Points of rupture in keratin morphant embryos are marked with asteriks. Scale bar: $100~\mu m$.

Video 7: Keratin network maturation in EVL cells of embryos with reduced keratin type II expression Time-lapse of keratin expression in representative Tg(krt18:Krt18-GFP) embryos injected at the one-cell stage either with 2 ng control MO (control, left) or 1 ng krt4 plus 1 ng krt8 MO (right) imaged from 4.5-8.4 hpf. Lateral view. Frame rate10 min/frame. Scale bar: $25~\mu m$.

Video 8: Changes in keratin expression upon EVL aspiration Time lapse of EVL aspiration in a representative Tg(krt18:Krt18-GFP) embryo using a 60 μ m pipette imaged by brightfield (left) and confocal (keratin, green, right) microscopy. Z-plane in the centre of the pipette. Frame rate 1 sec/frame. Scale bar: 25 μ m.

Video 9: Changes in keratin expression during EVL wound closure after cell ablation Time lapse of EVL in a representative Tg(actb2:Utrophin-mcherry, krt18:Krt18-GFP) embryo imaged

before (pre) and after (post) UV laser-mediated cell ablation showing keratin (right, green) and actin (left, orange). Frame rate 20 sec/frame. Scale bar: 25 μm .

Video 10: Wound closure in control and keratin-deficient embryos Time lapse of EVL response in representative Tg(actb2:Utrophin-mcherry) embryo imaged before (pre) and after (post) UV laser-mediated cell ablation injected at the one-cell stage either with 2 ng control MO (control, left) or 1 ng krt4 plus 1 ng krt8 MO (right). Frame rate 20 sec/frame. Scale bar: 25 μm .

Video 11: E-cadherin expression in control and keratin-deficient embryos Time lapse of E-cadherin expression in Tg(cdh1-YFP)xt17 embryos injected at the one-cell stage either with 2 ng control MO (control, left) or 1 ng krt4 plus 1 ng krt8 MO (right) starting at the beginning of epiboly (4 hpf) to failure of EVL integrity (14 hpf). Frame rate 10 min/frame. Scale bar: $25~\mu m$.

Video 12: Occludin-b expression in control and keratin-deficient embryos Time lapse of Occludin b expression in Tg(oclnb-GFP)pd1126 embryos injected at the one-cell stage either with 2 ng control MO (control, left) or 1 ng krt4 plus 1 ng krt8 MO (right) starting at the beginning of epiboly (4 hpf) to the end of epiboly (10 hpf). Frame rate 10 min/frame. Scale bar: 25 μm .

Video 13: Jup-a expression in control and keratin-deficient embryos Time lapse of Jup-a expression in Tg(her4.1:jupa-EGFP) embryos injected at at the one-cell stage either with 2 ng control MO (control, left) or 1 ng krt4 plus 1 ng krt8 MO (right) starting at the beginning of epiboly (4 hpf) to the end of epiboly (10 hpf). Frame rate 10 min/frame. Scale bar: 25 μm .

Video 14: Simulated EVL wound closure in model with and without keratin feedback onto mechanics Time lapse of simulated wound closure following ablations in EVL model tissues without keratin mechanical feedback ('keratin deficient', top) and with keratin mechanical feedback ('control', bottom). Keratin concentration K_i in the cell is shown by colour (K_i : 0-150 red-yellow, K_i : 150-350 green). Tensile stress in the tissue t_i from the junctional tension of the cells around the wound is shown by the colour of the cell edges (rainbow t_i : 0.0 – 0.6).

Video 15: Simulated EVL tissue undergoing epiboly Time lapse of simulated EVL model tissue being stretched by radially outward forces increasing with time applied on the margin of the tissue, simulating the forces generated by the YSL on the EVL edge in the embryo. Keratin intensity K_i shown as the colour of the cells (left) increases with time in response to the stress experienced by the tissue under this force, starting from unpercolated levels ($K_i < K_{th}$, red-yellow) and progressing in each cell over the threshold keratin levels to percolated levels ($K_i > K_{th}$, green). Elevation of keratin levels in each cell over the threshold level is stochastic due to the heterogeneity in the mechanical effects on the disordered tissue. Tensile stress in the tissue t_i is shown by the colour of the cell edges (rainbow t_i : 0.0 - 0.6).

3.2 Keratin promotes persistence of AJs and TJs

Keratin morphants and mutants both showed large-scale defects in tissue properties and epithelial integrity. To test whether this effect was due to the loss of junctional components, we observed the localization of some adherens junction and tight junction components in the EVL after knocking down keratin 4/8. We utilized the keratin morpholinos to knock down both m keratin 4/8 and observed changes in fluorescent protein fused junctional constructs localization in the EVL.

3.2.1 Adherens junctions are dependent on keratin accumulation

For changes in adherens junctions, we utilized an Ecad knock-in line visualizing the endogenous Ecadherin via fluorescence (Fig 3.1 A). Ecadherin fluorescence intensity measured via live imaging Tg(mlanYFP)xt17 cdh1-YFP embryos during epiboly initially decreased until the shield stage (6 hpf) but then steadily increased as epiboly progressed (Fig 3.1 B). We observed that the fluorescence intensity of E-cadherin increased further once blastopore closure occurred (Fig 3.1 B). In keratin morphants, however, this increase was not observed (Fig 3.1 A and B). Instead, the keratin morphants showed an initial decrease similar as in control, followed by maintenance of a lower fluorescence intensity than that of the corresponding time points in the control. However, after blastopore closure, all junctional association of Ecad was lost in the EVL cells (Fig 3.1 B). This loss of Ecad localization preceded the break of epithelial integrity observed in morphants during the somitogenesis stages of development.

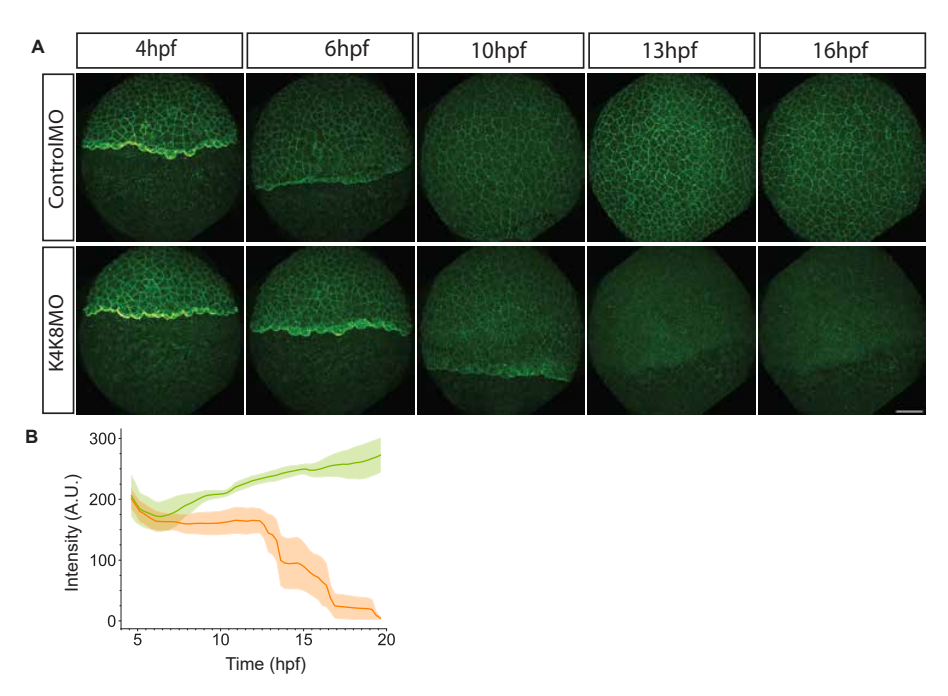


Figure 3.14: Ecadherin expression in the EVL upon keratin knockdown A Max intensity projection images of Ecad expression in Tg(mlanYFP)xt17 cdh1-YFP embryos upon control MO (top) and keratin 4/keratin8 MO (bottom) injection over developmental stages. Scale bar 100 μm .

B Plot of average Ecadherin intensity within the epiblast as a function of time during development (4.5hpf to 20 hpf) in control MO (green) (N=4, n=6 embryos) and keratin MO (orange)(N=4, n=7 embryos.) injected Tg(mlanYFP)xt17 cdh1-YFP embryos. Error bars as ribbons SD of mean.

The majority of the initial decrease could be attributed to the decrease of Ecad accumulation at the YSI as reported before [174]. However, the loss observed in the morphants later in development was specific to the loss of junctional accumulation in the EVL. This decrease did not coincide with the global breakdown of epithelial integrity observed in the EVL, but could potentially play a role in the initiation of local junctional breaks that occured as the epithelium is stretched.

It is interesting, however, that these defects in integrity and loss of adherens junctions are observed only later during development, while the effects observed due to loss of keratin have direct mechanical effects early during development with catastrophic consequences.

3.2.2 Tight junction components require keratin for junctional association

Tight junctions play a crucial role in maintaining epithelial integrity, forming a barrier that helps maintain homeostasis. Tight junction components accumulate increasingly in the EVL as epiboly progresses. Tight junction proteins accumulate during epiboly, with the expression of their components observed as apico-basal polarity is established in the forming EVL [174, 175].

We observed that some tight junction components were mislocalized upon keratin knockdown in the embryo. We observed that OccludinB-GFP fluorescence measured in TgBAC(oclnb-GFP)pd1126 upon control MO injection (Fig 3.2 A). Occludin B fluorescence, during epiboly, increased on EVL-EVL junctions, as epiboly progressed. Occludin B fluorescence was negligible before initiation of epiboly, regarding the maternal deposition observed in the yolk. Some embryos also showed an additional accumulation of Occludin in the nucleus; however, this accumulation was not consistently observed among different clutches of embryos from the same parents (data not shown). In keratin morphant embryos, the accumulation of Occludin B on the junctions was perturbed, and junctions lacked any Occludin B junctional accumulation (Fig 3.2 A and B). The yolk maternal deposition and the nuclear accumulation were unperturbed in the morphants.

ZO1 localization, on the other hand, was unperturbed upon keratin knockdown.

The lack of occludin but not ZO1 junctional accumulation during epiboly suggested a perturbation of junctional barriers, but not complete loss of barrier integrity upon keratin loss in the EVL. This perturbation underscores the critical role of keratins in maintaining epithelial barrier integrity beyond mechanical resilience. In keratinocytes, it has been suggested that this interaction with barrier proteins depends indirectly through changes in resilience leading to formation of actin stress fibers [176]. In the EVL, such fibers are unseen. However, the clear junctional association of the rim network could play spatio-temporally regulated roles in junctional maintenance.

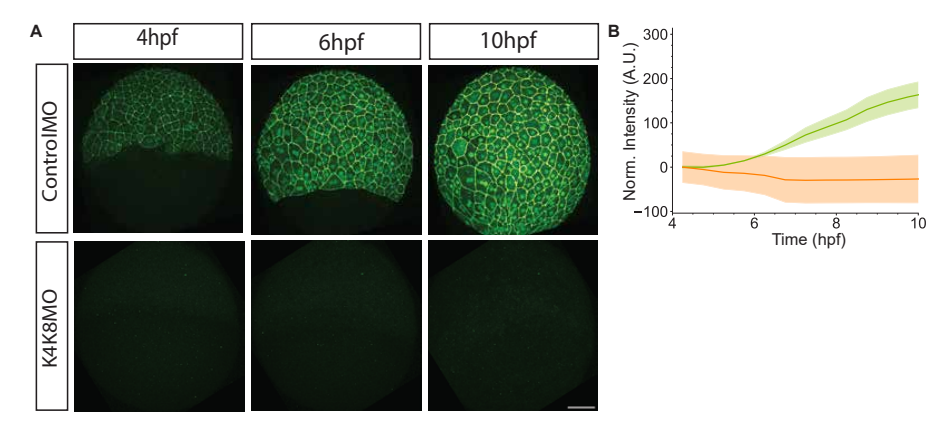


Figure 3.15: Occludin-GFP expression in the EVL upon keratin knockdown A Max intensity projection images of Occludin B expression in TgBAC(oclnb-GFP)pd1126 embryos upon injection of control MO (top) and keratin 4/keratin8 MO (bottom) embryos over epiboly stages. Scale bar 100 μm.

B Plot of average normalized Occludin B intensity within the epiblast as a function of time during development (4.5hpf to 10 hpf) in control MO (green)(N=3, n=5 embryos) (nand keratin MO (orange)(N=3, n=6 embryos) injected TgBAC(oclnb-GFP)pd1126 embryos. All curves were normalized to measure the increase over the initial intensity. Error bars as ribbons SD of mean.

3.3 Microtubular and Actin interactions stabilize keratin networks

Interactions with the microtubular cytoskeleton have been extensively studied for vimentin intermediate filaments, with even evidence for direct transport and interactions with microtubule networks [177]. However, such interactions with microtubules have not been observed for keratin intermediate filaments. In the EVL, we observed evidence for keratin organization and structure dependent on the organization of microtubules.

3.3.1 Nocadazole treatment leads to disorganized keratin network organization

We detected keratin expression in embryos subjected to $100~\mu M$ nocodazole treatment either prior to the onset of epiboly or at the shield stage (6 hpf), when the keratin network was more organized. Disruption of microtubules at early stages (3.5 hpf) impaired the temporal progression of keratin network assembly, interfering with initial minifilament formation as well as keratin enrichment at cell–cell junctions and around the nucleus (Fig 3.3 A). Using Dclk-GFP as a microtubule marker, we confirmed the efficacy of nocodazole treatment, which led to a rapid loss of Dclk signal in the EVL and a more gradual disassembly of the microtubule network in the YSL (Fig 3.3 A).

Despite these cytoskeletal perturbations, total keratin expression levels remained comparable to those of untreated controls (Fig 3.3 B). These findings indicate strongly that the increase of keratin during epiboly is largely determined by the mechanical feedback to the stress faced. However, through these experiments, we observed unique changes in the keratin network structure at the filament scale, suggesting that microtubules may be essential for organizing the network into the classical rim and spoke structure of intermediate filaments in the EVL.

Microtubule dissolution after shield stage, however, showed an arrest of network maturation

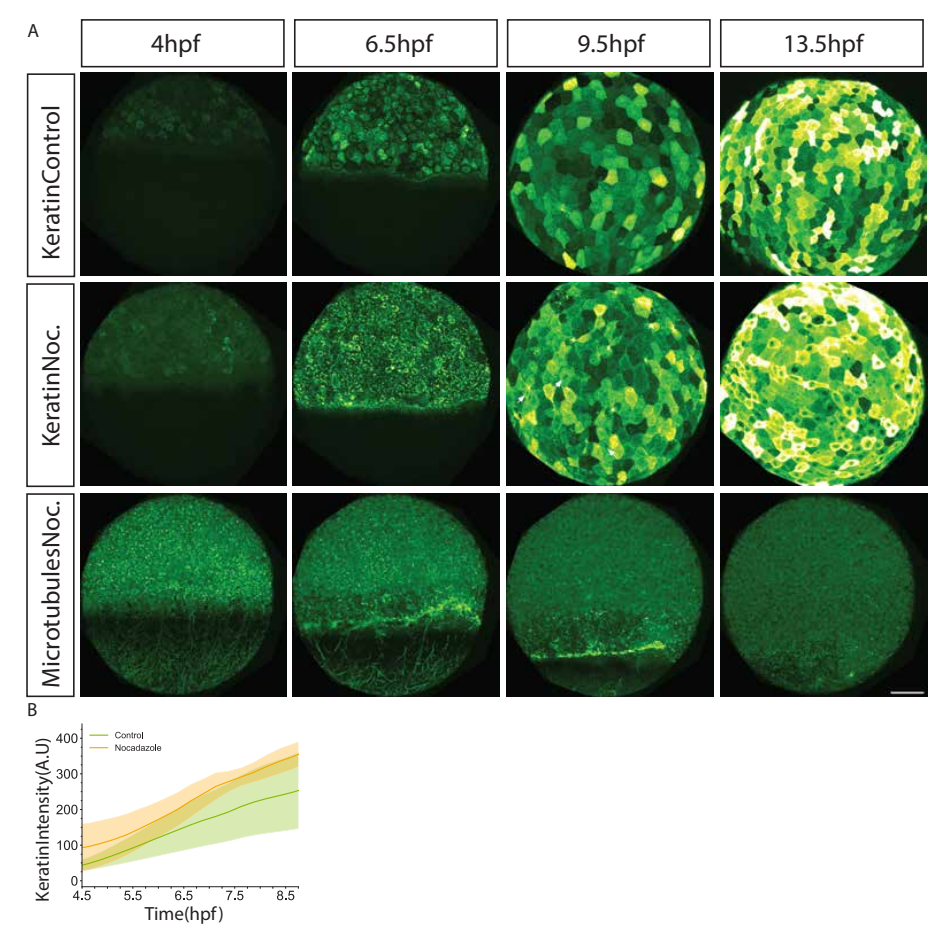


Figure 3.16: Keratin structure upon dissolution of microtubules before epiboly initiation A Max intensity projection images of keratin 18 expression in Tg(krt18:krt18-GFP) embryos upon treatment at 3.5 hours post-fertilization with DMSO control (top) and Nocadazole (middle) embryos over epiboly stages. Max intensity projection of microtubule expression in Tg(XIEef1a1:dclk2-GFP) embryos upon treatment with Nocadazole (bottom) over epiboly stages. Scale bar 100 μ m.

B Plot of average keratin intensity as a function of time (hours post fertilization) in Tg(krt18:KrtGFP) control (green, N=4, n= 5 embryos) and Nocadazole treatment (orange, N=4, n=6 embryos)

dependent on the level of expression of keratin in the cells (Fig 3.4). Cells exhibiting a higher expression and consequently a higher densly matured network progression was as observed in control cells. However, cells with a sparse network and limited distribution of keratin showed an arrested, delayed maturation, with some cells showing thick bundles that failed to branch and percolate throughout the cell.

Most notably, both of these treatments lead to peculiar holes at the nucleus in the network. These holes were created most prominently after 80% network density was reached, where the network looked percolated on the apical surface. Additionally, when microtubules were dissociated early in epiboly, the junctional association of keratin was perturbed.

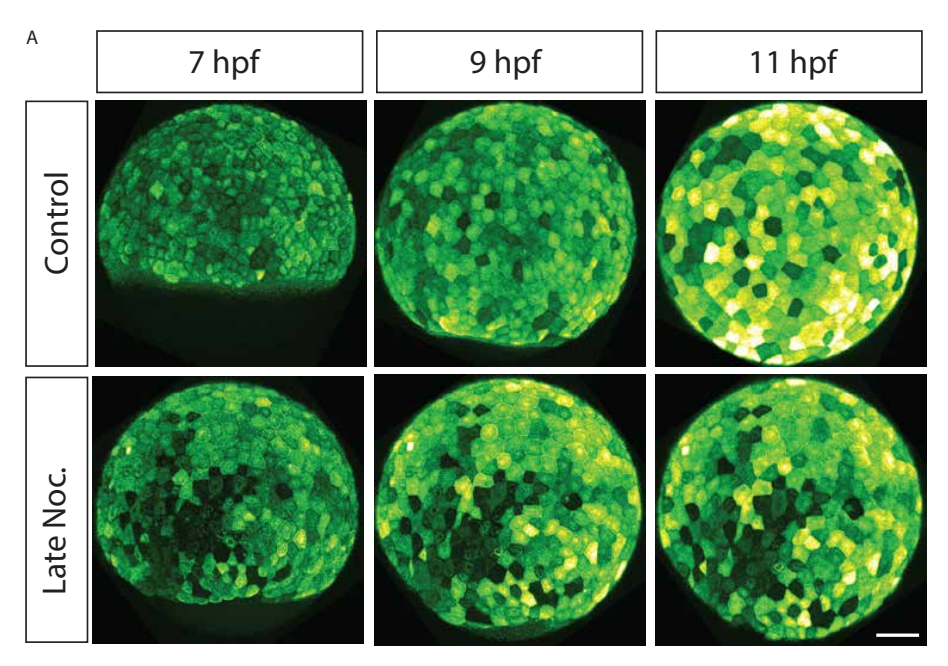


Figure 3.17: Keratin structure upon dissolution of microtubules after shield stage A Max intensity projection images of keratin 18 expression in Tg(krt18:krt18-GFP) embryos upon treatment at 5.5 hours post-fertilization with DMSO control (top) and Nocadazole 20 μ M(middle) embryos over epiboly stages. Scale bar 100 μ m.

3.3.2 Junctional keratin association is perturbed upon microtubule dissociation

We observed that early dissolution of microtubules leads to perturbed network dynamics, especially during the transition from the minifilament stage to connected filaments and further on to the junctional transition. We observed a keratin expression level-dependent perturbation of filament formation. Cells that would show a greater amount of keratin expression showed a similar initial network density as those seen in similarly expressing control cells. However, cells that were lower in expression showed perturbed minifilament formation at the apical surface. The network progression from minifilaments to longer filaments in higher-expressing cells showed thicker bundles that did not mature into denser networks at the same dynamics as seen in control cells.

All cells showed keratin expression as lower intensity cells showing bigger filaments without characteristic initial minifilaments at the apical surface being observed. Instead these cells showed a sparse network of thick filaments. On average upon nocadazole treatment the networks showed reduced connectivity and slower network maturation dynamics (Fig 3.5). An interesting observation to note was that the movements of the filaments were exaggerated as compared to the controls, which could arise due to perturbed keratin attachments in a microtubule-dependent process.

Additionally, we also observed perturbed junctional association of keratin filaments when microtubules were disrupted. Junctional filaments showed larger deviations, exhibiting undulating filaments along the junctions upon nocadazole treatment as compared to control embryos. Occasionally, we also observed disruptions of junctionally associated filaments or dynamic movements of the filaments towards the contractile junctions (Fig 3.6). These events lead to a collapse of the formed filaments towards the junction. This, however, was only observed in early treatments, suggesting a temporal dependence on this interaction with the microtubules.

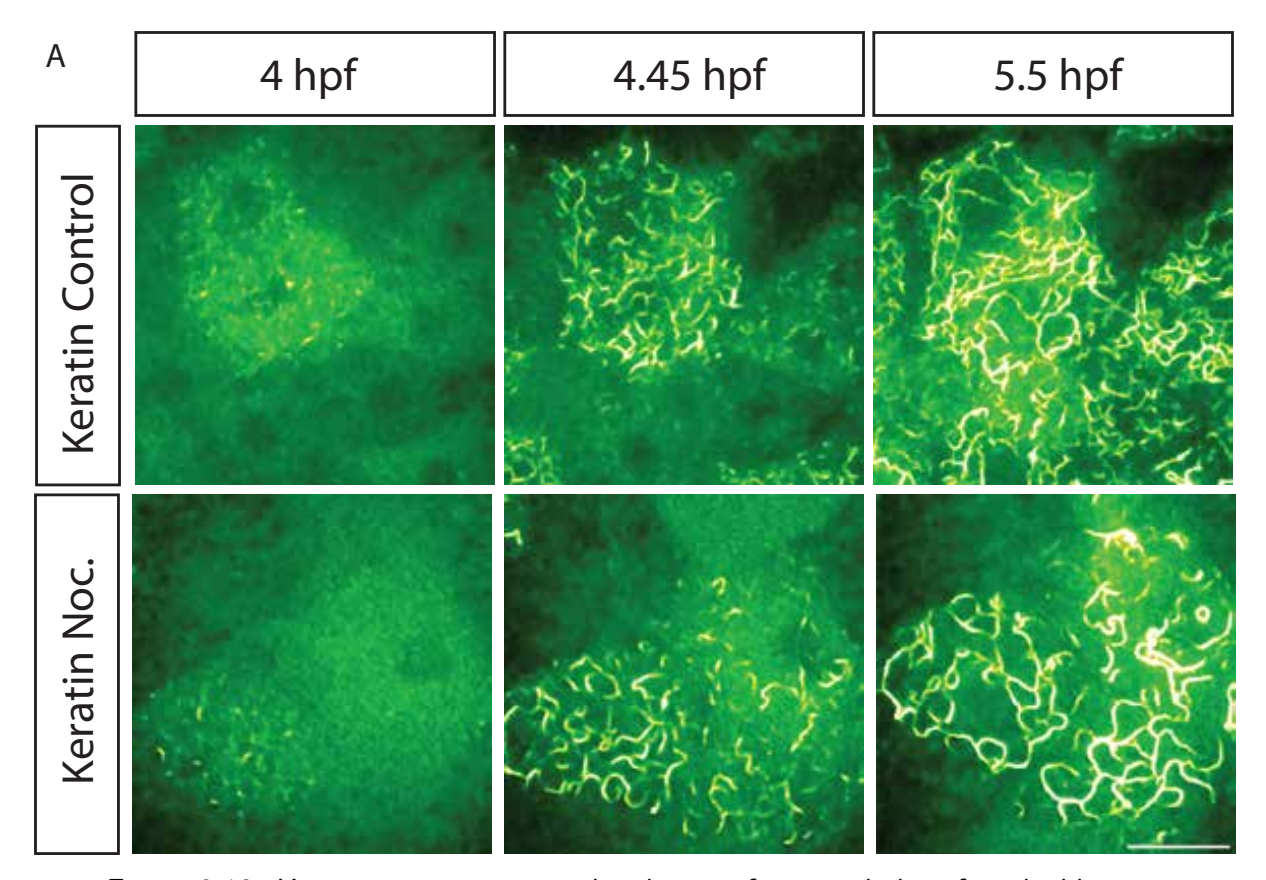


Figure 3.18: Keratin structure upon dissolution of microtubules after shield stage bryos A. Max intensity projection images of keratin expression in Tg(krt18:krt18-GFP) emat early stages with DMSO-treated controls (top) and Nocadazole treatments(bottom). A cluster of cells for each condition are followed from initial minifilaments to network before junctional transition from 4hpf to 5hpf. Scale bar: 25 μ m

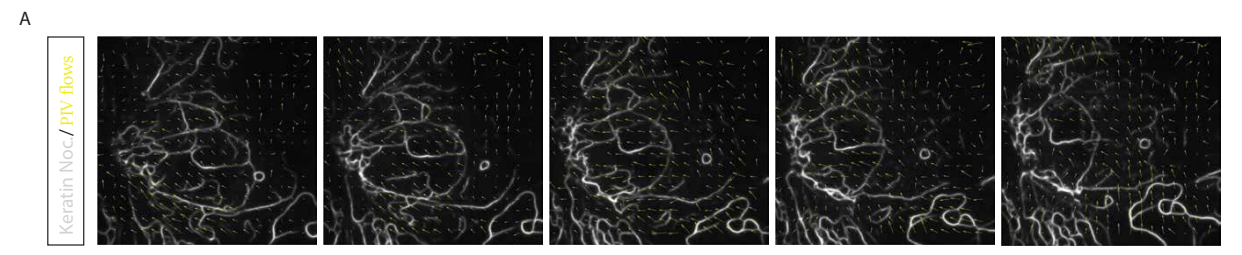


Figure 3.19: Keratin structure upon dissolution of microtubules after shield stage bryos A. PIV flow graphs on consecutive frames of a junctional flow event of keratin filaments in Tg(krt18:krt18-GFP) upon early Nocadazole treatments. Keratin filaments are shown in grey wherease PIV flow vectors are represted as yellow arrows. Each frame represents the instaneous flow in 2 min intervals as the network clears in the cell.

Once the network was formed, maintenance was not dependent on microtubules; however, its maturation and localization could be regulated by a microtubule-dependent process.

3.3.3 Nuclear keratin cage regulated by a microtubule dependent process

To further understand the nuclear hole phenotype, we imaged keratin filaments at high spatiotemporal resolution (Fig 3.7). Interestingly, we observed the nuclear holes in most

cells regardless of the amount of keratin. The holes appeared most often after 8 hours of development, when the network was well developed.

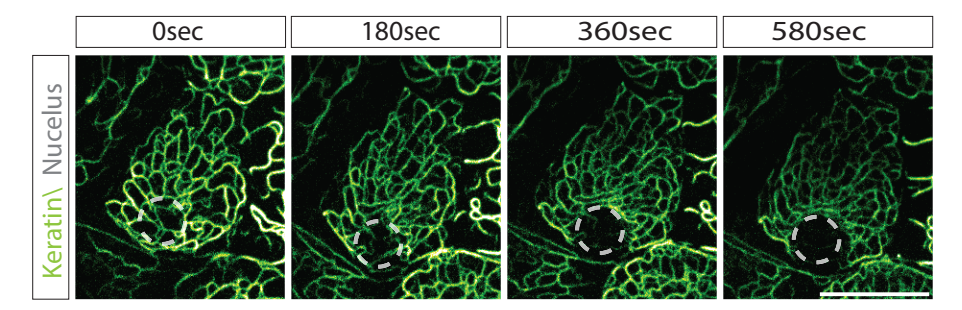


Figure 3.20: Keratin structure reorganization leading to clearing around the nucleus upon microtubule dissolution

A Maximum intensity projection image of keratin expression in Tg(krt18:Krt18GFP) embryos upon nocadazole treatment, showing the nuclear outline as a dashed line. Scale bar: 25 µm

We hypothesize that as the cells flattened, the filaments could be pushed away from the nucleus. As the cells flattened, the nucleus could be seen deforming the filament structure in the vicinity. Filaments were directed to the vicinity with deformations, rearranging filaments to the periphery of the nucleus instead of organizing over the nucleus as in control embryos. The reorganization time scale and tracking movements of the filaments around the nucleus suggested a direct contractility and physical occlusion of filaments around the nucleus. This suggests that currently unknown microtubule-mediated processes are involved in the nuclear lamina attachment of keratin filaments.

Intermediate filaments have long been known to work synergistically with other cytoskeletal systems both in the cytoplasm and in the nucleus. In the nucleus, these interactions are mainly made through nesprin proteins that mediate direct interactions with the nuclear lamina[88?]. We hypothesize that the localization of nesprins could be microtubule-dependent in the later stages of epiboly.

CHAPTER 4

Discussion

Keratins have always been thought to be important as a "security belt" essential for mechanical resilience functions in cells [178]. While intermediate filaments are broadly important in stabilizing cells, their roles in dynamic interactions with other developmental cytoskeletal systems are largely unknown. Our findings reveal a sophisticated mechanical interplay in which keratins orchestrate a balance between tissue spreading forces and structural resilience during zebrafish epiboly movements.

In our work, we elucidate a mechanistic role of keratins in affecting tissue properties as well as a mechanosensitive cross-talk between the keratin network maturation and hitherto unknown functions in actin mechanosensation. We observed that keratins are the first cytoplasmic intermediate filaments that are expressed in the zebrafish embryo. Specifically, they are expressed right at the beginning of gastrulation movements (epiboly) in the newly formed epithelial tissue, the EVL. Generally, keratin proteins form heterodimeric pairs consisting specifically of one type I (acidic) and one type II (basic) keratin. In zebrafish, the keratin gene family displays a notably different genomic organization compared to mammals, especially with respect to the organization of keratin Type II genes. Zebrafish possess at least 17 type I keratin genes distributed across five chromosomes, but only three identified type II keratin genes located on two chromosomes [179]. Expression data from our studies and previously published RNA transcriptomic analyses indicate that all three type II keratins are actively expressed in the zebrafish's enveloping layer (EVL) during early embryonic development [180]. In contrast, only a subset of type I keratins is expressed at this stage with keratin 18 being the most expressed gene. Additional type I keratins become expressed progressively as the epithelium further differentiates after gastrulation is completed, as seen in the periderm of zebrafish [98]. These genes, scattered throughout the genome rather than clustered, have seemingly consolidated essential functional roles. In zebrafish specifically, keratin gene expression peaks prominently in the enveloping layer (EVL) and continues robustly within epidermal lineages during larval developmental stages, underscoring their critical developmental roles [180].

A recent intriguing discovery in zebrafish concerns the distinct differences in isoforms of type I and type II keratin proteins compared to mammals such as humans and mice. In most mammals, these keratin pair genes are tightly correlated in their genomic position and expression patterns even when they are not in the same gene locus [179, 181]. All terrestrial vertebrates possess two distinct keratin gene clusters: one for type I (acidic) keratins and another for type II (basic) keratins. Phylogenetic and genomic analyses support the hypothesis that the distinct type I (acidic) and type II (basic) keratin lineages emerged prior to the

4. Discussion

evolutionary transition of vertebrates from aquatic to terrestrial environments. Terrestrial vertebrates consistently exhibit two well-defined keratin gene clusters, each highly conserved in structure and orientation. However, mammalian keratin clusters contain an increased gene number, primarily due to the evolution of specialized keratins, such as hair keratins and inner root sheath keratins, which represent mammalian-specific adaptations. In contrast, bird and amphibian keratin clusters contain fewer genes, reflecting their absence of these specialized mammalian keratins. In the human genome, genes encoding all type I keratin genes are clustered on 17q12-q21 except k18, while all keratin type II genes are on 12q11-q13 with the addition of keratin 18 [182]. This compact organization is thought to be a mechanism for coordinated keratin gene expression, resulting in a 1:1 molar ratio expression of required keratin genes. In zebrafish, however, keratin4 is on chromosome 6 along with keratin 18b, while keratin4 and keratin5, along with keratin18a isoforms, are present on chromosome 23. A strikingly conserved feature across vertebrates, including fish, is the genomic proximity of type I keratin 18 and type II keratin 8. These two keratin genes are widely expressed across various human tissues, a reflection of their fundamental roles in epithelial integrity. Their closely coordinated expression patterns both in humans and zebrafish as we have observed, further underscore their evolutionary significance as ancient, fundamental epithelial keratins, likely directly early diverged from ancestral lamin-like genes.[179].

In teleost fish, such as zebrafish, the type II keratin gene family has undergone significant evolutionary pressures, resulting in fewer gene copies compared to mammals[183, 179]. An intriguing distinction arises when comparing keratin gene structures across zebrafish and other commonly studied model organisms, such as frogs, mice, and humans. Our sequence analysis reveals notable differences in the highly conserved rod domains of type II keratins among these species. This differential structural conservation pattern of keratin isoforms during zebrafish embryogenesis suggests a unique functional requirement and regulation for keratin filament assembly and stability, distinct from that described in terrestrial vertebrates. Affinity and structural data that define the affinity of keratins and their binding partners in other organisms may not be true in zebrafish. This is also of particular interest as these specific rod domains are highly conserved domains in the protein responsible and required for its mechanical function and properties. Post-translational modification of the protein by protein kinases such as ERK and Akt is crucial for their organization and functions. A non-insignificant number of post-translational modifications that are mediated by ERK and Akt are within this sequence of rod forming domains. While zebrafish keratin genes generally share considerable sequence similarity with those of terrestrial vertebrates, specific variations within the rod domain point to evolutionary divergence events[179, 184].

A potential explanation or evolutionary feature for these modifications could be due to the differences in early development environment requirements. Embryos for mammals with a few notable exceptions develop in-utero with specialized extra-embryonic tissues providing essential nutritional and protective roles. The eggs of zebrafish are in contrast protected by a very thin chorion. The characteristic expression and the evolutionary peculiarities of keratin structures in the developing embryo suggest environmental challenges that could shape the evolutionary and developmental trajectories of keratin genes in teleosts. Intermediate filaments in early metazoans show genes with more significant similarities to lamins than keratin. Keratins from cnidarians (jellyfish) are lost and regained in Testitudes (turtles) [179]. This supports the idea that keratin genes are lost and can evolve depending on environmental requirements, especially as animals evolved from sea to land. Keratin 24 is a gene that is expressed in the corneal epithelium in the terminally differentiated cells [185]. In multiple aquatic mammals: cetaceans, Otaroidea as well as Camels which have specific environmental requirements. Camels have

a thick corneal epithelium which prevents abrasion, potentially requiring the expression of different pattern of keratin genes in their eyes than keratin24. Keratin genes around keratin24 are genes that are involved in hair follicles specifically, which are lost in cetaceans. It has been proposed that keratin24 is associated with the evolution of these specific phenotypic changes.

It is interesting to consider what evolutionary challenges could have affected the evolution of keratin genes in zebrafish. An interesting evolutionary difference to consider in this respect is the distinction between the mechanics of evolutionarily similar zebrafish and medaka eggs. Medaka eggs are lined with hairlike filaments and a harder chorion than zebrafish eggs. Upon dechorionation, these eggs are also softer and more fragile than zebrafish. EVL cells in medaka are similarly organized but show dramatically elongated cells at the end of epiboly [186]. Keratin architecture in medaka EVL cells, in contrast to the organization in zebrafish EVL, could be helpful in understanding the differential organization of similar keratins in structurally distinct cellular architectures in response to their adaptations to their different environment and development.

As the EVL spreads during epiboly, we discovered that the keratin network matures and undergoes a transformation of the network from a spare collection of apically distributed unconnected bundles to a dense network that spans throughout the apical surface and lining the junctions. We observed, however, that the density of the network increases at a remarkable rate with a network unlike in any other system/cell and the net density of the network is much larger than any system imaged in this detailed resolution so far. Keratin bundles organize in the cell in a rim and spoke fashion, with a ring of filaments around the cells connecting desmosomal junctions and spoke-like filaments organizing from the periphery to the nucleus [95, 94]. This entire change and maturation of the network into what has been classically thought of as a rim and spoke organization happens within a few hours, faster than any other model system that can be studied to understand the early maturation and formation of keratin networks. While the structure of keratin networks in different cells is remarkably diverse, the general structure is conserved [100]. This architecture of the network is remarkably similar in different cells and is crucial in terms of the response to mechanical deformations. In MDCK cell layers, for example, keratin intermediate filaments show massive reorganization when cells extend at extremely high strains, transforming from a disorganized network spread all over the cell to a bundled spoke arrangement around the nucleus [102].

In the EVL, however, we noted that the dynamically regulated organization of keratin intermediate filaments during development does not show a clear ring and spoke pattern. Instead, the mini filaments that begin forming the network are distributed on the apical surface in a regularly spaced manner attached to the cortex by an unknown plectin isoform. As the network matured, additional filaments were added that joined together to form longer filaments, forming prominent thick bundles that spanned across the cell, excluding the junction in the beginning. Nuclear association through Linc complex proteins leads to a network of keratin filaments around the nucleus called a nuclear cage [187]. In the EVL, we did not observe a clear nuclear organization surrounding the nucleus, suggesting a lack/minimal nuclear cage at the early stages of the network development. EVL cells are extremely squamous, with minimal distance between the nucleus and the cortex. Additionally, the keratin network, once matured, is extremely dense, creating an expansive cover over the entire apical surface. Unlike other developing organisms, we note that the keratin network in zebrafish EVL cells is much more robust and dense [188, 189, 95]. We suggest that the "spoke" network that connects the nucleus is modified in the EVL due to these modified physical constraints of the cell, allowing the network to be expansive over the entire tissue rather than limited into a cage at

4. Discussion

every cell. This is additionally supported by the presence of similar supracellular networks in the extra-embryonic tissues in mice [190]. Despite this altered organization, we noted that the mechanical reorganization observed in keratin networks in other systems is also true for keratin networks in zebrafish. This amplification and reorganization of the bundles is most evident after the junctional association of these filaments, suggesting the association with desmosomes is important for this process. We observed that the junctional accumulation of keratin was not equal in all cells. In different EVL cells the amount of mini-filaments seen was unequal, with some cells showing an increased number/density of these initiating filaments. As the network matured, the relative amount of keratin in different cells did not change, i.e., the cells with initially more initiating filaments showed a faster maturation and brighter fluorescence of keratin18 tagged with GFP. We observed that the presence of junctional keratin was closely correlated to the apical network of each cell. While all cells end up showing a junctional network at the end of the shield stage (7hpf), there is a broad transition period where cells with different densities show junctional accumulation at slightly different times. This unequal distribution of keratin in different cells of the same tissue is also seen in the mouse trophectoderm, although the difference is less pronounced due to the lack of a mature, dense keratin network in these cells [188].

Junctional keratin is usually associated with a desmosomal scaffold through desmosomal proteins such as desmoplakin, plakophilin, and plakoglobin to desmosomal cadherins desmoglein and desmocollin. Interestingly, in zebrafish, desmosomal proteins are expressed at shield stage (6hpf) significant levels with a very low level of expression seen at cleavage stages that further decline at the start of epiboly [191]. This correlates very closely with the junctional accumulation we observe with filaments attaching to the junction right as this increased expression of desmosomes is observed. Plakoglobin and plakophilin are armadillo family proteins similar in structure and function to β -catenin [192]. Protein tyrosine kinases (EGFR, Src, Fer, Fyn) phosphorylate distinct tyrosine residues on plakoglobin, differing from the phosphorylation pattern observed in β -catenin, a vital member of the armadillo family proteins. Phosphorylation at these sites affects plakoglobin's association with E-cadherin and α -catenin. This switch changes binding to desmoplakin, shifting plakoglobin from adherens junctions towards desmosomes, hence changing the availability of factors such as β -catenin in the nucleus and intermediate filament binding to desmosomes. Lack of these plaque linkers leads to not only changes in the organization of these junctional components but also prevents linkage of intermediate filaments across cells [193]. In plakoglobin-deficient cells, the presence of transcellular networks is perturbed. Interestingly, the defects observed by loss of plakoglobin in zebrafish do not show a severe effect during early development with few embryos showing a delayed midbrain-hindbrain border formation [194]. More severe defects are seen as the embryo develops further at 72 hrs with heart oedema and a kinked tail. Desmoplakin mediates interactions with the keratins inside the cell at desmosomal plaque through plakoglobin. Desmoplakin-deficient zebrafish have cardiac abnormalities and altered Wnt/ β -catenin, Yap-Taz, Tgf β /Smad signalling, impairing cardiac function. [195].

The keratin-desmosomal scaffold is mechanically crucial for a functional keratin network [96]. However, the most commonly associated desmosomal junctional molecules do not seem to be involved in the precise junction association of keratin that we observed in the EVL early in development. We propose that the molecules involved in the initial cortical attachment and the initial junctional attachment differ from those that are involved later in development. This is further supported by our observation that EVPL and PPL mutants and MO do not show a defective keratin network in the EVL. It is also interesting to consider what signals regulate this precise spatiotemporal regulation of the keratin-desmosomal scaffold, potentially in keratin or

an unknown upstream control-mediated manner. In the trophectoderm, it has been suggested that keratin expression is directly correlated to the nuclear accumulation of BAF transcriptional factors [188]. However, a mosaic of transcription factors from the Kruppel-like, p53 family and Sox genes are involved in the regulation of keratin expression [181]. In our work, we did not investigate any direct upstream regulation of keratin expression, but our observations point towards interesting mechanisms of precise expression and translational control for keratin.

We do observe that keratin expression is dependent on the force applied by the YSL onto the EVL. This we observed was as possible mechanism that could explain the dynamics of keratin maturation in the embryo. We noted that actomyosin contractility, both in the YSL pulling the EVL and the EVL itself, is responsible for the increased expression and maturation of the keratin network in an epiboly stage-independent manner. Lowering contractility by injecting myosin phosphatase into the ysl or into the EVL led to lower keratin fluorescence observed in the EVL. Additionally, we observed that ectopic force application with a pipette leads to reorganization and an increase in the fluorescence of keratin filaments. This increase is at a timescale that is much faster than any transcriptional or translational increase in keratin in the aspirated cell. Therefore, we propose it results from a direct restructuring of the network in response to stress. Mechanical effects on intermediate filament network maturation are relatively unknown in cells, but insights from their structure and organization give us hints about their functional abilities. On the filament level, studies have shown the many notable properties of intermediate filaments, especially for the most basic level of its organization, the filament. Among cytoplasmic intermediate filaments, keratins and vimentin are filaments with functions that are similar to each other. Vimentin filaments are hyperelastic, with no plastic deformations seen even under large strains under direct mechanical loads [196]. Vimentin filaments are stiffer than keratin for strains of up to 0.15 and show no plastic deformation upon strain. Vimentins soften upon repeated stretching due to changes in their molecular structure. Keratins, on the other hand, though they perform similar functions, show very different mechanics already at the single filament level. Keratins undergo plastic deformation but maintain their mechanical properties under stress [197]. Even though the secondary structure of these intermediate filaments is conserved, which is valid for most members of the IF family, changes in the amino acid sequence give these filaments different surface charges and interactivity. For example, keratin filaments also do not change their mechanical properties as dramatically as vimentin filaments under physiological levels of ion concentrations 198. Vimentin forms compact tetramers that potentially favor α helix unfolding rather than subunit sliding when stretched. Keratin filaments, on the other hand, are much more permissive to subunit exchanges and movement upon stress despite performing similar mechanical attenuation as vimentin filaments at the molecular level. It is important to note, although, that the properties of keratin at a filament level may not be similar to the mechanics of a keratin bundle being pulled. However, these observations are useful to understand the dynamics of these filaments under stress.

Intermediate filaments, unlike other cytoskeletal proteins, can exchange subunits throughout their length rather than specific sites at the ends of the filament [199]. Subunit exchange, allowed by the chemical properties of the core protein structure of keratin together with the ability of intermediate filaments to exchange subunits within length, could explain a mechanism for the mechanical recruitment of new subunits within a bundle. As a keratin filament is stretched, new sites are opened up in the filament where subunits in the cytoplasm could exchange and be added into the filament. The ability of keratin intermediate filaments to respond and restructure on force application is crucial to this ability, but examples of how keratin bundles respond to stress in vivo are limited. Pulling forces applied ectopically with a

4. Discussion

pipette could lead to rapid reorganization of the keratin network, possibly by incorporating new monomers from the cytosol into the bundled filaments upon force application.

Direct interaction of the actin cytoskeleton and the keratin network is mediated by plakin proteins as well. In mammals, these proteins include BPAG1, desmoplakin, plectin, envoplakin, periplalkin, epiplakin, and MACF1. They act as direct linkers and affect the mechanics of all the cytoskeletons in vivo. Desmoplakin, as discussed above, is a crucial component of the desmosome and forms its most abundant component [200]. In mice, the loss of desmoplakin leads to embryonic developmental failure due to dissociation of extra-embryonic tissues (ectoplacental cone, EPC; extra-embryonic ectoderm, EXE; visceral endoderm, VE; and parietal endoderm, PE). But additionally, in the embryo, it also leads to defects in proliferation and [201]. In the skin desmoplakin loss leads to lesser number of desmosomes as well as adherens junction formation. Consequently, actin reorganization to undergo membrane sealing during epithelial sheet formation is affected in these mice [99]. Envoplakin and periplakin are essential for micro-ridge stabilization by forming a ring around the growing actin microridges in the mucosal cells of zebrafish epithelium. The presence of these plakins is regulated such that keratin can be associated to these long epidermal protrusions and stabilize actin filaments in the ridges. Loss of either of these plakins leads to a destabilization of the micro ridges and a shortening of their length [98]. These proteins are also regulated in a dynamic manner by phosphorylation on all plakin proteins, especially at the C-terminal region, which are important for IF binding [105]. As mechanisms and interactions of plakins that could mediate these posttranslational modifications are not well understood, we could not verify the involvement of such interactions/mechanisms playing a dynamic, fast-acting role in keratin mechanosensation. We did observe that envoplakin and periplakin MO did not have any siginificant effect on the accumulation of keratin filaments during epiboly. However, we did not probe the other plakin family proteins in their roles in keratin regulation, especially by actomyosin-mediated stress. Based on the flows of keratin seen in the YSL it is plausible to consider that keratin and actin cytoskeletons do interact through any of these potential plakin candidates or other unknown interactions. In the EVL, before the network is denser than 60%-70% filaments show wiggling movements that occur at lengthscales of a few nm. In cell culture such wiggles have been also seen in keratin bundles and have been associated to localized pulling by plectins [202]. Dynamic reorganization of keratin binding proteins, especially mediated by phosphorylation changes induced in response to mechanical stress, could be an interesting mechanism that is utilized by the embryo to regulate the maturation of the keratin network during development.

Intermediate filaments have been shown to be interacting and dependent on other cytoskeletal systems in the cells, but evidence supporting the role of microtubules in organizing keratins had been limited. In the zebrafish, EVL microtubules may be important in transporting and maintaining keratin on the junctions. We observed that nocadazole treated embryos showed an effect on the recruitment of keratins to the apical surface, with embryos treated with nocadazole before the start of epiboly showing a reduced keratin network. Additionally embryos treated with nocadazole leads to direct loss of keratins from the junctions as a complete network. Evidence supporting the interaction of microtubules with vimentin, on the other hand, is numerous [196, 177]. Surprisingly, vimentin can directly bind to microtubules via electrostatic interactions [196]. Vimentin intermediate filament networks stabilize microtubules and prevent catastrophe when in culture [177]. This stabilization occurs due to direct mechanical transient interactions between the two cytoskeletons. In Retinal pigment epithelial cells, this interaction leads to templating for microtubules and more remarkable persistence of cell movements. Microtubules plus end grow on the vimentin filaments and can regrow on existing vimentin filaments if induced to reduce using nocadazole [203]. Despite the lack of such evidence for

keratin maintenance or growth, we provide some evidence suggesting a dual role of microtubules in regulating the keratin network. Microtubules may be involved in the recruitment of unknown plakin linkers on the apical cortex and junctions that regulate the interaction of keratins with these components of the cell.

The various methods we utilized to study the effect of loss of keratins relied on the limited number of type II keratins in the zebrafish genome [179]. Keratin knockouts have been of interest in the field due to the direct evidence with keratin defects leading to epidermal lysis effects grouped together in the disease named Epidermla bullosa (EB). A host of different symptoms usually arising out of mutations in the keratin5/keratin17 genes have an epithelialspecific phenotype. A most interesting fact about the symptoms of these diseases is the fact that mutations in particular keratin lead to specific defects, which give further insights into their roles in physiology and development. However, this syndrome exemplifies the ability of keratins to compensate due to a significant amount of redundancy in their structural functions. For example in keratin8/keratin19 negative mice keratin7 and keratin 18 filaments form a compensatory network showcasing the robustness and felxibility of these networks [204, 205]. Previous reports have shown the ability of zebrafish genome to express homologus genes upon mutant mRNA degradation [206]. Additionally given the interactive mechanisms seen in the EVL that show interactions of keratins with other cytoskeletal proteins in the EVL a stable knockout of keratins that abrogated the network entirely was necessary. A major challenge in understanding the specific role of loss of keratins has been the relatively mild effect on development shown by large-scale perturbations of keratins quite often due to extra embryonic tissues that support failing before developmentally critical failure points are reached. Most defects seen in early embryonic death upon knockouts of keratins can be attributed to stress-mediated damage as well as apoptosis triggered due to increased apoptotic signalling in the extra-embryonic tissues such as the placenta and yolk. Therefore that , we utilized methods that lead to an entire locus knockout for keratin or morpholino-mediated loss of keratin mRNA directly. With the large number of keratin Type I isoforms, despite keratin18 MO showing the critical defects due to loss of keratin network in the EVL, we resorted to knocking out keratin Type II. In contrast with the mouse embryonic structure, the extra-embryonic tissues are vital structurally and signaling-wise to zebrafish development starting at the beginning of embryonic development.

Loss of type II keratins keratin 8 and keratin 4 early during development in the zebrafish embryo leads to failure of bundle formation and network maturation despite the epithelium spreading and stress applied to the epithelium. A limited amount of keratin 18 filaments seen in the morphant and mutant embryos could be attributed to potential keratin isoforms crossbinding. However, we observed that loss of keratins via morpholinos or via CRISPR-mediated genome knockouts leads to delayed epiboly movements and fragility of the epithelium. Unfortunately, despite various different methods used to create mutants by single spot introductions, as well as whole locus deletions, stable lines could not be generated as none of the embryos survived. This underscores the importance of the keratin cytoskeletal network in early development in zebrafish. We propose that this difference in the crucial requirement of keratin early in development especially arises due to the differential structure of the zebrafish embryo. During epiboly, the EVL undergoes a dramatic increase in the surface area over a very short time, with limited cell divisions seen for most of this process. The yolk and EVL are tissues that directly line the embryo, serving as a physical boundary against which the cells develop. Consequently, the rapid development of the network and the criticality of the loss of keratins could be a direct effect of the unique requirements of the development of the first epithelial tissue in the zebrafish embryo.

4. Discussion

We observed that the breaking of the EVL happened most often coincidentally with the convergence of the body axis and the formation of the head. Suggesting that a potential mechanical function plays a critical role in epithelial fragility and developmental defects. This aligns with the idea in the field that keratins function primarily as a mechanical protection for the cell cortex and are most important in tissues under stress [207, 103]. Using laser cutting experiments to ablate the cell cortex, we observed that both with single keratin and complete network knockdowns, the recoil velocity of the tissue is increased. Keratins have also been known to increase the rigidity of the tissue [208]. With our pipette aspiration experiments, we confirmed that the loss of keratins leads to a less viscous EVL. The recoil after cortical ablation is dependent on the contractility as well as the mechanical properties of the ablated medium [209]. Taken together, we hypothesize that the increased recoil could be a direct effect of the reduced viscosity of the EVL upon keratin loss. Hence, the effect on tissue properties is more critical for the mechanical changes in the EVL due to keratins. A question in the field of tissue mechanics relies on whether tissues behave viscously or elastically on a developmental timescale. Actomyosin is the primary force-generating system in embryonic tissues, with the recoils observed in viscoelastic tissues being primarily driven by active myosin force. Degrading myosin in the Drosophila wing hints toward the mechanical properties of tissues at timescales of ablations being elastic [210]. However, our experiments as well as evidence from previous research suggest strongly that tissue properties are dominated largely by their viscous properties [71, 209]. A potential explanation for this distinction could be the presence of cytoplasmic intermediate filaments in zebrafish and C. elegans tissues, a distinct difference from Drosophila tissues. Indeed, the difference in tissue properties and recoil suggests that keratins are an essential determinant of tissue viscosity in embryonic tissues.

The reduced viscosity of the tissue was not sufficient to explain the delayed movement of the EVL. We also observed an additional effect on the oriented elongation of the EVL, which suggested a defective transmission of forces between EVL cells. During development, the EVL cells align as they stretch in the Animal-vegetal (AV) axis, with the longest axis of cells preferentially aligning towards the AV axis. This is a direct effect of the pulling force on the margin as increased YSL pulling mediated locally by caRhoA led to elongated cells in the region with increased contractility. However the embryos lacking any keratin network formation showed a reduced coordinated movements. In cell culture, the roles of intermediate filaments in collective migration are distributing forces through the migrating sheet [211, 203]. In wound healing assays in the developing embryo, this led us to understand the role of keratins in efficiently transmitting forces throughout the epithelium. In keratin morphants, although the healing epithelium is unperturbed, the forces and stretching of the EVL cells around the cell were limited to the wound edge. While in the control embryos, up to 3 cell layers could respond to the injury and move together to close it, in the keratin morphant embryos, the movements were limited to a single cell layer at the boundary. In stratified epithelia, it has been seen that the tissues can co-ordinate oriented migration as well as proliferation in a Rac dependent manner [212]. Both of these experimental results we obtained show a direct role of supra-cellular intermediated filament networks in mediating force propagation over a tissue length scale. Desmosomal connections are likely crucial in mediating these force across cell boundaries. Identifying the interactions with the intermediate filament network would be critical in probing the supra-cellular mechanics of keratin intermediate filament networks. In experiments with monolayers which express keratin show the critical features that such a interaction could affect tissues [103, 102]. In the EVL we see a massive coordinated movement of a squamous epithelium that is dependent on mechanical force transmission by an intermediate filament network.

YSL is the mechanical driver exerting the majority of the forces driving epiboly movement and spreading of the EVL [71, 213]. Specifically the force is generated by flow of actin in the tissue. Keratins are expressed in the YSL at the shield stage (6hpf) once the network in the EVL is around the junctional transitional stage. It is interesting to note that the network initially arises as mini filaments similar to the initial EVL network. We observed a compressive flow that forms a thick band of dense filaments at the EVL, YSL margin. Keratin particles have been shown to travel on actin filaments before they are integrated into a network [214]. Our preliminary experiments have also shown an internal YSL (iYSL; under the epiblast) spanning network that forms over the entire yolk cell; however, it is much sparser than the network seen in the EVL or the external YSL (eYSL; the YSL seen at the front of the migrating embryo). The connection at the margin is most likely mediated through segregated desmosomal proteins at the margin [191]. This could suggest an accumulation of desmosomal plaques at the margin, which is also supported by the blastodisc detachment phenotype exhibited by desmosomal knockout embryos. With keratin morphants, however, we did not observe such detachments. This is despite the numerous pieces of evidence suggesting the bidirectional cross-regulation of desmosomes and keratin recruitment [215, 216]. Specific keratin isoform binding to desmosomes is associated not just with the strength of binding by desmosomes, but also with their number. An interesting observation seen from the YSL keratin network is unlike the EVL network the filaments don't associate into long bundles rather a denser less ordered filament system. The evident junctional keratin associated with the EVL margin is seen instead as a band similar to the distribution of other junctional components in the YSL such as tight junction proteins. This suggests that desmosomal proteins could be organized in a similar manner in the YSL as ZO proteins. However, this network perturbation by YSL-specific knockout of keratins leads to slower EVL movements. This is due to direct perturbation of the actin flows as keratin are expressed in the YSL. Interstingly what is seen among these flows is a lack of alignment and more variance in their directionality, in direct parallel to the alignment defects seen in the cells. However, the direct cause and hence control of these flows are so far unknown. Keratins may be a key factor playing a role in the mechanics of these flows, perhaps acting as a frictional substrate interacting and affecting the actin cortex via plakin linkers.

The Actin band in the YSL increases in intensity and thins as the EVL is pulled during epiboly [71]. This is mediated through recruitment of actin specifically to the YSL band as the band moves over the yolk. We observed no significant differences between the thickness of the YSL band as would be expected from the defects in the flows. However, our pipette aspirations on the YSL demonstrated that the recruitment of actin in response to force is dependent on keratin. Without the presence of keratin in the YSL, actin cannot be accumulated in the YSL efficiently, and the intensity of the band after aspiration is reduced. Similar to other cytoskeletal proteins and tight junction proteins, keratins also flowed with actin, but the speed of these movements was halved compared to that of actin. This could suggest a role of keratins as a frictional substrate for the flowing actin cortex.

Bibliography

- [1] Suyash Naik, Yann-Edwin Keta, Kornelija Pranjic-Ferscha, Édouard Hannezo, Silke Henkes, and Carl-Philipp Heisenberg. Keratins coordinate tissue spreading by balancing spreading forces with tissue material properties. *bioRxiv*, 2025.
- [2] AM Turing. A theory of morphogenesis. *Phil. Trans. B*, 12, 1952.
- [3] Sally P Leys and Ana Riesgo. Epithelia, an evolutionary novelty of metazoans. *Journal of Experimental Zoology Part B: Molecular and Developmental Evolution*, 318(6):438–447, 2012.
- [4] Johannes Holtfreter. A study of the mechanics of gastrulation. part i. *Journal of experimental zoology*, 94(3):261–318, 1943.
- [5] Johannes Holtfreter. A study of the mechanics of gastrulation. *Journal of experimental zoology*, 95(2):171–212, 1944.
- [6] Carl-Philipp Heisenberg and Yohanns Bellaïche. Forces in tissue morphogenesis and patterning. *Cell*, 153(5):948–962, 2013.
- [7] Yvette G. Langdon and Mary C. Mullins. Maternal and Zygotic Control of Zebrafish Dorsoventral Axial Patterning. *Annual Review of Genetics*, 45(Volume 45, 2011):357–377, December 2011.
- [8] Gabriel N. Santos-Durán, Rory L. Cooper, Ebrahim Jahanbakhsh, Grigorii Timin, and Michel C. Milinkovitch. Self-organized patterning of crocodile head scales by compressive folding. *Nature*, 637(8045):375–383, January 2025.
- [9] Ping Wu, Ting-Xin Jiang, Jen-Yee Shen, Randall Bruce Widelitz, and Cheng-Ming Chuong. Morphoregulation of Avian Beaks: Comparative Mapping of Growth Zone Activities and Morphological Evolution. *Developmental dynamics: an official publication of the American Association of Anatomists*, 235(5):1400–1412, May 2006.
- [10] Thomas Lecuit and Loïc Le Goff. Orchestrating size and shape during morphogenesis. *Nature*, 450(7167):189–192, November 2007.
- [11] Ian Conlon and Martin Raff. Size Control in Animal Development. *Cell*, 96(2):235–244, January 1999.
- [12] Shruthi Balachandra, Sharanya Sarkar, and Amanda A. Amodeo. The Nuclear-to-Cytoplasmic Ratio: Coupling DNA Content to Cell Size, Cell Cycle, and Biosynthetic Capacity. *Annual Review of Genetics*, 56(1):165–185, November 2022.

- [13] Thomas P. Neufeld, Aida Flor A. de la Cruz, Laura A. Johnston, and Bruce A. Edgar. Coordination of Growth and Cell Division in the Drosophila Wing. *Cell*, 93(7):1183–1193, June 1998.
- [14] Jody Rosenblatt, Martin C Raff, and Louise P Cramer. An epithelial cell destined for apoptosis signals its neighbors to extrude it by an actin-and myosin-dependent mechanism. *Current biology*, 11(23):1847–1857, 2001.
- [15] Yapeng Gu, Tetyana Forostyan, Roger Sabbadini, and Jody Rosenblatt. Epithelial cell extrusion requires the sphingosine-1-phosphate receptor 2 pathway. *Journal of Cell Biology*, 193(4):667–676, 2011.
- [16] Andrea Hartsock and W. James Nelson. Adherens and Tight Junctions: Structure, Function and Connections to the Actin Cytoskeleton. *Biochimica et biophysica acta*, 1778(3):660–669, March 2008.
- [17] Andrew P. Kowalczyk, Elayne A. Bornslaeger, Suzanne M. Norvell, Helena L. Palka, and Kathleen J. Green. Desmosomes: Intercellular Adhesive Junctions Specialized for Attachment of Intermediate Filaments. In Kwang W. Jeon, editor, *International Review of Cytology*, volume 185, pages 237–302. Academic Press, January 1998.
- [18] Andrew P. Kowalczyk and Kathleen J. Green. Structure, Function and Regulation of Desmosomes. *Progress in molecular biology and translational science*, 116:95–118, 2013.
- [19] Tony Y.-C. Tsai, Mateusz Sikora, Peng Xia, Tugba Colak-Champollion, Holger Knaut, Carl-Philipp Heisenberg, and Sean G. Megason. An adhesion code ensures robust pattern formation during tissue morphogenesis. *Science*, 370(6512):113–116, October 2020.
- [20] Jean-Léon Maître, Hélène Berthoumieux, Simon Frederik Gabriel Krens, Guillaume Salbreux, Frank Jülicher, Ewa Paluch, and Carl-Philipp Heisenberg. Adhesion Functions in Cell Sorting by Mechanically Coupling the Cortices of Adhering Cells. *Science*, 338(6104):253–256, October 2012.
- [21] Frans Van Roy and Geert Berx. The cell-cell adhesion molecule e-cadherin. *Cellular and molecular life sciences*, 65:3756–3788, 2008.
- [22] Barry M Gumbiner. Cell adhesion: the molecular basis of tissue architecture and morphogenesis. *Cell*, 84(3):345–357, 1996.
- [23] Elizabeth D Hay. *Cell biology of extracellular matrix*. Springer Science & Business Media, 2013.
- [24] Cornelia Schwayer, Mateusz Sikora, Jana Slováková, Roland Kardos, and Carl-Philipp Heisenberg. Actin rings of power. *Developmental cell*, 37(6):493–506, 2016.
- [25] Tatyana M Svitkina. Actin cell cortex: structure and molecular organization. *Trends in cell biology*, 30(7):556–565, 2020.
- [26] Damien Démoulin, Marie-France Carlier, Jérôme Bibette, and Jean Baudry. Power transduction of actin filaments ratcheting in vitro against a load. *Proceedings of the National Academy of Sciences*, 111(50):17845–17850, 2014.

- [27] Laurent Blanchoin, Rajaa Boujemaa-Paterski, Cécile Sykes, and Julie Plastino. Actin dynamics, architecture, and mechanics in cell motility. *Physiological reviews*, 94(1):235– 263, 2014.
- [28] M. Lisa Manning, Ramsey A. Foty, Malcolm S. Steinberg, and Eva-Maria Schoetz. Coaction of intercellular adhesion and cortical tension specifies tissue surface tension. *Proceedings of the National Academy of Sciences*, 107(28):12517–12522, July 2010.
- [29] Michael F. Olson. Actin-Myosin Cytoskeleton Regulation and Function. *Cells*, 12(1):9, December 2022.
- [30] Gary Laevsky and David A. Knecht. Cross-linking of actin filaments by myosin II is a major contributor to cortical integrity and cell motility in restrictive environments. *Journal of Cell Science*, 116(Pt 18):3761–3770, September 2003.
- [31] Hailing Yang, Anutosh Ganguly, and Fernando Cabral. Inhibition of Cell Migration and Cell Division Correlates with Distinct Effects of Microtubule Inhibiting Drugs. *The Journal of Biological Chemistry*, 285(42):32242–32250, October 2010.
- [32] Bruno Carmona, H. Susana Marinho, Catarina Lopes Matos, Sofia Nolasco, and Helena Soares. Tubulin Post-Translational Modifications: The Elusive Roles of Acetylation. *Biology*, 12(4):561, April 2023.
- [33] Natasha T. Snider and M. Bishr Omary. Post-translational modifications of intermediate filament proteins: Mechanisms and functions. *Nature Reviews Molecular Cell Biology*, 15(3):163–177, March 2014.
- [34] Anne L. Hitt and Elizabeth J. Luna. Membrane interactions with the actin cytoskeleton. *Current Opinion in Cell Biology*, 6(1):120–130, February 1994.
- [35] Elizabeth J. Luna and Anne L. Hitt. Cytoskeleton-Plasma Membrane Interactions. *Science*, 258(5084):955–964, 1992.
- [36] Panayotis A. Theodoropoulos, Christos Stournaras, Barbara Stoll, Emmanuel Markogiannakis, Florian Lang, Achilles Gravanis, and Dieter Häussinger. Hepatocyte swelling leads to rapid decrease of the G-/total actin ratio and increases actin mRNA levels. *FEBS Letters*, 311(3):241–245, 1992.
- [37] E. A. Papakonstanti, E. A. Vardaki, and C. Stournaras. Actin cytoskeleton: A signaling sensor in cell volume regulation. *Cellular Physiology and Biochemistry: International Journal of Experimental Cellular Physiology, Biochemistry, and Pharmacology*, 10(5-6):257–264, 2000.
- [38] Seth Tyler. Epithelium—the primary building block for metazoan complexity. *Integrative and comparative biology*, 43(1):55–63, 2003.
- [39] Miri Adler, Arun R Chavan, and Ruslan Medzhitov. Tissue biology: in search of a new paradigm. *Annual Review of Cell and Developmental Biology*, 39(1):67–89, 2023.
- [40] Hassiba Belahbib, Emmanuelle Renard, Sébastien Santini, Cyril Jourda, Jean-Michel Claverie, Carole Borchiellini, and André Le Bivic. New genomic data and analyses challenge the traditional vision of animal epithelium evolution. *BMC genomics*, 19:1–15, 2018.

- [41] Clare E Buckley and Daniel St Johnston. Apical-basal polarity and the control of epithelial form and function. *Nature reviews Molecular cell biology*, 23(8):559–577, 2022.
- [42] Claudia G Vasquez, Eva L de la Serna, and Alexander R Dunn. How cells tell up from down and stick together to construct multicellular tissues—interplay between apicobasal polarity and cell–cell adhesion. *Journal of cell science*, 134(21):jcs248757, 2021.
- [43] Joseph P Campanale, Thomas Y Sun, and Denise J Montell. Development and dynamics of cell polarity at a glance. *Journal of cell science*, 130(7):1201–1207, 2017.
- [44] Jingwen Zeng, Shanshan Feng, Bin Wu, and Wei Guo. Polarized exocytosis. *Cold Spring Harbor Perspectives in Biology*, 9(12):a027870, 2017.
- [45] Melissa A Pickett, Victor F Naturale, and Jessica L Feldman. A polarizing issue: diversity in the mechanisms underlying apico-basolateral polarization in vivo. *Annual Review of Cell and Developmental Biology*, 35(1):285–308, 2019.
- [46] Matthew C Gibson and Norbert Perrimon. Apicobasal polarization: epithelial form and function. *Current opinion in cell biology*, 15(6):747–752, 2003.
- [47] Sophie Quintin, Christelle Gally, and Michel Labouesse. Epithelial morphogenesis in embryos: asymmetries, motors and brakes. *Trends in genetics*, 24(5):221–230, 2008.
- [48] Kunyoo Shin, Vanessa C Fogg, and Ben Margolis. Tight junctions and cell polarity. *Annu. Rev. Cell Dev. Biol.*, 22(1):207–235, 2006.
- [49] LM Godsel, S Getsios, AC Huen, and KJ Green. The molecular composition and function of desmosomes. *Cell adhesion*, pages 137–193, 2004.
- [50] John R Stanley, David T Woodley, Stephen I Katz, and George R Martin. Structure and function of basement membrane. *Journal of Investigative Dermatology*, 79(1):69–72, 1982.
- [51] Christine-Maria Horejs, Andrea Serio, Alan Purvis, Adam J. Gormley, Sergio Bertazzo, Anna Poliniewicz, Alex J. Wang, Peter DiMaggio, Erhard Hohenester, and Molly M. Stevens. Biologically-active laminin-111 fragment that modulates the epithelial-to-mesenchymal transition in embryonic stem cells. *Proceedings of the National Academy of Sciences*, 111(16):5908–5913, April 2014.
- [52] Isabelle Bonnet, Philippe Marcq, Floris Bosveld, Luc Fetler, Yohanns Bellaïche, and François Graner. Mechanical state, material properties and continuous description of an epithelial tissue. *Journal of The Royal Society Interface*, 9(75):2614–2623, May 2012.
- [53] Edouard Hannezo, Jacques Prost, and Jean-Francois Joanny. Theory of epithelial sheet morphology in three dimensions. *Proceedings of the National Academy of Sciences*, 111(1):27–32, January 2014.
- [54] Marine Luciano, Marie Versaevel, Eléonore Vercruysse, Anthony Procès, Yohalie Kalukula, Alexandre Remson, Amandine Deridoux, and Sylvain Gabriele. Appreciating the role of cell shape changes in the mechanobiology of epithelial tissues. *Biophysics Reviews*, 3(1):011305, March 2022.

- [55] Dianne Fristrom. The cellular basis of epithelial morphogenesis. a review. *Tissue and Cell*, 20(5):645–690, 1988.
- [56] J Arthur Thomson. On growth and form, 1917.
- [57] Marta N Shahbazi. Mechanisms of human embryo development: from cell fate to tissue shape and back. *Development*, 147(14):dev190629, 2020.
- [58] Charles B Kimmel, William W Ballard, Seth R Kimmel, Bonnie Ullmann, and Thomas F Schilling. Stages of embryonic development of the zebrafish. *Developmental dynamics*, 203(3):253–310, 1995.
- [59] Andreas Janshoff. Viscoelastic properties of epithelial cells. *Biochemical society transactions*, 49(6):2687–2695, 2021.
- [60] C. A. Ettensohn. Mechanisms of epithelial invagination. *The Quarterly Review of Biology*, 60(3):289–307, September 1985.
- [61] Jingjing Li, Andrew D. Economou, and Jeremy B. A. Green. Epithelial invagination by vertical telescoping, September 2019. Pages: 515981 Section: New Results.
- [62] Lance A. Davidson. No strings attached: new insights into epithelial morphogenesis. *BMC Biology*, 10(1):105, December 2012.
- [63] Robert J. Tetley, Michael F. Staddon, Davide Heller, Andreas Hoppe, Shiladitya Banerjee, and Yanlan Mao. Tissue fluidity promotes epithelial wound healing. *Nature Physics*, 15(11):1195–1203, November 2019. Number: 11 Publisher: Nature Publishing Group.
- [64] Matteo Rauzi. Cell intercalation in a simple epithelium. *Philosophical Transactions of the Royal Society B: Biological Sciences*, 375(1809):20190552, August 2020. Publisher: Royal Society.
- [65] Rastko Sknepnek, Ilyas Djafer-Cherif, Manli Chuai, Cornelis Weijer, and Silke Henkes. Generating active T1 transitions through mechanochemical feedback. eLife, 12:e79862, April 2023. Publisher: eLife Sciences Publications, Ltd.
- [66] Dhananjay T. Tambe, C. Corey Hardin, Thomas E. Angelini, Kavitha Rajendran, Chan Young Park, Xavier Serra-Picamal, Enhua H. Zhou, Muhammad H. Zaman, James P. Butler, David A. Weitz, Jeffrey J. Fredberg, and Xavier Trepat. Collective cell guidance by cooperative intercellular forces. *Nature Materials*, 10(6):469–475, June 2011. Publisher: Nature Publishing Group.
- [67] Tamal Das, Kai Safferling, Sebastian Rausch, Niels Grabe, Heike Boehm, and Joachim P. Spatz. A molecular mechanotransduction pathway regulates collective migration of epithelial cells. *Nature Cell Biology*, 17(3):276–287, March 2015. Publisher: Nature Publishing Group.
- [68] D. Nathaniel Clarke and Adam C. Martin. Actin-based force generation and cell adhesion in tissue morphogenesis. *Current Biology*, 31(10):R667–R680, May 2021.
- [69] Ashley EE Bruce. Zebrafish epiboly: Spreading thin over the yolk. *Developmental Dynamics*, 245(3):244–258, 2016.

- [70] Takashi Iwamatsu. Stages of normal development in the medaka oryzias latipes. *Mechanisms of development*, 121(7-8):605–618, 2004.
- [71] Martin Behrndt, Guillaume Salbreux, Pedro Campinho, Robert Hauschild, Felix Oswald, Julia Roensch, Stephan W Grill, and Carl-Philipp Heisenberg. Forces driving epithelial spreading in zebrafish gastrulation. *Science*, 338(6104):257–260, 2012.
- [72] Ashley EE Bruce and Carl-Philipp Heisenberg. Mechanisms of zebrafish epiboly: A current view. *Current topics in developmental biology*, 136:319–341, 2020.
- [73] Tomoko Kondo, Toshiharu Yanagawa, Noriyuki Yoshida, and Masakane Yamashita. Introduction of cyclin b induces activation of the maturation-promoting factor and breakdown of germinal vesicle in growing zebrafish oocytes unresponsive to the maturation-inducing hormone. *Developmental biology*, 190(1):142–152, 1997.
- [74] Peng Xia, Daniel Gütl, Vanessa Zheden, and Carl-Philipp Heisenberg. Lateral inhibition in cell specification mediated by mechanical signals modulating taz activity. *Cell*, 176(6):1379–1392, 2019.
- [75] Florence L Marlow and Mary C Mullins. Bucky ball functions in balbiani body assembly and animal–vegetal polarity in the oocyte and follicle cell layer in zebrafish. *Developmental biology*, 321(1):40–50, 2008.
- [76] Ricardo Fuentes and Juan Fernández. Ooplasmic segregation in the zebrafish zygote and early embryo: pattern of ooplasmic movements and transport pathways. *Developmental Dynamics*, 239(8):2172–2189, 2010.
- [77] Shayan Shamipour, Roland Kardos, Shi-Lei Xue, Björn Hof, Edouard Hannezo, and Carl-Philipp Heisenberg. Bulk actin dynamics drive phase segregation in zebrafish oocytes. *Cell*, 177(6):1463–1479, 2019.
- [78] Alexandra Schauer, Diana Pinheiro, Robert Hauschild, and Carl-Philipp Heisenberg. Zebrafish embryonic explants undergo genetically encoded self-assembly. *Elife*, 9:e55190, 2020.
- [79] Alexandra Schauer, Kornelija Pranjic-Ferscha, Robert Hauschild, and Carl-Philipp Heisenberg. Robust axis elongation by nodal-dependent restriction of bmp signaling. *Development*, 151(4), 2024.
- [80] Nikhil Mishra, Yuting I Li, Edouard Hannezo, and Carl-Philipp Heisenberg. Geometry-driven asymmetric cell divisions pattern cell cycles and zygotic genome activation in the zebrafish embryo. *bioRxiv*, pages 2025–02, 2025.
- [81] Fengzhu Xiong, Wenzhe Ma, Tom W. Hiscock, Kishore R. Mosaliganti, Andrea R. Tentner, Kenneth A. Brakke, Nicolas Rannou, Arnaud Gelas, Lydie Souhait, Ian A. Swinburne, Nikolaus D. Obholzer, and Sean G. Megason. Interplay of Cell Shape and Division Orientation Promotes Robust Morphogenesis of Developing Epithelia. *Cell*, 159(2):415–427, October 2014.
- [82] CG Sagerstrom, LS Gammill, RV Veale, and HL Sive. Determination of the enveloping layer and lack of autoneutralization in zebrafish embryos. *EMBL/GenBank/DDBJ databases, accession number AF084461*, 1998.

- [83] Sung-Kook Hong, Carly S. Levin, Jamie L. Brown, Haiyan Wan, Brad T. Sherman, Da Wei Huang, Richard A. Lempicki, and Benjamin Feldman. Pre-gastrula expression of zebrafish extraembryonic genes. *BMC Developmental Biology*, 10(1):42, April 2010.
- [84] Wuhong Pei, Houtan Noushmehr, Justin Costa, Maia V Ouspenskaia, Abdel G Elkahloun, and Benjamin Feldman. An early requirement for maternal foxh1 during zebrafish gastrulation. *Developmental biology*, 310(1):10–22, 2007.
- [85] Martina Lachnit, Esther Kur, and Wolfgang Driever. Alterations of the cytoskeleton in all three embryonic lineages contribute to the epiboly defect of pou5f1/oct4 deficient mzspg zebrafish embryos. *Developmental biology*, 315(1):1–17, 2008.
- [86] Jaime L Sabel, Claudia d'Alençon, Erin K O'Brien, Eric Van Otterloo, Katie Lutz, Tawny N Cuykendall, Brian C Schutte, Douglas W Houston, and Robert A Cornell. Maternal interferon regulatory factor 6 is required for the differentiation of primary superficial epithelia in danio and xenopus embryos. *Developmental biology*, 325(1):249– 262, 2009.
- [87] Peter M. Steinert, Robert H. Rice, Dennis R. Roop, Benes L. Trus, and Alasdair C. Steven. Complete amino acid sequence of a mouse epidermal keratin subunit and implications for the structure of intermediate filaments. *Nature*, 302(5911):794–800, April 1983.
- [88] Harald Herrmann and Ueli Aebi. Intermediate Filaments: Structure and Assembly. *Cold Spring Harbor Perspectives in Biology*, 8(11), November 2016.
- [89] Sherif A. Eldirany, Ivan B. Lomakin, Minh Ho, and Christopher G. Bunick. Recent insight into intermediate filament structure. *Current Opinion in Cell Biology*, 68:132–143, February 2021.
- [90] Sergei V. Strelkov, Harald Herrmann, and Ueli Aebi. Molecular architecture of intermediate filaments. *BioEssays*, 25(3):243–251, 2003.
- [91] Maria Galou, Jie Gao, Jeanne Humbert, Mathias Mericskay, Zhenlin Li, Denise Paulin, and Patrick Vicart. The importance of intermediate filaments in the adaptation of tissues to mechanical stress: Evidence from gene knockout studies. *Biology of the Cell*, 89(2):85–97, 1997. _eprint: https://onlinelibrary.wiley.com/doi/pdf/10.1111/j.1768-322X.1997.tb00997.x.
- [92] Annette Peter and Reimer Stick. Evolutionary aspects in intermediate filament proteins. Current Opinion in Cell Biology, 32:48–55, February 2015. Publisher: Elsevier Current Trends.
- [93] Annette Peter and Reimer Stick. Evolution of the lamin protein family: What introns can tell. *Nucleus*, 3(1):44–59, 2012. Number: 1 Publisher: Taylor and Francis Inc.
- [94] Roy A. Quinlan, Nicole Schwarz, Reinhard Windoffer, Christine Richardson, Tim Hawkins, Joshua A. Broussard, Kathleen J. Green, and Rudolf E. Leube. A rim-and-spoke hypothesis to explain the biomechanical roles for cytoplasmic intermediate filament networks. *Journal of Cell Science*, 130(20):3437–3445, October 2017.
- [95] Marcin Moch, Nicole Schwarz, Reinhard Windoffer, and Rudolf E. Leube. The keratin–desmosome scaffold: Pivotal role of desmosomes for keratin network morphogenesis. *Cellular and Molecular Life Sciences*, 77(3):543–558, February 2020.

- [96] Emmanuella Delva, Dana K. Tucker, and Andrew P. Kowalczyk. The Desmosome. Cold Spring Harbor Perspectives in Biology, 1(2):a002543, January 2009. Company: Cold Spring Harbor Laboratory Press Distributor: Cold Spring Harbor Laboratory Press Institution: Cold Spring Harbor Laboratory Press Label: Cold Spring Harbor Laboratory Press Publisher: Cold Spring Harbor Lab.
- [97] Kaelyn D. Sumigray and Terry Lechler. Desmoplakin controls microvilli length but not cell adhesion or keratin organization in the intestinal epithelium. *Molecular Biology of the Cell*, 23(5):792–799, March 2012.
- [98] Yasuko Inaba, Vasudha Chauhan, Aaron Paul van Loon, Lamia Saiyara Choudhury, and Alvaro Sagasti. Keratins and plakin family cytolinker proteins control the length of epithelial microridge protrusions. *Elife*, 9:e58149, 2020.
- [99] Valeri Vasioukhin, Ethan Bowers, Christoph Bauer, Linda Degenstein, and Elaine Fuchs. Desmoplakin is essential in epidermal sheet formation. *Nature Cell Biology*, 3(12):1076–1085, December 2001.
- [100] Reinhard Windoffer, Nicole Schwarz, Sungjun Yoon, Teodora Piskova, Michael Scholkemper, Johannes Stegmaier, Andrea Bönsch, Jacopo Di Russo, and Rudolf E. Leube. Quantitative Mapping of Keratin Networks in 3D, December 2021.
- [101] Chang-Hun Lee, Min-Sung Kim, Byung Min Chung, Daniel J. Leahy, and Pierre A. Coulombe. Structural basis for heteromeric assembly and perinuclear organization of keratin filaments. *Nature Structural & Molecular Biology*, 19(7):707–715, July 2012. Publisher: Nature Publishing Group.
- [102] Ernest Latorre, Sohan Kale, Laura Casares, Manuel Gómez-González, Marina Uroz, Léo Valon, Roshna V. Nair, Elena Garreta, Nuria Montserrat, Aránzazu del Campo, Benoit Ladoux, Marino Arroyo, and Xavier Trepat. Active superelasticity in three-dimensional epithelia of controlled shape. *Nature*, 563(7730):203–208, November 2018.
- [103] Julia Duque, Alessandra Bonfanti, Jonathan Fouchard, Lucia Baldauf, Sara R. Azenha, Emma Ferber, Andrew Harris, Elias H. Barriga, Alexandre J. Kabla, and Guillaume Charras. Rupture strength of living cell monolayers. *Nature Materials*, 23(11):1563–1574, November 2024.
- [104] Ruth Meyer, Ulrike Rölleke, Nicole Schwarz, Amaury Perez-Tirado, Anna V. Schepers, Andreas Janshoff, and Sarah Köster. The keratin cortex stabilizes cells at high strains, February 2025. Pages: 2025.02.24.639846 Section: New Results.
- [105] Jamal-Eddine Bouameur, Bertrand Favre, and Luca Borradori. Plakins, a Versatile Family of Cytolinkers: Roles in Skin Integrity and in Human Diseases. *Journal of Investigative Dermatology*, 134(4):885–894, April 2014.
- [106] Monte Westerfield. The zebrafish book; a guide for the laboratory use of zebrafish (danio rerio). (No Title), 2007.
- [107] Marius Pachitariu and Carsen Stringer. Cellpose 2.0: how to train your own model. *Nature methods*, 19(12):1634–1641, 2022.
- [108] Karine Guevorkian and J-L Maître. Micropipette aspiration: A unique tool for exploring cell and tissue mechanics in vivo. In *Methods in cell biology*, volume 139, pages 187–201. Elsevier, 2017.

- [109] William Thielicke and René Sonntag. Particle image velocimetry for matlab: Accuracy and enhanced algorithms in pivlab. 2021.
- [110] Sébastien Herbert, Léo Valon, Laure Mancini, Nicolas Dray, Paolo Caldarelli, Jérôme Gros, Elric Esposito, Spencer L Shorte, Laure Bally-Cuif, Nathalie Aulner, et al. Localzprojector and deproj: a toolbox for local 2d projection and accurate morphometrics of large 3d microscopy images. *BMC biology*, 19:1–13, 2021.
- [111] Feyza Nur Arslan, Edouard Hannezo, Jack Merrin, Martin Loose, and Carl-Philipp Heisenberg. Adhesion-induced cortical flows pattern e-cadherin-mediated cell contacts. *Current Biology*, 34(1):171–182, 2024.
- [112] Laurent Saias, James Swoger, Andrea D'Angelo, Patrick Hayes, Julien Colombelli, James Sharpe, Guillaume Salbreux, and Julia Solon. Decrease in cell volume generates contractile forces driving dorsal closure. *Developmental Cell*, 33:611–621, 2015.
- [113] P. E. Young, A. M. Richman, A. S. Ketchum, and D. P. Kiehart. Morphogenesis in *Drosophila* requires nonmuscle myosin heavy chain function. *Genes & Development*, 7:29–41, 1993.
- [114] Antonio Jacinto, Will Wood, Torsten Balayo, Mark Turmaine, Alfonso Martinez-Arias, and Paul Martin. Dynamic actin-based epithelial adhesion and cell matching during *Drosophila* dorsal closure. *Current Biology*, 10:1420–1426, 2000.
- [115] V. P. Losick, D. T. Fox, and A. C. Spradling. Polyploidization and cell fusion contribute to wound healing in the adult *Drosophila* epithelium. *Current Biology*, 23:2224–2232, 2013.
- [116] R. M. Brown and C. A. Middleton. Contact-induced spreading in cultures of corneal epithelial cells. *Journal of Cell Science*, 51:143–152, 1981.
- [117] Thomas Lecuit and Loïc Le Goff. Orchestrating size and shape during morphogenesis. *Nature*, 450:189–192, 2007.
- [118] C. B. Kimmel, W. W. Ballard, S. R. Kimmel, B. Ullmann, and T. F. Schilling. Stages of embryonic development of the zebrafish. *Developmental Dynamics*, 203:253–310, 1995.
- [119] A. E. E. Bruce. Zebrafish epiboly: Spreading thin over the yolk. *Developmental Dynamics*, 245:244–258, 2016.
- [120] S. Lepage and A. Bruce. Zebrafish epiboly: Mechanics and mechanisms. *The International Journal of Developmental Biology*, 54:1213–1228, 2010.
- [121] M. Behrndt, G. Salbreux, P. Campinho, R. Hauschild, F. Oswald, J. Roensch, S. W. Grill, and C.-P. Heisenberg. Forces driving epithelial spreading in zebrafish gastrulation. *Science*, 338:257–260, 2012.
- [122] Christian Schwayer, Shayan Shamipour, Katharina Pranjic-Ferscha, Alexandra Schauer, Mönica Balda, Masazumi Tada, Karl Matter, and Carl-Philipp Heisenberg. Mechanosensation of tight junctions depends on zo-1 phase separation and flow. *Cell*, 179:937–952.e18, 2019.

- [123] Hidenori Morita, Silvia Grigolon, Martin Bock, Sander F. G. Krens, Guillaume Salbreux, and Carl-Philipp Heisenberg. The physical basis of coordinated tissue spreading in zebrafish gastrulation. *Developmental Cell*, 40:354–366.e4, 2017.
- [124] Pedro Campinho, Martin Behrndt, Jonas Ranft, Thomas Risler, Nicolas Minc, and Carl-Philipp Heisenberg. Tension-oriented cell divisions limit anisotropic tissue tension in epithelial spreading during zebrafish epiboly. *Nature Cell Biology*, 15:1405–1414, 2013.
- [125] Nicoletta I. Petridou and Carl-Philipp Heisenberg. Tissue rheology in embryonic organization. *The EMBO Journal*, 38:e102497, 2019.
- [126] Antoine C. Laly, Kristina Sliogeryte, Olivier J. Pundel, Ruth Ross, Michelle C. Keeling, Divya Avisetti, Alykhan Waseem, Nicolas Gavara, and John T. Connelly. The keratin network of intermediate filaments regulates keratinocyte rigidity sensing and nuclear mechanotransduction. *Science Advances*, 7:eabd6187, 2021.
- [127] Franziska Loschke, Katharina Seltmann, Jean-Emmanuel Bouameur, and Thomas M. Magin. Regulation of keratin network organization. *Current Opinion in Cell Biology*, 32:56–64, 2015.
- [128] Harald Herrmann, Markus Häner, Manfred Brettel, Nam-On Ku, and Ueli Aebi. Characterization of distinct early assembly units of different intermediate filament proteins. *Journal of Molecular Biology*, 286:1403–1420, 1999.
- [129] Harald Herrmann, Harald Bär, Laurent Kreplak, Sergei V. Strelkov, and Ueli Aebi. Intermediate filaments: from cell architecture to nanomechanics. *Nature Reviews Molecular Cell Biology*, 8:562–573, 2007.
- [130] Christoph Lorenz, Jens Forsting, Annika V. Schepers, Johannes Kraxner, Sabine Bauch, Holger Witt, Stefan Klumpp, and Sarah Köster. Lateral subunit coupling determines intermediate filament mechanics. *Physical Review Letters*, 123:188102, 2019.
- [131] Laurent Kreplak, Ueli Aebi, and Harald Herrmann. Molecular mechanisms underlying the assembly of intermediate filaments. *Experimental Cell Research*, 301:77–83, 2004.
- [132] Hermann H. Bragulla and Dominique G. Homberger. Structure and functions of keratin proteins in simple, stratified, keratinized and cornified epithelia. *Journal of Anatomy*, 214:516–559, 2009.
- [133] Roy A. Quinlan, Nina Schwarz, Reinhard Windoffer, Clare Richardson, Tavia Hawkins, Jennifer A. Broussard, Kathleen J. Green, and Rudolf E. Leube. A rim-and-spoke hypothesis to explain the biomechanical roles for cytoplasmic intermediate filament networks. *Journal of Cell Science*, 130:3437–3445, 2017.
- [134] Derya Acehan, Christian Petzold, Ingo Gumper, Diego D. Sabatini, Eva J. Müller, Pamela Cowin, and David L. Stokes. Plakoglobin is required for effective intermediate filament anchorage to desmosomes. *Journal of Investigative Dermatology*, 128:2665–2675, 2008.
- [135] Claudia Kröger, Franziska Loschke, Nina Schwarz, Reinhard Windoffer, Rudolf E. Leube, and Thomas M. Magin. Keratins control intercellular adhesion involving pkc- α -mediated desmoplakin phosphorylation. *Journal of Cell Biology*, 201:681–692, 2013.

- [136] Reinhard Windoffer, Nina Schwarz, Sun Yoon, Tereza Piskova, Matthias Scholkemper, Johannes Stegmaier, Alexander Bönsch, José D. Russo, and Rudolf E. Leube. Quantitative mapping of keratin networks in 3d. *bioRxiv*, 2021.
- [137] Pablo J. Salas, Rosana Forteza, and Anastasiya Mashukova. Multiple roles for keratin intermediate filaments in the regulation of epithelial barrier function and apico-basal polarity. *Tissue Barriers*, 4:e1178368, 2016.
- [138] Jan Kayser, Harald Grabmayr, Michael Harasim, Harald Herrmann, and Andreas R. Bausch. Assembly kinetics determine the structure of keratin networks. *Soft Matter*, 8:8873–8879, 2012.
- [139] Eduardo Latorre, Sagar Kale, Luis Casares, María Gómez-González, Miguel Uroz, Laurent Valon, Raghavan V. Nair, Elisa Garreta, Nuria Montserrat, Agustín del Campo, et al. Active superelasticity in three-dimensional epithelia of controlled shape. *Nature*, 563:203–208, 2018.
- [140] Javier Duque, Andrea Bonfanti, Jérémy Fouchard, Lukas Baldauf, Sérgio R. Azenha, Eugen Ferber, Adam Harris, Eva H. Barriga, Alexandre J. Kabla, and Guillaume Charras. Rupture strength of living cell monolayers. *Nature Materials*, 23:1563–1574, 2024.
- [141] Harry Y. G. Lim, Yann D. Alvarez, Morgan Gasnier, Ye Wang, Paul Tetlak, Sophie Bissiere, Hao Wang, Maté Biro, and Nicolas Plachta. Keratins are asymmetrically inherited fate determinants in the mammalian embryo. *Nature*, 585:404–409, 2020.
- [142] Wahbi Nahaboo, Selma E. Eski, Emilie Despin-Guitard, Marijn Vermeersch, Maxime Versaevel, Batoul Saykali, Delphine Monteyne, Sylvain Gabriele, Thomas M. Magin, Nina Schwarz, et al. Keratin filaments mediate the expansion of extra-embryonic membranes in the post-gastrulation mouse embryo. *The EMBO Journal*, 41:e108747, 2022.
- [143] Elaine Fuchs. Keratins and the skin. *Annual Review of Cell and Developmental Biology*, 11:123–154, 1995.
- [144] Markus Homberg and Thomas M. Magin. Beyond expectations: Novel insights into epidermal keratin function and regulation. In Kwang W. Jeon, editor, *International Review of Cell and Molecular Biology*, pages 265–306. Academic Press, 2014.
- [145] Xian Pan, Robin P. Hobbs, and Pierre A. Coulombe. The expanding significance of keratin intermediate filaments in normal and diseased epithelia. *Current Opinion in Cell Biology*, 25:47–56, 2013.
- [146] Michael Ho, Beth Thompson, Jeffrey N. Fisk, Daniel W. Nebert, Elspeth A. Bruford, Vasilis Vasiliou, and Christopher G. Bunick. Update of the keratin gene family: evolution, tissue-specific expression patterns, and relevance to clinical disorders. *Human Genomics*, 16:1, 2022.
- [147] Jacob A. Farrell, Yuanhao Wang, Samantha J. Riesenfeld, Karthik Shekhar, Aviv Regev, and Alexander F. Schier. Single-cell reconstruction of developmental trajectories during zebrafish embryogenesis. *Science*, 360:eaar3131, 2018.
- [148] Wei Pei, Houtan Noushmehr, Joaquim Costa, Maria V. Ouspenskaia, Abbas G. Elkahloun, and Brian Feldman. An early requirement for maternal foxh1 during zebrafish gastrulation. *Developmental Biology*, 310:10–22, 2007.

- [149] Sundarapandiyan Sivaramakrishnan, Joseph L. Schneider, Alexander Sitikov, Robert D. Goldman, and Karen M. Ridge. Shear stress induced reorganization of the keratin intermediate filament network requires phosphorylation by protein kinase c zeta. *Molecular Biology of the Cell*, 20:2755–2765, 2009.
- [150] A. Hernández-Vega, M. Marsal, P. Pouille, S. Tosi, J. Colombelli, T. Luque, D. Navajas, I. Pagonabarraga, and E. Martín-Blanco. Polarized cortical tension drives zebrafish epiboly movements. *The EMBO Journal*, 36:25–41, 2017.
- [151] Varsha Jayashankar, Michael J. Nguyen, Bethany W. Carr, Daniel C. Zheng, Jose B. Rosales, Jocelyn B. Rosales, and Daniel C. Weiser. Protein phosphatase 1 β paralogs encode the zebrafish myosin phosphatase catalytic subunit. *PLoS ONE*, 8:e75766, 2013.
- [152] Sylvain Chanet, Christopher J. Miller, Evan D. Vaishnav, Bard Ermentrout, Lance A. Davidson, and Adam C. Martin. Actomyosin meshwork mechanosensing enables tissue shape to orient cell force. *Nature Communications*, 8:15014, 2017.
- [153] Binyue He, Adam Martin, and Eric Wieschaus. Flow-dependent myosin recruitment during *Drosophila* cellularization requires zygotic *dunk* activity. *Development*, 143:2417–2430, 2016.
- [154] N. Sabine Werner, Reinhard Windoffer, Peter Strnad, Christian Grund, Rudolf E. Leube, and Thomas M. Magin. Epidermolysis bullosa simplex-type mutations alter the dynamics of the keratin cytoskeleton and reveal a contribution of actin to the transport of keratin subunits. *Molecular Biology of the Cell*, 15:990–1002, 2004.
- [155] Annette Kölsch, Reinhard Windoffer, and Rudolf E. Leube. Actin-dependent dynamics of keratin filament precursors. *Cell Motility and the Cytoskeleton*, 66:976–985, 2009.
- [156] Julien Colombelli and Julia Solon. Force communication in multicellular tissues addressed by laser nanosurgery. *Cell and Tissue Research*, 352:133–147, 2013.
- [157] Dapeng Bi, Xiang Yang, M. Cristina Marchetti, and M. Lisa Manning. Motility-driven glass and jamming transitions in biological tissues. *Physical Review X*, 6:021011, 2016.
- [158] Reza Farhadifar, Jens-Christian Röper, Benoit Aigouy, Suzanne Eaton, and Frank Jülicher. The influence of cell mechanics, cell-cell interactions, and proliferation on epithelial packing. *Current Biology*, 17:2095–2104, 2007.
- [159] Yassine-Eddine Keta and Silke Henkes. cells. https://github.com/yketa/cells. GitHub repository, MIT License.
- [160] Fang Wang, Shun Chen, Hong Liu, Carine Parent, and Pierre Coulombe. Keratin 6 regulates collective keratinocyte migration by altering cell–cell and cell–matrix adhesion. *Journal of Cell Biology*, 217:jcb.201712130, 2018.
- [161] Sebastian Karsch, Florian Büchau, Thomas M. Magin, and Andreas Janshoff. An intact keratin network is crucial for mechanical integrity and barrier function in keratinocyte cell sheets. *Cellular and Molecular Life Sciences*, 77:4397–4411, 2020.
- [162] Valentin Lulevich, Hong Yang, Rivkah Isseroff, and Gang-yu Liu. Single cell mechanics of keratinocyte cells. *Ultramicroscopy*, 110:1435–1442, 2010.

- [163] Ping Wong and Pierre A. Coulombe. Loss of keratin 6 (k6) proteins reveals a function for intermediate filaments during wound repair. *Journal of Cell Biology*, 163:327–337, 2003.
- [164] Carl-Gustaf A. Stenvall, Muhammad Tayyab, Teemu J. Grönroos, Miia A. Ilomäki, Kirsi Viiri, Karen M. Ridge, Leo Polari, and Diana M. Toivola. Targeted deletion of keratin 8 in intestinal epithelial cells disrupts tissue integrity and predisposes to tumorigenesis in the colon. *Cellular and Molecular Life Sciences*, 79:10, 2021.
- [165] Joanna Deek, Florian Hecht, Livia Rossetti, Katharina Wißmiller, and Andreas R. Bausch. Mechanics of soft epithelial keratin networks depend on modular filament assembly kinetics. *Acta Biomaterialia*, 43:218–229, 2016.
- [166] Florian Büchau, Franziska Vielmuth, Jens Waschke, and Thomas M. Magin. Bidirectional regulation of desmosome hyperadhesion by keratin isotypes and desmosomal components. *Cellular and Molecular Life Sciences*, 79:223, 2022.
- [167] Andrew P. Kowalczyk, Elisabeth A. Bornslaeger, Staci M. Norvell, Heather L. Palka, and Kathleen J. Green. Desmosomes: Intercellular adhesive junctions specialized for attachment of intermediate filaments. In Kwang W. Jeon, editor, *International Review of Cytology*, pages 237–302. Academic Press, 1998.
- [168] Jin Sun Kim, Chan-Ho Lee, Bryan Y. Su, and Pierre A. Coulombe. Mathematical modeling of the impact of actin and keratin filaments on keratinocyte cell spreading. *Biophysical Journal*, 103:1828–1838, 2012.
- [169] Jean-Emmanuel Bouameur, Beatrice Favre, and Luca Borradori. Plakins, a versatile family of cytolinkers: Roles in skin integrity and in human diseases. *Journal of Investigative Dermatology*, 134:885–894, 2014.
- [170] Yutaka Inaba, Vishakha Chauhan, A. Peter van Loon, Lokeshwar S. Choudhury, and Alvaro Sagasti. Keratins and plakin family cytolinker proteins control the length of epithelial microridge protrusions. *eLife*, 9:e58149, 2020.
- [171] Gregory F. Weber, Margaret A. Bjerke, and Douglas W. DeSimone. A mechanoresponsive cadherin-keratin complex directs polarized protrusive behavior and collective cell migration. *Developmental Cell*, 22:104–115, 2012.
- [172] Harald Herrmann and Sergei V. Strelkov. History and phylogeny of intermediate filaments: Now in insects. *BMC Biology*, 9:16, 2011.
- [173] Akanksha Jain, Vladimír Ulman, Arghyadip Mukherjee, Manoj Prakash, Marco B. Cuenca, Leena G. Pimpale, Sören Münster, Rainer Haase, Kristen A. Panfilio, Florian Jug, et al. Regionalized tissue fluidization is required for epithelial gap closure during insect gastrulation. *Nature Communications*, 11:5604, 2020.
- [174] Cornelia Schwayer, Shayan Shamipour, Kornelija Pranjic-Ferscha, Alexandra Schauer, Maria Balda, Masazumi Tada, Karl Matter, and Carl-Philipp Heisenberg. Mechanosensation of Tight Junctions Depends on ZO-1 Phase Separation and Flow. *Cell*, 179(4):937–952.e18, October 2019.
- [175] Mathias Köppen, Beatriz García Fernández, Lara Carvalho, Antonio Jacinto, and Carl-Philipp Heisenberg. Coordinated cell-shape changes control epithelial movement in zebrafish and Drosophila. *Development*, 133(14):2671–2681, July 2006.

- [176] Susanne Karsch, Fanny Büchau, Thomas M. Magin, and Andreas Janshoff. An intact keratin network is crucial for mechanical integrity and barrier function in keratinocyte cell sheets. *Cellular and Molecular Life Sciences*, 77(21):4397–4411, November 2020.
- [177] Laura Schaedel, Charlotta Lorenz, Anna V. Schepers, Stefan Klumpp, and Sarah Köster. Vimentin intermediate filaments stabilize dynamic microtubules by direct interactions. *Nature Communications*, 12(1):3799, June 2021.
- [178] L. Kreplak, H. Bär, J. F. Leterrier, H. Herrmann, and U. Aebi. Exploring the Mechanical Behavior of Single Intermediate Filaments. *Journal of Molecular Biology*, 354(3):569–577, December 2005.
- [179] Minh Ho, Brian Thompson, Jeffrey Nicholas Fisk, Daniel W. Nebert, Elspeth A. Bruford, Vasilis Vasiliou, and Christopher G. Bunick. Update of the keratin gene family: Evolution, tissue-specific expression patterns, and relevance to clinical disorders. *Human Genomics*, 16(1):1, January 2022.
- [180] Jeffrey A. Farrell, Yiqun Wang, Samantha J. Riesenfeld, Karthik Shekhar, Aviv Regev, and Alexander F. Schier. Single-cell reconstruction of developmental trajectories during zebrafish embryogenesis. *Science*, 360(6392):eaar3131, June 2018.
- [181] Ekaterina P. Kalabusheva, Anastasia S. Shtompel, Alexandra L. Rippa, Sergey V. Ulianov, Sergey V. Razin, and Ekaterina A. Vorotelyak. A Kaleidoscope of Keratin Gene Expression and the Mosaic of Its Regulatory Mechanisms. *International Journal of Molecular Sciences*, 24(6):5603, March 2023.
- [182] Roland Moll, Markus Divo, and Lutz Langbein. The human keratins: biology and pathology. *Histochemistry and cell biology*, 129:705–733, 2008.
- [183] Alexander Zimek and Klaus Weber. Terrestrial vertebrates have two keratin gene clusters; striking differences in teleost fish. *European Journal of Cell Biology*, 84(6):623–635, July 2005.
- [184] Bhaja Krushna Padhi, Marie-Andrée Akimenko, and Marc Ekker. Independent expansion of the keratin gene family in teleostean fish and mammals: An insight from phylogenetic analysis and radiation hybrid mapping of keratin genes in zebrafish. *Gene*, 368:37–45, March 2006.
- [185] Florian Ehrlich, Maria Laggner, Lutz Langbein, Pamela Burger, Andreas Pollreisz, Erwin Tschachler, and Leopold Eckhart. Comparative genomics suggests loss of keratin K24 in three evolutionary lineages of mammals. *Scientific Reports*, 9(1):10924, July 2019.
- [186] Tetsuo Kageyama. CELLULAR BASIS OF EPIBOLY OF THE ENVELOPING LAYER IN THE EMBRYO OF MEDAKA, ORYZIAS LATIPES. I. CELL ARCHITECTURE RE-VEALED BY SILVER STAINING METHOD. *Development, Growth and Differentiation*, 22(4):659–668, August 1980.
- [187] Carl-Gustaf A. Stenvall, Joel H. Nyström, Ciarán Butler-Hallissey, Theresia Jansson, Taina R. H. Heikkilä, Stephen A. Adam, Roland Foisner, Robert D. Goldman, Karen M. Ridge, and Diana M. Toivola. Cytoplasmic keratins couple with and maintain nuclear envelope integrity in colonic epithelial cells. *Molecular Biology of the Cell*, 33(13):ar121, November 2022. Publisher: American Society for Cell Biology (mboc).

- [188] Hui Yi Grace Lim, Yanina D Alvarez, Maxime Gasnier, Yiming Wang, Piotr Tetlak, Stephanie Bissiere, Hongmei Wang, Maté Biro, and Nicolas Plachta. Keratins are asymmetrically inherited fate determinants in the mammalian embryo. *Nature*, 585(7825):404–409, 2020.
- [189] Jens Bohnekamp, Diane E Cryderman, Achim Paululat, Gabriel C Baccam, Lori L Wallrath, and Thomas M Magin. A drosophila model of epidermolysis bullosa simplex. Journal of Investigative Dermatology, 135(8):2031–2039, 2015.
- [190] Wallis Nahaboo, Sema Elif Eski, Evangéline Despin-Guitard, Marjorie Vermeersch, Marie Versaevel, Bechara Saykali, Daniel Monteyne, Sylvain Gabriele, Thomas M. Magin, Nicole Schwarz, Rudolf E. Leube, An Zwijsen, David Perez-Morga, Sumeet Pal Singh, and Isabelle Migeotte. Keratin filaments mediate the expansion of extra-embryonic membranes in the post-gastrulation mouse embryo. *The EMBO journal*, 41(7):e108747, April 2022.
- [191] Alexander Goonesinghe, Xing-Ming Luan, Adam Hurlstone, and David Garrod. Desmosomal cadherins in zebrafish epiboly and gastrulation. *BMC Developmental Biology*, 12:1–16, 2012.
- [192] Susana Miravet, José Piedra, Julio Castaño, Imma Raurell, Clara Francí, Mireia Duñach, and Antonio García de Herreros. Tyrosine Phosphorylation of Plakoglobin Causes Contrary Effects on Its Association with Desmosomes and Adherens Junction Components and Modulates β -Catenin-Mediated Transcription. *Molecular and Cellular Biology*, October 2003.
- [193] Devrim Acehan, Christopher Petzold, Iwona Gumper, David D. Sabatini, Eliane J. Müller, Pamela Cowin, and David L. Stokes. Plakoglobin Is Required for Effective Intermediate Filament Anchorage to Desmosomes. *Journal of Investigative Dermatology*, 128(11):2665–2675, November 2008.
- [194] Eva D Martin, Miriam A Moriarty, Lucy Byrnes, and Maura Grealy. Plakoglobin has both structural and signalling roles in zebrafish development. *Developmental biology*, 327(1):83–96, 2009.
- [195] Alice Giuliodori, Giorgia Beffagna, Giulia Marchetto, Chiara Fornetto, Francesco Vanzi, Stefano Toppo, Nicola Facchinello, Mattia Santimaria, Andrea Vettori, Stefania Rizzo, Mila Della Barbera, Kalliopi Pilichou, Francesco Argenton, Gaetano Thiene, Natascia Tiso, and Cristina Basso. Loss of cardiac Wnt beta-catenin signalling in desmoplakin-deficient AC8 zebrafish models is rescuable by genetic and pharmacological intervention. *Cardiovascular Research*, 114(8):1082–1097, July 2018.
- [196] Anna V. Schepers, Charlotta Lorenz, Peter Nietmann, Andreas Janshoff, Stefan Klumpp, and Sarah Köster. Multiscale mechanics and temporal evolution of vimentin intermediate filament networks. *bioRxiv*, page 2021.01.30.428887, January 2021.
- [197] Charlotta Lorenz, Johanna Forsting, Robert W. Style, Stefan Klumpp, and Sarah Köster. Keratin filament mechanics and energy dissipation are determined by metal-like plasticity. *Matter*, 6(6):2019–2033, June 2023.
- [198] Charlotta Lorenz, Johanna Forsting, Anna V. Schepers, Julia Kraxner, Susanne Bauch, Hannes Witt, Stefan Klumpp, and Sarah Köster. Lateral Subunit Coupling Determines

- Intermediate Filament Mechanics. *Physical Review Letters*, 123(18):188102, November 2019.
- [199] Gülsen Çolakoğlu and Anthony Brown. Intermediate filaments exchange subunits along their length and elongate by end-to-end annealing. *Journal of Cell Biology*, 185(5):769–777, May 2009.
- [200] Helga Mueller and Werner W. Franke. Biochemical and immunological characterization of desmoplakins I and II, the major polypeptides of the desmosomal plaque. *Journal of Molecular Biology*, 163(4):647–671, February 1983.
- [201] G. Ian Gallicano, Christoph Bauer, and Elaine Fuchs. Rescuing desmoplakin function in extra-embryonic ectoderm reveals the importance of this protein in embryonic heart, neuroepithelium, skin and vasculature. *Development*, 128(6):929–941, March 2001.
- [202] Jens-Friedrich Nolting, Wiebke Möbius, and Sarah Köster. Mechanics of Individual Keratin Bundles in Living Cells. *Biophysical Journal*, 107(11):2693–2699, December 2014.
- [203] Zhuo Gan, Liya Ding, Christoph J. Burckhardt, Jason Lowery, Assaf Zaritsky, Karlyndsay Sitterley, Andressa Mota, Nancy Costigliola, Colby G. Starker, Daniel F. Voytas, Jessica Tytell, Robert D. Goldman, and Gaudenz Danuser. Vimentin intermediate filaments template microtubule networks to enhance persistence in cell polarity and directed migration. *Cell systems*, 3(3):252–263.e8, September 2016.
- [204] Preethi Vijayaraj, Goran Söhl, and Thomas M. Magin. Keratin Transgenic and Knockout Mice. In Mouldy Sioud, editor, *Target Discovery and Validation Reviews and Protocols: Volume 1, Emerging Strategies for Targets and Biomarker Discovery*, pages 203–251. Humana Press, Totowa, NJ, 2007.
- [205] Yoshitaka Tamai, Tomo-o Ishikawa, Michael R. Bösl, Masahiko Mori, Masami Nozaki, Heléne Baribault, Robert G. Oshima, and Makoto M. Taketo. Cytokeratins 8 and 19 in the Mouse Placental Development. *Journal of Cell Biology*, 151(3):563–572, October 2000.
- [206] Mohamed A. El-Brolosy, Zacharias Kontarakis, Andrea Rossi, Carsten Kuenne, Stefan Günther, Nana Fukuda, Khrievono Kikhi, Giulia L. M. Boezio, Carter M. Takacs, Shih-Lei Lai, Ryuichi Fukuda, Claudia Gerri, Antonio J. Giraldez, and Didier Y. R. Stainier. Genetic compensation triggered by mutant mRNA degradation. *Nature*, 568(7751):193–197, April 2019.
- [207] Sivaraj Sivaramakrishnan, Jaime L. Schneider, Albert Sitikov, Robert D. Goldman, and Karen M. Ridge. Shear stress induced reorganization of the keratin intermediate filament network requires phosphorylation by protein kinase C zeta. *Molecular Biology of the Cell*, 20(11):2755–2765, June 2009.
- [208] Valentin Lulevich, Hsin-ya Yang, R Rivkah Isseroff, and Gang-yu Liu. Single cell mechanics of keratinocyte cells. *Ultramicroscopy*, 110(12):1435–1442, 2010.
- [209] Mirjam Mayer, Martin Depken, Justin S. Bois, Frank Jülicher, and Stephan W. Grill. Anisotropies in cortical tension reveal the physical basis of polarizing cortical flows. *Nature*, 467(7315):617–621, September 2010.

- [210] Amanda Nicole Goldner, Salena M. Fessehaye, Nataly Rodriguez, Kelly Ann Mapes, Miriam Osterfield, and Konstantin Doubrovinski. Evidence that tissue recoil in the early Drosophila embryo is a passive not active process. *Molecular Biology of the Cell*, 34(10):br16, September 2023.
- [211] Chiara De Pascalis, Carlos Pérez-González, Shailaja Seetharaman, Batiste Boëda, Benoit Vianay, Mithila Burute, Cécile Leduc, Nicolas Borghi, Xavier Trepat, and Sandrine Etienne-Manneville. Intermediate filaments control collective migration by restricting traction forces and sustaining cell–cell contacts. *Journal of cell biology*, 217(9):3031–3044, 2018.
- [212] Sangbum Park, David G. Gonzalez, Boris Guirao, Jonathan D. Boucher, Katie Cockburn, Edward D. Marsh, Kailin R. Mesa, Samara Brown, Panteleimon Rompolas, Ann M. Haberman, Yohanns Bellaïche, and Valentina Greco. Tissue-scale coordination of cellular behaviour promotes epidermal wound repair in live mice. *Nature Cell Biology*, 19(3):155–163, March 2017.
- [213] Pedro Campinho, Martin Behrndt, Jonas Ranft, Thomas Risler, Nicolas Minc, and Carl-Philipp Heisenberg. Tension-oriented cell divisions limit anisotropic tissue tension in epithelial spreading during zebrafish epiboly. *Nature Cell Biology*, 15(12):1405–1414, December 2013.
- [214] Anne Kölsch, Reinhard Windoffer, and Rudolf E. Leube. Actin-dependent dynamics of keratin filament precursors. *Cell Motility*, 66(11):976–985, 2009. _eprint: https://onlinelibrary.wiley.com/doi/pdf/10.1002/cm.20395.
- [215] Fanny Loschke, Melanie Homberg, and Thomas M. Magin. Keratin Isotypes Control Desmosome Stability and Dynamics through PKCalpha. *Journal of Investigative Dermatology*, 136(1):202–213, January 2016.
- [216] Fanny Büchau, Franziska Vielmuth, Jens Waschke, and Thomas M. Magin. Bidirectional regulation of desmosome hyperadhesion by keratin isotypes and desmosomal components. *Cellular and Molecular Life Sciences: CMLS*, 79(5):223, April 2022.